CATALYTICALLY ENHANCED SYSTEMS FOR HYDROGEN STORAGE

FINAL REPORT

Craig M. Jensen[1], Carmen Andrei[2], Hendrik Brinks[3], Rosario Cantelii[4], Sandra Eaton[5], Sandrine Gomes[6], Hans Hagemann[6], Bjorn Haubach[3], Randi Holmstead[2], Kristin K. Kumashiro[1], Brad Lewandowski[1], Meredith Kuba[1], David Morales-Morales[1], Keeley Murphy[1], Walter Niemczura[1], Oriele Palumbo[4], Annalisa Paolone[4], G. Renaudin[6], Sesha Srinivasan[1], Martin Sulic[1], Dalin Sun[1], J.C. Walmsley[2], Zhouhui Wang[1], and Klaus Yvon[5]

1) Department of Chemistry, University of Hawaii, Honolulu, HI 96822.
2) Department of Physics, Norwegian University of Science and Technology, 7491 Trondheim, Norway.
3) Department of Chemistry, University of Denver, Denver, CO 80208.
4) Dipartimento di Fisca, Università di Roma "La Sapienza", Piazzale A. Moro 2, I-00185 Roma, Italy.
5) Institute for Energy Technology, P.O. Box 40, 2007 Kjeller, Norway.
6) Laboratoire de Cristallograhie, Université de Genève, 24 quai E. Ansermet, CH-1211 Geneva 4, Switzerland.

Contractor: University of Hawaii, Honolulu, HI; cooperative agreement DE-FC36-00GO10537
Start Date: 8/1/00
End Date: 9/30/05

Contact information: email: jensen@gold.chem.hawaii.edu; phone: 808-956-2769; fax 808-956-5908.

Table of Contents

List of Tables, Figures, and Schemes

Executive Summary

Previous U.S. DOE sponsored research at the University of Hawaii resulted in the development of methods of doping of sodium aluminum hydride, $NaAlH_4$ with titanium, zirconium and other catalysts such that: dehydriding occurs at temperatures as low as 100 ˚C; rehydriding requires less than 1 h; and >4 weight percent hydrogen can be repeatedly cycled through dehydriding/rehydriding. These materials appeared to be on the threshold of practical viability as hydrogen carriers for onboard fuel cells. However, it was apparent that further kinetic enhancement was required to achieve commercial viability. One of the primary goals of this project was to develop the requisite improved catalysts. Over the course of this project, a variety of titanium and zirconium dopant precursors were investigated. Moreover, our approach was to conduct of guided search for improved catalysts by obtaining a fundamental understanding of the chemical nature of the titanium dopants their mechanism of action. Therefore, we also determined the chemical nature of the titanium species that are formed upon mechanical milling of $NaAlH_4$ with the dopant precursors through synchrotron X-ray and neutron diffraction as well as transmission electron microscopy, scanning electron microscopy, and electron paramagnetic resonance (EPR) spectroscopy. In addition to kinetic studies, insight into the mechanism of action of the dopants was gained through studies of the destabilization of hydrogen in $NaAlH_4$ by the dopants through infrared, NMR, and anelastic spectroscopy.

Our previous efforts had also resulted in the discovery a class of catalysts that could provide the key to a practical hydrogen storage system based on the reversible dehydrogenation of liquid organic compounds. The PCP pincer complex, $IrH_2\{C_6H_3\text{-}2,6\text{-}(CH_2PBu^t{}_2)_2\}$ was the first reported homogeneous catalysts for the dehydrogenation of cycloalkanes to arenes. Unlike the heterogeneous catalysts for this reaction, our homogeneous catalyst also showed appreciable activity at low concentrations at temperatures as low as 100 ˚C. We had also found that the pincer complex also catalyzes the hydrogenation of arenes to cycloalkanes under moderate (10 atm) pressures of hydrogen. The two-way, hydrogenation/dehydrogenation activity of the catalyst suggests its application in a hydrogen storage system. The major obstacle to the practical

application of the pincer catalyst is that pronounced product inhibition occurs after about 10% dehydrogenation of cycloalkanes. The second major goal of this project was to develop an improved PCP catalyst which would not be inhibited by the dehydrogenated form of organic hydrogen carriers.

Abstract

The dehydriding rates of NaAlH4 doped with 2 mol % $Ti(O^nBu)_4$ or β-$TiCl_3$ are adequate to meet the demands of a PEM fuel cell operating under practical conditions. Mixtures NaH and Al doped with 2 mol % $Zr(O^nPr)_4$ will undergo hydriding to $NaAlH_4$ in 15 minutes under 120 atm of hydrogen at 120 ˚C. Alternate classes of Ti-dopants were found to be ineffective. Synchrotron X-ray and neutron diffraction studies of $NaAlH_4$, Na_3AlH_6 , and NaH/Al doped with 2 mol of Ti additives show, that after several cycles of dehydrogenation and re-hydrogenation, a shoulder appears on the high-angle side of the Al reflections that we interpret as $Al_{0.93}Ti_{0.07}$ This conclusion is confirmed by a combination of transmission microscopy and scanning electron microscopy studies of $NaAlH_4$ doped with 2 mol % TiF_3. The studies showed immediately following ball milling most of the Ti present was unreacted TiF_3 while Ti had been incorporated into an Al containing phase in samples which had undergone 15 cycles of dehydrogenation/re-hydrogenation.

Electron paramagnetic resonance spectroscopy indicates the evolution of the incorporated Ti results from the initial Ti(III) transforming through a series of Ti(0) species during the first 5 cycles. While it was observed that the conversion of Ti(III) to Ti(0) occurs much more readily for $TiCl_3$ than TiF_3, it was seen in both cases that the evolution of Ti follows the same sequence involving 3 distinguishable Ti(0) species and ends in the predominance of the same single Ti(0) species. Since only a relatively minor change in the hydrogen cycling kinetics is observed during the first 10 cycles of dehydrogenation/re-hydrogenation, our results indicate that the profoundly enhanced hydrogen cycling kinetics of Ti-doped $NaAlH_4$ are apparently due to a minority Ti species and that the majority of the Ti is in a resting state. Solid state ^1H NMR studies have revealed that there is a population of highly mobile hydrogen in both doped and undoped $NaAlH_4$ and that Ti-doping results in a significant increase in the proportion of

mobile hydrogen in the **bulk** material. Evidence that Ti-doping perturbs Al-H bonding throughout the bulk of the hydride was also obtained from infrared (IR) and anelastic spectroscopy. The latter indicates the formation of a point defect involving hydrogen that has a very high mobility (~$5x10^3$ jumps/s at 70K) upon thermal treatment of the hydride. Rietveld analysis of this broadening of the X-ray diffraction peaks that occurs upon mechanical milling of the hydride results not only in reduction of hydride grain size, but also a distortion of the lattice thus indicating the enhanced hydrogen cycling kinetics are linked to a distortion of the hydride's microstructure. The arsino pincer complex, $IrH_2\{C_6H_3\text{-}2,6\text{-}(CH_2AsBu^t{}_2)_2\}$ was synthesized and found to be an active catalyst for the dehydrogenation of a variety of cycloalkanes to arenes as well as the reverse hydrogenation reaction. However, development of a hydrogen storage system based on this technology seems impractical, as only a maximum 20 % conversion to the arene can be achieved.

Introduction

A major obstacle to the conversion of the world to a "hydrogen economy" is the problem of onboard hydrogen storage. Despite decades of extensive effort no material has been found which has the combination of a high gravimetric hydrogen density, adequate hydrogen dissociation energetics, long-term cyclability, and low cost required for commercial vehicular application. A priori, sodium aluminum hydride, $NaAlH_4$ would seem to be viable candidate for application as a practical onboard hydrogen storage material. It has a high weight percent available hydrogen content (5.6 %), relatively low cost, and is readily available in bulk. However, thermal activated evolution of hydrogen from $NaAlH_4$ occurs at appreciable rates only at temperatures well above its melting point of 183 ˚C. Additionally, this process can be reversed only under severe conditions. Thus, until recently, complex aluminum hydrides were not considered as rechargeable hydrogen carriers. This situation was changed by recent studies which have shown that upon doping with selected transition metals, the dehydriding of anionic aluminum hydrides could be kinetically enhanced and rendered reversible under moderate conditions in the solid state (Bogdanovic and Schwickardi, 1997; Jensen et al., 1999; Zidan et al., 1999; Bogdanovic et al., 2000; Jensen and Gross, 2001). We have

developed methods of doping sodium aluminum hydride, $NaAlH_4$, with titanium and/or zirconium that have given rise to state-of-the-art hydrogen storage materials. However, less than ~5 weight percent hydrogen can be reversibly released from these materials under conditions that are required for the practical operation of an onboard fuel cell. In light of this and other practical limitations, it has become apparent that improved variations of this material must be produced to achieve commercial viability. A better understanding of the fundamental basis of the enigmatic kinetic enhancement of reversible dehydrogenation of the doped materials in the solid state would be invaluable to the effort to improve the hydrogen cycling kinetics of these materials.

We have also been investigating hydrogen storage through the reversible dehydrogenation of cycloalkanes to arenes. Cycloalkanes are cheap and abundant. The dehydrogenation of cycloalkanes to arenes releases approximately 7 weight percent hydrogen. As such this storage system also meets the criteria of low cost and high hydrogen density required for practical applications. However, it is, generally considered to be impractical as their dehydrogenation occurs at adequate rates only in the presence of high loadings of heterogeneous, precious metal catalysts at temperatures in excess of 300 ^{o}C. We found that the PCP pincer complex, $IrH_2\{C_6H_3\text{-}2,6\text{-}(CH_2PBu^t_2)_2\}$ (1) is a uniquely active and robust catalyst for aliphatic dehydrogenations (Gupta et al., 1996; Gupta, Hagen et al., 1997; Gupta, Kaska et al., 1997; Xu et al, 1997; Liu et al., 1999; Jensen, 2000). In contrast to most catalysts that have been reported for thermochemical dehydrogenation of alkanes, the pincer catalyst does not require a sacrificial hydrogen acceptor. Thus in the presence of the pincer catalyst, alkanes are efficiently dehydrogenated to alkenes with the direct evolution of H_2 (Gupta, Hagen et al., 1997; Jensen, 2000). The pincer catalyst is also the first reported homogeneous catalysts for the dehydrogenation of cycloalkanes to arenes (Gupta, Hagen et al., 1997). Unlike the heterogeneous catalysts that are known for this reaction, it shows appreciable activity at temperatures as low as 100 ˚C and very low catalyst loadings (Gupta, Hagen et al., 1997; Jensen, 2000). We have also found that the pincer complex also catalyzes the hydrogenation of arenes to cycloalkanes under moderate (10 atm) pressures of hydrogen. The two-way, hydrogenation/dehydrogenation activity of the catalyst suggests its application in a hydrogen storage system based on the reversible

dehydrogenation of a cycloalkane to its arene analog, such as the methylcyclohexane-toluene system seen in Scheme 1.

Scheme 1

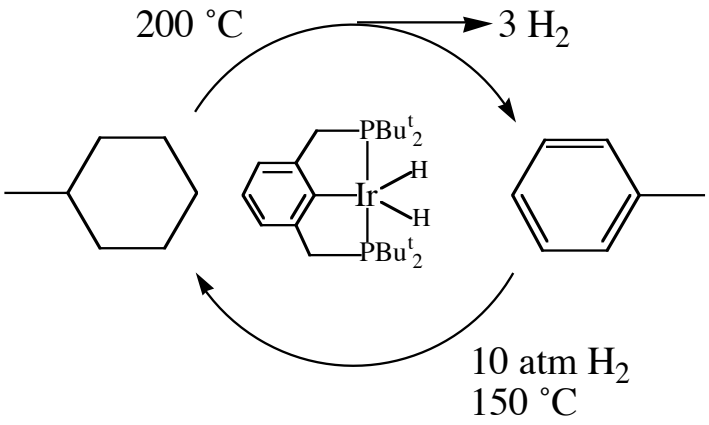

Scheme 1. Iridium pincer catalyzed toluene/ methylcyclohexane hydrogenation/dehydrogenation cycle.

Temperatures in excess of 200 ˚C are thermodynamically required to achieve a usable pressure of hydrogen from the dehydrogenation of alkanes. However, unlike solid hydrogen storage materials, liquid cycloalkanes can be easily transported within a system. Thus a small portion can be continuously fed into a small hot tube at a rate that ensures an adequate supply of hydrogen for the onboard application. This system is also attractive since it is compatible with existing gasoline infrastructure. The major drawback to homogenous, pincer complex catalyzed systems is that pronounced product inhibition occurs after dehydrogenation of about 10% of the cycloalkane to arene. The dissociation of product from the catalyst is apparently reversible and, at high concentrations, arenes effectively compete with alkanes for coordination to the complex. An alteration of the electronic environment at the metal center may improve the alkane/arene binding selectivity. Therefore substitution of the phosphorous donor atoms by arsenic atoms was investigated as a means of improving the level of conversion of methylcyclohexane to toluene.

Results

Task 1. Testing of Aluminum-Transition Metal Catalysts for the Reversible Dehydriding of $NaAlH_4$. (Amended in FY03 to: Determination and Quantification of Effective Dopant Ions and extended with Task 3: Determination of the Hydrogen Cycling Kinetics and Thermodynamics of Newly Formulated Doped $NaAlH_4$; and further extended in FY04 with Task 7. Synthesis and Characterization of Sodium-Titanium Alanate).

The aluminum-transition metal alloys: TiAl, Ti_3Al, Zr_3Al, and Ni_3Al, the transition metal-aluminum hydrido complexes: $\{(C_5H_5)_2ZrH(\mu\text{-}H)_2AlH_2(NMe_3)\}$, and $\{(C_5H_5)_2Ti(\mu\text{-}H)_2AlH_2(THF)\}$ were studied as catalysts for the reversible dehydriding of $NaAlH_4$. The complexes were synthesized through methods that have been reported in the literature (Khan et al., 1997; Fryzuk et al., 1997). The alloys were purchased from Alfa Aesar. Small amounts (~2 mol %) of the alloys and complexes were introduced into bulk $NaAlH_4$ through ball milling techniques under an inert atmosphere. The dehydriding behavior of the doped hydrides were screened by thermal programmed desorption and isothermal desorption studies using a modified Sievert's type apparatus. As seen in **Figure 1**, little or no kinetic enhancement was observed in all of the samples doped with aluminum alloys. Hydrogen desorption was accelerated in the samples doped

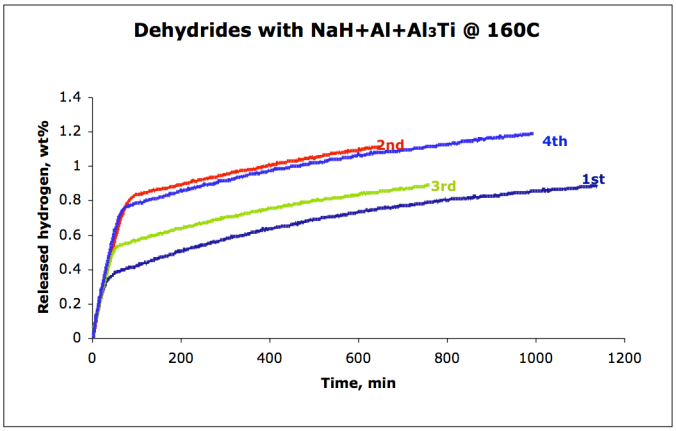

Figure 1. Dehydrogenation profile at 160˚C for NaH/Al + 3 mol% Al_3Ti powder mechanically milled for 30 minutes and charged under 100 atm H_2 for 10 h at 120˚C.

with the transition metal-aluminum hydride complexes. However, the desorption rates were much lower than those observed for samples doped with $Ti(O^nBu)_4$ or $Zr(O^nPr)_4$. In order to obtain a meaningful comparison of the relative catalytic enhancement produced by the various dopants, we conducted isothermal desorption studies of samples of the hydrides under the practical relevant conditions of 100˚C while maintaining a constant pressure of 1 atm. Table 1 summarizes the results of our studies of the hydride undergoing the initial dehydrogenation reaction seen in equation 1. The rates of

$$3\ NaAlH_4 \text{ ----------> } Na_3AlH_6 + 2\ Al + 3\ H_2 \qquad (1)$$

Table 1. Rates of dehydriding of NaAlH4 containing 2 mol % dopant at 100˚C, against a constant pressure of 1 atm

Catalyst Precursor	Rate of desorption (wt %/h)
$Ti(O^nBu)_4$	1.8
β-$TiCl_3$	1.8
$TiCl_4$	1.8
$Zr(O^nPr)_4$	0.6
$\{(C_5H_5)_2ZrH(\mu\text{-}H)_2AlH_2(NMe_3)\}$	0.2
$\{(C_5H_5)_2Ti(\mu\text{-}H)_2AlH_2(THF)\}$	0.2

dehydrogenation that were observed for hydride doped with either $Ti(O^nBu)_4$ or β-$TiCl_3$ corresponds to a hydrogen flow rate of 0.01 g H_2/s per kg of $NaAlH_4$ which is adequate to meet the demands of a fuel cell operating under practical conditions. We have also found that acceptable rates of re-hydrogenation could be achieved with a ball milled 50:50 mixture of NaH and Al doped with 2 mole percent $Zr(O^nPr)_4$. We observed absorption of 4.4 weight percent hydrogen within 15 min at 120˚C under 125 atm of hydrogen. Unfortunately, the rates observed for the second dehydrogenation reaction, seen in equation 2, were an order of magnitude slower and thus hydrogen is liberated by this

$$Na_3AlH_6 \text{ ----------> } 3\ NaH + Al + 3/2\ H_2 \qquad (2)$$

reaction at rates too slowly to be utilized for onboard PEM fuel cell applications.

In order to characterize the Ti dopant, samples of $NaAlH_4$, Na_3AlH_6, and NaH/Al doped with 2 mol of Ti additives were studied by synchrotron X-ray and neutron diffraction in a collaborative effort with the Hauback group at the Institute for Energy Technology, Norway (Brinks et al., 2004). Directly after ball milling, there are no signs of any Ti-containing phases. However, ass seen in **Figure 2**, after several cycles of

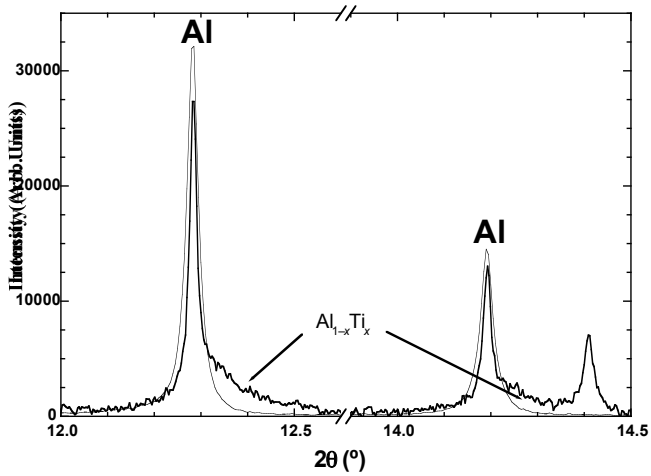

Figure 2. Comparison of the Al peaks observed by synchrotron X-ray diffraction for NaAlH4 doped with 2 mol % $TiCl_3$ before and after 7 cycles of dehydrogenation-re-hydrogenation

dehydrogenation and re-hydrogenation, a shoulder on the high-angle side of the Al reflections appears that is interpreted as the face-centered-cubic (fcc) solid solution, with an approximate composition of $Al_{0.93}Ti_{0.07}$.

The conclusions of our diffraction studies were confirmed in studies of $NaAlH_4$ that was doped with 2 mol % TiF_3 by a combination of transmission electron microscopy and scanning electron microscopy, both with energy-dispersive spectroscopic X-ray analysis (Andrei et al., 2005). These studies were carried out in collaboration with the Walmsley group at the Norwegian University of Science and Technology. After samples of $NaAlH_4$ doped with 2 mol % TiF_3 had undergone 15 cycles of dehydrogenation-rehydrogenation energy dispersive spectroscopic X-ray analysis showed that Ti had been incorporated into an Al containing phase. However, analysis of samples of the doped hydride immediately following ball-milling indicates that the distribution of Ti is quite

uneven. As seen in **Figure 3**, a variety of methods, including selected-area diffraction and high-resolution imaging confirmed that most of Ti was present as unreacted TiF_3.

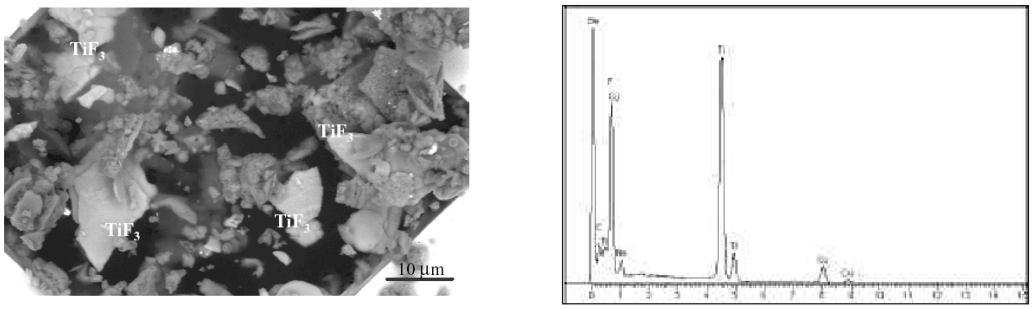

Figure 3. Left, SEM image taken with backscattered electrons (BSE). Right, energy Dispersive X-ray spectrum of a particle observed in uncycled $NaAlH_4$ doped with 2 mol % TiF_3 shows strong Ti and F peaks.

Further insight as to how the Ti dopants enhance the kinetics of hydrogen cycling in NaAlH4 was gained in collaborative studies with the Yvon group of the University of Geneva (Gomes et al., 2005). We observed that ball-milling of the doped hydride results in a broadening of the X-ray diffraction peaks. Rietveld analysis of this broadening indicates that mechanical milling of the hydride results not only in reduction of hydride grain size, but also a distortion of the lattice primarily in the c direction. Thus the enhanced hydrogen cycling kinetics that arise following the mechanical doping process are not only a consequence of hydride particle size reduction and Ti dispersal but also appear to be linked to a distortion of the hydride's microstructure

Task 2. Solid State Magnetic Resonance Spectroscopic Studies of the Reversible Dehydriding of NaAlH4. (Amended in FY03 to: Characterization of "Mobile Hydrogen in Doped NaAlH4 by Solid State Nuclear Magnetic Resonance Spectroscopy and Neutron Diffraction).

We obtained wide-line solid state ^1H nuclear magnetic resonance (NMR) spectra of a ball-milled sample of undoped $NaAlH_4$. As seen in **Figure 4**, the spectrum of both materials contains a broad and a narrow component. The narrow feature has a chemical shift of ca. 2 ppm and an unusually narrow linewidth of ca. 1-2 kHz while broad feature

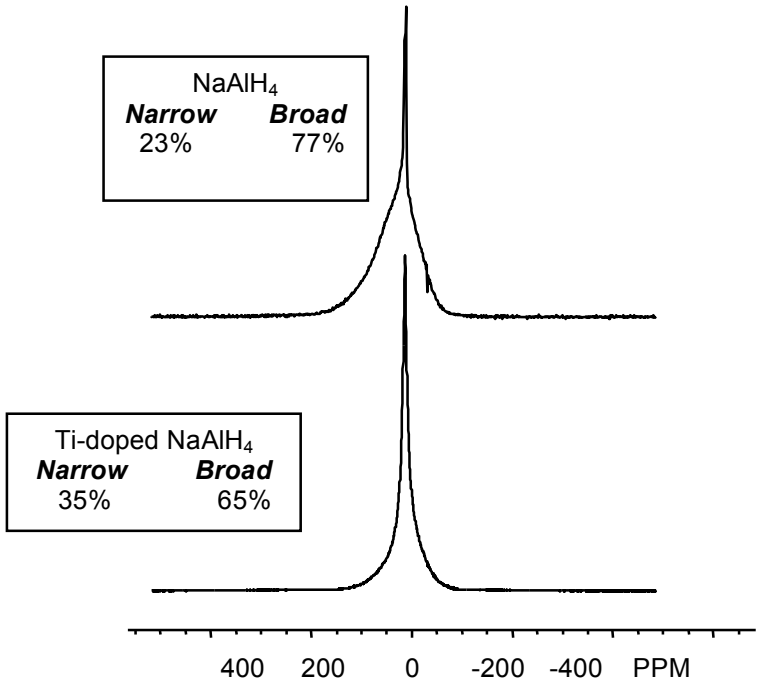

Figure 4. Solid state ^{1}H NMR spectra of $NaAlH_4$ with and without doping with 2 mol % $Ti(O^nBu)_4$.

has a more typical linewidth of ca. 40 kHz. Using inversion-recovery experiments, the T_1 of the narrow and broad features were determined to be 32 msec and 25 seconds, respectively. The former is particularly striking, because this short T_1 is atypical for protons in the solid-state. The relative intensity of the narrow component was unchanged upon heating a ball-milled sample under dynamic vacuum at 100 ˚C for 24 h. Thus it would seem unlikely that the narrow feature is associated with residual organic solvent as this treatment would remove the majority of this type of impurity. Additionally, the infrared spectrum of this material was devoid of any absorption in the C-H stretching region. Furthermore, the relative intensity of the narrow component increases as the hydride is doped or subjected to ball milling for longer periods of time. Obviously, this should not increase the level of organic solvent in the material. The remarkably short T_1 of the narrow feature suggests that the second population hydrogen is metal bound hydrogen which is not in a discrete, rigid $[AlH_4]^-$ environment and that a significant population of hydrogen in NaAlH4 is highly mobile at even ambient temperature. We

have observed that samples of the hydride that are doped with titanium have a significant increase in the proportion of mobile hydrogen in the **bulk** material.

In hopes of elucidating the changes occur in the structural environment of the hydrogen atom upon doping the hydride, we carried out neutron diffraction structure determination of $NaAlD_4$. In contrast to the X-ray structure determination $NaAlH_4$ in which only the atomic position of the Na and Al could be located (Belskii et al, 1983) the atomic positions of the deuterium atoms can be reliably located by neutron diffraction Due to the inherent problem of incoherent neutron scattering by ^1H, it was necessary to develop a method for the synthesis of high purity $NaAlD_4$. This was accomplished through the reaction of $LiAlD_4$ with NaF in the presence of an aluminum alkyl catalyst. Neutron diffraction data was collected in Norway at the Institute for Energy Technology from a sample of $NaAlD_4$ that was prepared through this method. Final refinement of this data gave the structure of the hydride seen in **Figure 5**. The deuterium atoms were

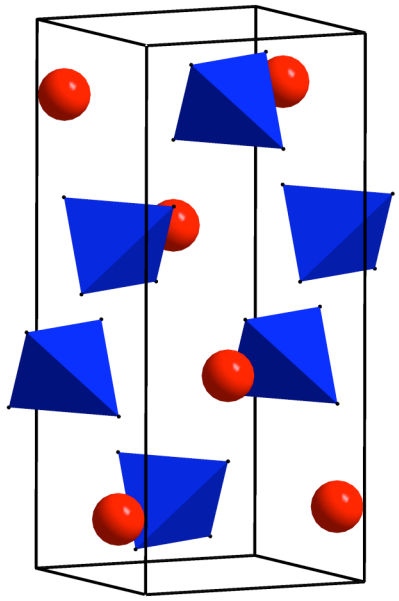

Figure 5. The crystal structure of $NaAlD_4$.

well located giving a structure with two unique Al-D distances of 1.627(2), 1.626(2) Å and two unique D-Al-D angles of 107.30(1) and 113.90(1) (Hauback et al., 2003). Unfortunately, no significant structural differences were found upon refinement of the neutron diffraction data that was collected from a sample of the doped hydride.

Task 4 (added in FY 04): Characterization and Quantification of Effective Dopant through Paramagnetic Resonance Studies

Further confirmation and information about the Ti-dopant was provided through studies of doped $NaAlH_4$ by electron paramagnetic resonance (EPR) spectroscopy that were conducted in collaboration with the Eaton group at the University of Denver (Kuba et al., 2005). The EPR spectra were obtained for samples of Ti-doped $NaAlH_4$ that were subjected to different numbers of cycles of dehydrogenation/re-hydrogenation. As seen in **Figure 6**, Ti was observed to evolve from its initial Ti(III) state through a series of Ti(0) species during the first 5 cycles. Although the conversion of Ti(III) to Ti(0) occurs much more readily for $TiCl_3$ doped samples than those prepared with TiF_3, in both cases the evolution of Ti follows the same sequence that involves 3 distinguishable Ti(0) species and ends in the predominance of the same single Ti(0) species. The spectra of samples of $NaAlH_4$ containing 2 mol % of cubic Al_3Ti and Ti powder are distinctly different than any of those observed for the Ti(0) species that arise during the hydrogen cycling of the hydride. We observe only a relatively minor change in the hydrogen cycling kinetics during the first 10 cycles of dehydrogenation/re-hydrogenation. This finding in conjunction with the electron microscopy and EPR studies strongly suggests that the hydrogen cycling kinetics are unaffected whether a Ti(III) to Ti(0) species predominates. **Thus the profoundly enhanced hydrogen cycling kinetics of Ti-doped $NaAlH_4$ are apparently due to a minority Ti species and that the majority of the Ti is in a resting state**. This conclusion is supported by our finding that all known TiAl alloys are ineffective in promoting the dehydrogenation/re-hydrogenation kinetics of $NaAlH_4$.

Task 5 (added in FY04). Characterization of Dynamic Processes by Solid State Nuclear Magnetic Resonance and Raman Spectroscopy

As discussed in the Task 2 section, nuclear magnetic resonance (NMR) spectroscopic studies indicated that titanium doping significantly increases in the proportion of mobile. hydrogen in the **bulk** material. Further evidence that Ti doping perturbs Al-H bonding throughout the bulk of the hydride was obtained from infrared spectroscopy (collaboration with the Yvon group at the University of Geneva). As seen

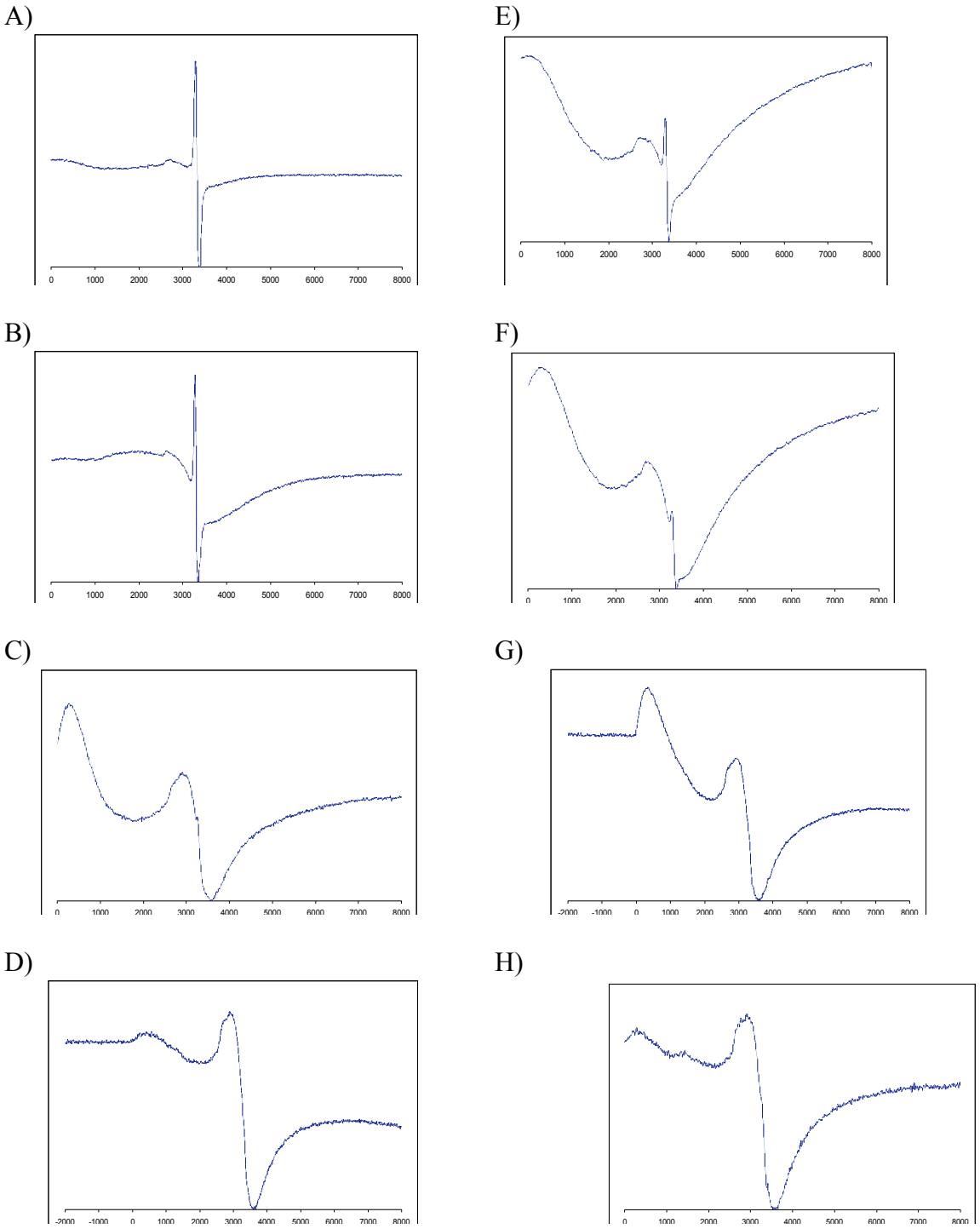

Figure 6. EPR spectrum of: A) 2 mol % TiF_3 doped $NaAlH_4$, uncycled. B) 2 mol % TiF_3 doped $NaAlH_4$, after 3 cycles. C) 2 mol % TiF_3 doped $NaAlH_4$, after 5 cycles. D) 2 mol % TiF_3 doped $NaAlH_4$, after 10 cycles. E) 2 mol % $TiCl_3$ doped $NaAlH_4$, uncycled. F) 2 mol % $TiCl_3$ doped $NaAlH_4$, after 3 cycles. G) 2 mol % $TiCl_3$ doped $NaAlH_4$, after 5 cycles. H) 2 mol % $TiCl_3$ doped $NaAlH_4$, after 10 cycles.

in **Figure 7**, upon doping the hydride, the infrared absorption corresponding to the

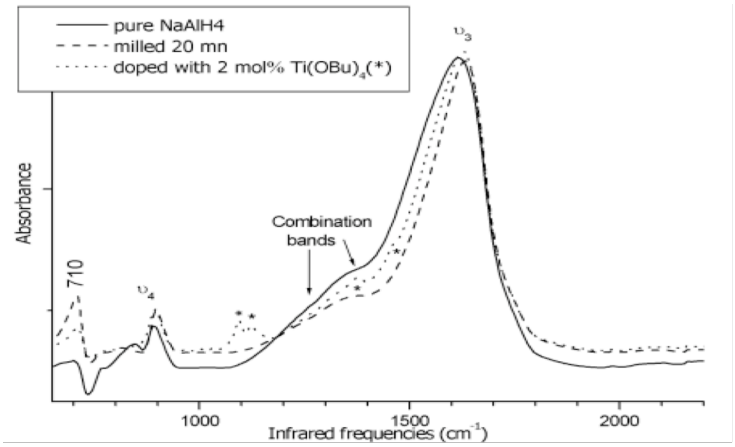

Figure 7. Comparison of the infra red spectra of doped and undoped $NaAlH_4$.

asymmetric stretching mode shifts by ~15 cm^{-1} to higher frequency while the H-Al-H asymmetric bending mode shifts by ~20 cm^{-1} to lower frequency (Gomes et al., 2005). We initially planed to study the dynamics of the mobilized population of hydrogen through solid state NMR and Raman spectroscopy. However, we found anelastic spectroscopy to be a much more insightful method by which to study the titanium induced mobilization of hydrogen. These measurements were carried out in collaboration with the Cantelli group at the University of Rome (Palumbo et al., 2005). Heating NaAlH4 doped with 2 mol % $TiCl_3$ to 436 K introduces a thermally activated relaxation process with a frequency of 1 kHz at 70 K. This denotes the formation of a point defect with a very high mobility (~$5x10^3$ jumps/s at 70K). The relaxation involves the reorientation of H around Ti.

Task 6. Determination of the Effects of Doping on Plateau Pressures of $NaAlH_4$.

Our initial studies of the equilibrium hydrogen pressures of Ti-doped $NaAlH_4$ were conducted with samples of $NaAlH_4$ that were doped 1.3 – 2.0 mole % $Ti(OBu)_4$. The plateau pressure was seen to increase from 3.0(2) to 4.7(2) Mpa over the range of doping levels. However, we soon found that different plateau pressures were obtained at the same doping levels if different dopant precursors were used. We also found similar variation even among samples that were doped to the same level with the same dopant

precursor. This finding is consistent with several reports that the exceptionally flat isotherms reported in the literature (Bogdanovic et al., 2000) can not be reproduced. We and several other groups have instead observed plateaus that are severely sloped. Thus accurate determination of plateau pressures is impossible. We have also found significant variation among the pressures observed at the same points in the dehydrogenation of identically prepared samples. Therefore, we terminated experimental work in this area.

Task 8. Characterization and Evaluation of Silicon-$LiAlH_4$ System. (Added in FY04)

This task was undertaken to explore the possibility that, the dehydrogenation $LiAlH_4$ in the presence of the silicon might proceed according to equation 3 and kinetically favor

$$4\ LiAlH_4 + Si \text{ ----------> } Li_4Si + 4\ Al + 8\ H_2 \qquad (3)$$

the formation of the lithium-silicon alloy, Li_4Si instead of LiH. The theoretical hydrogen cycling based on this process and its reverse is 8.97 weight percent. Mixtures of $LiAlH_4$ and Si were Ti-doped through our mechanical (ball milling) method (Zidan et al. 1999). The dehydrogenation of the mixtures was monitored using an automated thermovolumetric analyzer (PCT) under a variety of conditions. Unfortunately, it all case analysis of the dehydrogenated reaction mixtures showed no signs of the lithium-silicon alloy.

Task 9. Further Studies of Advanced Complex Hydride. (added in FY04).

This task was added following preliminary studies of the Si/$LiAlH_4$ which indicated that a material which evolved >7.0 wt % hydrogen upon dehydrogenation at 125 ˚C could be fully re-hydrogenated at 150 ˚C and 150 atm of hydrogen. Many attempts were made to reproduce this result while monitoring the dehydrogenation and re-hydrogenation with a high accuracy, automated thermovolumetric analyzer (PCT). However, all samples showed no sign of hydrogen up take during attempted re-hydrogenation. Apparently, re-hydrogenation did not occur in the initial experiment and the observed pressure drop was

due to a leak in the system. Unfortunately, this hypothesis could not be verified as the "re-hydrogenated" sample was lost and could not be analyzed by X-ray diffraction.

Original Task 3 (terminated after FY02). Synthesis and Testing of an Arsino Pincer Catalyst for Reversible Alkane Dehydrogenation.

In order to improve the alkane/arene binding selectivity of the coordinate complex in dehydrogenation system we successfully synthesized the arsino pincer complex, $IrH_2\{C_6H_3\text{-}2,6\text{-}(CH_2AsBu^t_2)_2\}$ as seen in Scheme 2. Reaction of α,α'-dibromoxylene

Scheme 2. Synthesis of $IrH_2\{C_6H_3\text{-}2,6\text{-}(CH_2AsBu^t_2)_2\}$.

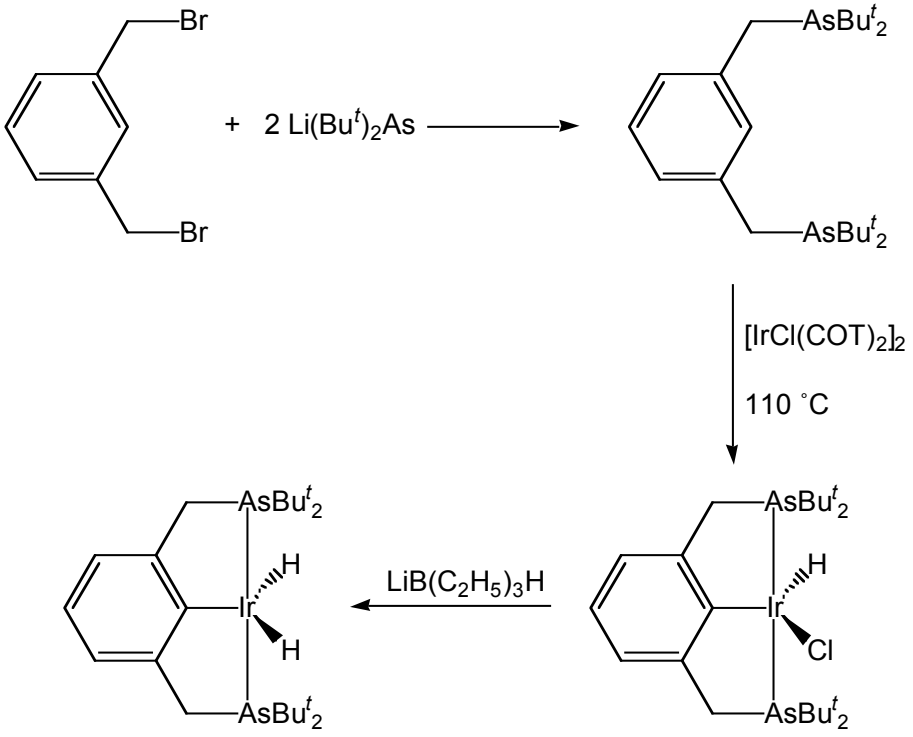

with two equivalents of lithium di-t-butylarsinide gave α,α'-bis(arsino)xylene in > 90 % yield. The hydrido chloride iridium complex, $IrHCl\{C_6H_3\text{-}2,6\text{-}(CH_2AsBu^t_2)_2\}$ was then synthesized by refluxing the α,α'-bis(arsino)xylene with $[Ir(COE)(\mu\text{-}Cl)]_2$ in toluene for 24 hours. Subsequent reaction of the hydrido chloride complex with $LiBEt_3H$ under an

atmosphere of H_2 gave the target dihydride complex that was characterized by ^1H, ^{13}C, and ^{31}P NMR spectroscopy. The catalytic activity of the arsino pincer complex for the dehydrogenation of methylcyclohexane to toluene at 200 ˚C was quantified by gas chromatography. We have observed that the dehydrogenation proceeds to >20% conversion compared to the ~10 % conversion that can be achieved with the phosphino catalyst. This result verifies our hypothesis that the σ-donor strength of the ligand greatly influences the attainable conversion level in the catalytic system. Unfortunately, the conversion level is still far short of practically significant >90 % mark and it seems unlikely that we will be able to adjust the catalytic system such that we can attain such high levels of (single-pass) conversion.

Conclusions

We have examined the effects of two classes of dopants on the rates of the dehydriding of doped $NaAlH_4$ to Na_3AlH_6 and Al under the practical relevant conditions of 100 ˚C and a constant pressure of 1 atm. Aluminum-transition metal alloys were found to have little or no effect while doping with transition metal-aluminum hydride complexes resulted in only modest kinetic enhancement. However, benchmarking the dehydriding rates of hydride doped with $Ti(O^nBu)_4$ and β-$TiCl_3$ has revealed that these materials undergo dehydriding at rates adequate to meet the demands of a fuel cell operating under practical conditions. We have also found that NaH and Al doped with 2 mol % $Zr(O^nPr)_4$ will undergo hydriding to $NaAlH_4$ more rapidly and under milder conditions that had been previously appreciated. Thus three key, practical kinetic parameters have now been established for $NaAlH_4$ at acceptable doping levels: 1) dehydriding of $NaAlH_4$ to Na_3AlH_6 and Al at the rate of 1.8 wt % per hour at 100 ˚C under 1 atm; 2) rehydriding of 4.4 wt % can be accomplished in only 15 minutes; and 3) >4.0 weight percent hydrogen can be repeatedly cycled through dehydriding/rehydriding at temperatures as low as 150 ˚C.

Our EPR, synchrotron XRD, XAFS, and TEM studies of $NaAlH_4$ doped with 2 mol % TiF_3, all indicate a change in Ti from a Ti(III) species (TiF_3) to an Al associated Ti(0) species. This change is shown to occur within the first few cycles of dehydrogenation/rehydrogenation. We observe only a relatively minor change in the

hydrogen cycling kinetics whether a Ti(III) to Ti(0) species predominates. Therefore, our studies strongly suggest that **the enhanced hydrogen cycling kinetics of Ti-doped $NaAlH_4$ are due to a minority Ti species and that the majority of the Ti is in a resting state**. This conclusion is supported by our findings that all known TiAl alloys are relatively ineffective in promoting the dehydrogenation/re-hydrogenation kinetics of $NaAlH_4$.

Studies of NaAlH4 by infrared spectroscopy show that doping perturbs Al-H bonding throughout the **bulk** of the hydride. This conclusion is supported by solid state ^1H NMR spectroscopy which indicates that there is a significant population of hydrogen in NaAlH4 that is highly mobile even at ambient temperature and that titanium doping results in an increase in the proportion of mobile hydrogen in the **bulk** material. Further complementary results were obtained through anelastic spectroscopy. These studies have shown that point defects arise upon thermal treatment of Ti-doped $NaAlH_4$. These entities apparently involve hydrogen and are highly mobile (~$5x10^3$ jumps/s at 70K).

Ball-milling of the doped hydride results in a broadening of the X-ray diffraction peaks. Rietveld analysis of this broadening indicates that in addition to increasing the surface área, the milling process produces a distortion of the crystasl lattice. This distortion in the hydride's microstructure appears to be linked to the enhanced hydrogen cycling kinetics that arise following the mechanical doping process.

We have successfully synthesized the arsino pincer complex, $IrH_2\{C_6H_3\text{-}2,6\text{-}(CH_2AsBu^t_2)_2\}$ and to found it to catalyze the dehydrogenation of methylcyclohexane to toluene. The >20% conversion obtained using this catalyst is much greater than the 10 % conversion obtained with the phosphino catalyst. This result verifies our hypothesis that the σ-donor strength of the ligand greatly influences the attainable conversion level in the catalytic system. Unfortunately the conversion level is still far short of a practically significant, >90 %, mark and it seems unlikely that we will be able to adjust the catalytic system such that we can attain such high levels of conversion.

Future Directions

Despite the recent flurry of recent activity that has been directed towards the development of alanates as onboard hydrogen carriers, no alanate-based material has been developed that meets the performance criteria set by the U.S. DOE. The level of success that has been achieved with the alanates has, however, been sufficient to push the frontier of the search for non-cyrogenic, onboard, reversible hydrogen carriers beyond hydrogen absorbing metals and alloys. The prospect of kinetic enhancement through the introduction of transition metal dopants, has led to the exploration of other materials that have favorable dehydrogenation thermodynamics but ostensibly insurmountably, slow dehydrogenation and/or re-hydrogenation kinetics. Indeed, it has recently been found that the phenomenon of kinetic enhancement upon transition metal doping extends beyond the alanates to the reversible dehydrogenation of $LiNH_2$ (Ichikawa et al 2004) and $MgH_2/LiBH_4$ (Vajo et al 2005). However, further improvement rates of dehydrogenation and re-hydrogenation remains on of the principal barriers to the practical application of these and other complex hydrides.

Clearly, the effort to improve the dehydrogenation and re-hydrogenation kinetics of complex hydrides would be greatly aided understanding of the mechanism of action of the dopants. Our initial approach to gain such insight into the Ti-doped $NaAlH_4$ was to characterize the active Ti species. However, described above, we have found that the active species must be a small minority of the Ti present in the material. Thus the identification and characterization of the true active species will be difficult if not impossible. On the other hand, during the course of this project we have discovered that Ti doping has the effect of generating hydrogen containing point defects in the hydride. It is evident that the generation of these defects is the key to enhancing the dehydrogenation/re-hydrogenation kinetics of complexes hydrides and thus it is imperative that they be characterized. As part of this research project, we have initiated an effort to characterize the "mobile population of hydrogen" that we have detected by solid state ^1H NMR. It is quite likely that the "mobile hydrogen" is that same species as the "hydrogen containing point defects" detected by anelastic spectroscopy. Thus the NMR studies will be continued and supplemented by solid state ^2H NMR spectroscopic studies to elucidate chemical natural of the detected species. While anelastic

spectroscopy is an excellent tool for detection of point defects, it gives little information about the composition or immediate chemical environment of the defects. Such information has been obtained about point defects in semi-conductors through positron inhalation and muon spin resonance studies. The study of Ti-doped $NaAlH_4$ by these methods is clearly an important future direction for this area of research. Finally, the detection of point defects in other potential capacity hydrogen storage materials such as lithium amide and lithium borohydride anelastic spectroscopy is topic for important future research.

References

Andrei, C.M., J. Walmsley, H.W. Brinks, R. Homestad, C.M. Jensen, B.C. Hauback. 2005. *Appl. Phys. A*., 80:709.

Brinks, HW., C. M. Jensen, S.S. Srinivasan, B.C. Hauback, D. Blanchard, and K. Murphy. 2004. *J. Alloys Compd.,* 376:215.

Belskii, V.K., B.M. Bulychev, A.V. Goulubeva. 1983 *Russ. J. Inorg. Chem.*, 28:1528.

Bogdanovic, B. and M. Schwickardi. 1997. *J. Alloys and Comp*., 1-9:253.

Bogdanovic, B., R.A. Brand, A. Marjanovic, M. Schwickardi, J. Tölle. 2000. *J. Alloys and Comp.*, 302:36.

Fryzuk, M.D., G.K.B. Clentsmith, S. J. Rettig. 1997. *Inorg. Chem. Acta* , 259:51.

Gomes, S., G. Renaudin, H. Hagemann, K. Yvon, M.P. Sulic, and C.M. Jensen. 2005. *J. Alloys Compd.***,** 390:305.

Gupta, M., C. Hagen, W.C. Kaska, R. Flesher, and C.M. Jensen. 1996. *J. Chem. Soc. Chem.Commun*., 2083.

Gupta, M., C. Hagen, W.C. Kaska, R.E. Cramer, C.M. Jensen. 1997. *J. Am. Chem. Soc.*, 119: 840.

Gupta, M., W.C. Kaska, and C.M. Jensen. 1997. *J. Chem. Soc., Chem. Commun*., 461.

Hauback, B., H.W. Brinks, C.M. Jensen, K. Murphy, and A.J. Maeland. 2003 *J. Alloys Compd.* 358:142.

Ichikawa, T., S. Isobe, N. Hanada, H. Fujii. 2004 *J. Alloys and Compds.* 365:271.

Jensen, C.M., R. Zidan, N. Mariels, A. Hee, C. Hagen. 1999. *Int. J. Hydrogen Energy*, 24:461.
Jensen, C.M. 1999. *J. Chem. Soc., Chem. Commun.*, 2443.

Jensen, C.M., K.J. Gross. 2001. *Appl. Phys. A*, 72:213.

Khan, K., C.L. Raston, J.E. McGrady, B.W. Skelton, A.H. White. 1997. *Organometallics*, 16:3252.

Kuba, M.T., S.S. Eaton, C. Morales, C.M. Jensen. 2005. *J. Mater. Res.*, 20:3265.

Liu, F., E.B. Pak, B. Singh, C.M. Jensen, and A.S. Goldman. 1999. *J. Am. Chem. Soc.*, 121:4086.

Palumbo, O., R. Cantelli, A. Paolone, S.S. Srinivasan, C.M. Jensen. 2005. *J. Phys. Chem. B.,* 109:1168.

Vajo, J., S. Skeith, F. Mertins. 2005. *J. Phys. Chem. B*, 109:3719.

Xu, X., G.P. Rosini, M. Gupta, C.M. Jensen, W.C. Kaska, K. Krough-Jespersen, and A.S. Goldman. 1997. *J. Chem. Soc. Chem. Commun.*, 2273.

Zidan, R.A., S. Takara, A.G. Hee, C.M. Jensen, 1999. *J. Alloys and Comp.*, 285:119.

Publications

1. "Development of Catalytically Enhanced Sodium Aluminum Hydride as a Hydrogen Storage Material Craig M. Jensen and Karl J. Gross; *Appl. Phys. A,* **2001**, *72*, 213. (invited contribution for special issue on Hydrogen Storage Technologies).

2. "Catalyzed Alanates for Hydrogen Storage. K.J. Gross, C.M. Jensen and G.J. Thomas; *J. Alloys Compd.* **2002**, *330-332*, 683.

3. "Engineering Considerations in the Use of Catalyzed Sodium Alanates for Hydrogen Storage" G. Sandrock, K. Gross, G. Thomas, C. Jensen, D. Meeker, and S. Takara; *J. Alloys Compd.* **2002**, *330-332*, 696.

4) "Mircrostructural Characterization of Catalyzed $NaAlH_4$." George J. Thomas, Karl J. Gross, N.Y.C. Yang, and Craig M. Jensen *J. Alloys Compd.* **2002**, *330-332*, 702.

5. "X-ray Diffraction Studies of Titanium and Zirconium Doped $NaAlH_4$: Elucidation of Doping Induced Structural Changes and Their Relationship to Enhanced Hydrogen Storage Properties" Dalin Sun, Tetsu Kiyobayashi, Hiroyuki T. Takeshita, Nobuhiro Kuriyama, and Craig M. Jensen; *J. Alloys Compd.* **2002**, *337*, 8.

6. "Neutron diffraction Structure Determination of $NaAlD_4$" B.C. Hauback, H.W. Brinks, C.M. Jensen, K. Murphy, and A.J. Maeland; *J. Alloys Compd.* **2003,** *358*, 142.

7. "Kinetic Study and Determination of the Enthalpies of Activation of Titanium and Zirconium Doped $NaAlH_4$ and Na_3AlH_6" Tetsu Kiyobayashi, Sesha S. Srinivasan, Dalin Sun, and Craig M. Jensen; *J. Phys. Chem. A* **2003**, *107*, 7671.

8. "Rehydrogenaton of Dehydrogenated $NaAlH_4$ at Low Temperature and Pressure" Dalin Sun, Sesha S. Srinivasan, Tetsu Kiyobayashi, Nobuhiro Kuriyama, and Craig M. Jensen; *J. Phys. Chem. B* **2003**, *107*, 10176.

9. "Diffraction Studies of Alanates" H. W. Brinks, B. C. Hauback, D. Blanchard, C. M. Jensen, M. Fichtner, and H. Fjellvåg; *Advanced Materials for Energy Conversion II*, **2004**, 153.

10. "Dehydrogenation Process of Titanium and Zirconium Doped Alanates, T. Kiyobayashi, Akita, S.S. Srinivasan, D. Sun, S. Sangawa, C.M. Jensen and N. Kuriyama; *Advanced Materials for Energy Conversion II*, **2004**, 157.

11. "Synchrotron X-ray and Neutron Diffraction Studies of $NaAlH_4$ Containing Ti Additives" H.W. Brinks, C. M. Jensen, S.S. Srinivasan, B.C. Hauback, D. Blanchard, and K. Murphy; *J. Alloys Compd.***2004**, *376*, 215.

12. "Rehydrogenation and Cycling Studies of Dehydrogenated $NaAlH_4$. Dalin Sun, Sesha S. Srinivasan, Guorong Chen and Craig M. Jensen; *J. Alloys Compd.* **2004**, *373*, 265.

13. "Dehydrogenation of Alkanes Catalyzed by an Iridium-Phosphinito PCP Pincer Complex" David Morales-Morales, Rocío Redón, Cathleen Yung, and Craig M. Jensen; *Inorg. Chim. Acta* **2004** *357*, 2953. (invited contribution for topical volume on Rhodium and Iridium Chemistry).

14. "Long Term Cycling Behavior of Titanium Doped $NaAlH_4$ Prepared through Solvent Mediated Milling of NaH and Al with Titanium Dopant Precursors" Sesha S. Srinivasan,Hendrik W. Brinks, Bjorn C. Hauback, Dalin Sun and Craig M. Jensen; *J. Alloys Compd.***2004** 377, 283.

15. "Structure and Hydrogen Dynamics of Pure and Ti-doped Sodium Alanate" Jorge Iniguez, T. Yildirim, T.J. Udovic, M. Sulic, and C. M. Jensen; *Phys. Rev. B.* **2004** *65,* 235433.

16. "Preparation of Ti-doped Sodium Aluminum Hydride from Mechanical Milling of NaH/Al with Off-the-Shelf Ti Power" P. Wang and C.M. Jensen; *J. Phys. Chem. B.* **2004** *108*, 15829.

17. "Method for Preparing Ti-doped $NaAlH_4$ using Ti powder: Observation of Unusual Reversible Dehydrogenation Behavior" Ping Wang and Craig M. Jensen; *J. Alloys Compd.* **2004** *379*, 99.

18. "Effects of Milling, Doping and Cycling of $NaAlH_4$ Studied by Vibration Spectroscopy and X-ray Diffraction" S. Gomes, G. Renaudin, H. Hagemann, K. Yvon, M.P. Sulic, and C.M. Jensen, *J. Alloys Compd.* **2005** *390*, 305.

19. "Point Defect Dynamics and Evolution of Chemical Reactions in Alanates by Anelastic Spectroscopy" Oriele Palumbo, Rosario Cantelli, Annalisa Paolone, Sesha S. Srinivasan, and Craig M. Jensen; *J. Phys. Chem. B.* **2005,** *109*, 1168.

20. "Electron Microscopy Studies of $NaAlH_4$ Doped with TiF_3: Hydrogen Cycling Effects" C.M. Andrei, J. Walmsley, H.W. Brinks, R. Homestad, C.M. Jensen, B.C. Hauback; *Appl. Phys. A*. **2005**, *80*, 709.

21. "Synthesis and Crystal Structure of Na_2LiAlD_6" H.W. Brinks, B.C. Hauback, C.M. Jensen, and R. Zidan; *J. Alloys Compd.* **2005** *392*, 27.

22. "Motion of Point Defects and Monitoring of Chemical Reactions in Sodium Aluminium Hydride" Oriele Palumbo, Rosario Cantelli, Annalisa Paolone, Craig M. Jensen, and Sesha S. Srinivasan; *J. Alloys Compd.* **2005**, *404-406, 748*.

23. "Characterization of Titanium Dopants in Sodium Alanate by Electron Paramagnetic Resonance Spectroscopy" Meredith T. Kuba, Sandra S. Eaton, Christine Morales, and Craig M. Jensen; *J. Mater. Res.* **2005**, *20*, 3265.

24. "Synchrotron X-ray Studies of $Al_{1-y}Ti_y$ Formation and Re-hydriding Inhibition in Ti-enhanced $NaAlH_4$" Hendrik W. Brinks, Bjørn C. Hauback, Sesha S. Srinivasan, and Craig M. Jensen; *J. Phys. Chem. B.* **2005** *109*, 15780.

Invited Presentations

1) 10/3/00 University of Queensland, Brisbane, Australia.
2) 10/5/00 International Symposium on Hydrogen-Metal Systems. Noosa, Australia.
3) 10/10/00 Australian National University, Canberra, Australia.
4) 10/12/00 University of Sydney, Australia.
5) 10/13/00 University of Auckland , New Zealand.
6) 3/18/01 Japan Steel Company, Muroran Laboratory, Muroran, Japan.
7) 4/17/01 United Technologies Technical Center, East Hartford, Connecticut.
8) 8/24/01 Hiroshima University, Japan.
9) 8/28/01 Osaka University, Toyonaka, Osaka, Japan.
10) 12/17/01 Symposium on the Chemistry and Application of Metal complexes of Mixed-Donor Polydenate Ligands; 2000 International Chemical Congress of the Pacific Basin Societies, Honolulu, Hawaii.
11) 10/25/01 University of Utah.
12) 12/14/01 2nd International Symposium on New Protium Function, Miyazaki, Japan.
13) 2/20/02 Symposium on the Fundamentals of Advanced Materials for Energy Conversion, 2002 meeting of the Minerals, Metals, and Materials Society, Seattle, Washington.
14) 2/24/02 University of Washington.
15) 3/27/02 81st meeting of the Chemical Society of Japan, Tokyo, Japan.
16) 5/13/02 Symposium on Hydrogen Storage Materials and Hydrogen Generators, 201st meeting of the Electrochemical Society, Philadelphia, PA.
17) 8/13/02 Universal Oil Products Research Center,Des Plaines, Illinois.
18) 9/5/02 International Symposium on Metal Hydrogen Systems, Annecy, France.
19) 9/13/02 California Institute of Technology.
20) 3/14/03 Research Association for the Development of Advanced Metal Hydrides Meeting , Osaka, Japan.
21) 6/11/03 European Materials Research Society 2003 Meeting, Symposium on Nanoscale Materials for Energy, Strasbourg, France.
22) 7/11/03 GE Global Research Center, Niskayuna, New York.
23) 7/15/03 Gordon Research Conference on Hydrogen-Metal Systems, Waterville, Maine.
24) 8/17/03 XII International Materials Research Congress, Cancun, Mexico.
25) 8/20/03 International Workshop on the Present Status of Hydrogen Techologies, Mexican Institute of Petroleum, Mexico City, Mexico.
26) 11/13/03 Department of Physics, University of Hawaii at Manoa.

27) 3/2/04 OSTEC Committee on Hydrogen Absorbing Materials, Osaka,Japan.
28) 3/14/04 Symposium on the Fundamentals of Advanced Materials for Energy Conversion II, 2004 meeting of the Minerals, Metals, and Materials Society, Charlotte, North Carolina.
29) 3/22/04 Invited Session on Perspectives on Hydrogen Storage, annual meeting of the American Physical Society, Montreal, Canada.
30) 5/10/04 Symposium on Hydrogen Storage Materials , 205th meeting of the Electrochemical Society, San Antonio, Texas.
31) 7/2/04 Durham University, United Kingdom.
32) 9/4/04 International Symposium on Metal Hydrogen Systems, Crakow, Poland.
33) 9/14//04 Leiden University, The Netherlands.
34) 9/15/04 Utrecht University, The Netherlands.
35) 10/18/04 Symposium on the Hydrogen Economy, meeting of the American Society for Materials , Columbus, Ohio.
36) 11/3/04 Symposium on Hydrogen Absorbing Materials, Fifth Pacific Rim International Conference on Advanced Materials and Processes (PRICM-5), Bejing, China.
37) 11/5/04 Nankai University, Tainjin, China.
38) 11/8/04 Fudan University, Shanghai, China.
39) 11/30/04 Cornell University.
40) 12/1/04 Symposium on Hydrogen Storage, 2004 Materials Research Society fall meeting, Boston, Massachusetts.
41) 1/12/05 Gordon Research Conference on Hydrocarbons, Ventura, California.
42) 1/14/05 Sandia National Laboratory, Livermore, California.
43) 5/31/05 Session on “Crystalline Hydrogen Storage Materials”, American Crystallographic Association , Orlando, Florida.
44) 6/20/05 Hydrogen Storage Technology Conference, International Partnership for the Hydrogen Economy, Lucca, Italy.
45) 8/26/05 Symposium on Hydrogen Storage and Utilization, American Chemical Society, Washington, D.C.

Appl. Phys. A 80, 709–715 (2005)
DOI: 10.1007/s00339-004-3106-z

Applied Physics A
Materials Science & Processing

Rapid communication

C.M. ANDREI[1]
J.C. WALMSLEY[2]
H.W. BRINKS[3]
R. HOLMESTAD[1,✉]
S.S. SRINIVASAN[4]
C.M. JENSEN[4]
B.C. HAUBACK[3]

Electron-microscopy studies of $NaAlH_4$ with TiF_3 additive: hydrogen-cycling effects

[1] Department of Physics, Norwegian University of Science and Technology, 7491 Trondheim, Norway
[2] SINTEF Materials and Chemistry, 7465 Trondheim, Norway
[3] Institute for Energy Technology, P.O. Box 40, 2007 Kjeller, Norway
[4] Department of Chemistry, University of Hawaii, Honolulu, HI 96822, USA

Received: 6 October 2004/Accepted: 22 October 2004
Published online: 25 November 2004 •

ABSTRACT $NaAlH_4$ is a promising candidate material for hydrogen storage. Ti additives are effective in reducing the reaction temperatures and improving kinetics. In this work, the microstructure of $NaAlH_4$ with 2% TiF_3 has been studied in different conditions using a combination of transmission electron microscopy and scanning electron microscopy, both with energy-dispersive spectroscopic X-ray analysis. The effect of the additive on particle and grain size was examined after the initial ball-milling process and after 15 cycles. The additive has an uneven distribution in the sample after ball milling. Selected-area diffraction and high-resolution imaging confirmed the presence of TiF_3. This phase accounts for most of the Ti in the material at this stage and showed limited mixing with the alanate. The grain size within particles for TiF_3 is larger than for the alanate particles. Diffraction from the latter was dominated by metallic aluminium. After cycling, the TiF_3 has decomposed and energy-dispersive spectroscopic X-ray analysis maps showed some combination of Ti with the alanate phase. There is no significant change in the measurable grain size of the Al-containing alanate particles between the ball-milled and the 15-cycled samples, but more cycles result in agglomeration of the material.

PACS 61.14.-x; 68.37.LP; 68.37.Hk

1 Introduction

Complex hydrides of aluminium such as sodium or lithium aluminium hydride ($NaAlH_4$ or $LiAlH_4$) are attractive as hydrogen-storage compounds for automotive use due to their high hydrogen content and low weight. These materials have received wide attention since Bogdanovic and Schwickardi's report in 1997 that Na alanates could be made reversible by the addition of catalysts [1]. The temperature required for rapid dehydriding of $NaAlH_4$ with Ti catalysts was found to be lowered to $\sim 150\,^{\circ}C$ and the conditions required for rehydriding were also reduced to 5 h at 170 °C and 152 bar [1]. As a result, Ti-doped $NaAlH_4$ has been investigated extensively with respect to hydrogen release [1–17] as well as structural phase determination and characterization of the active Ti species [18–25].

The transition metal obviously has an effect on the hydrogen-cycling kinetics but, until now, there has been no clear understanding of the chemical identity and distribution of the Ti. X-ray and neutron-diffraction studies of similar materials to those studied here could not identify Ti-containing phases after the ball-milling process used to mix the compounds [26]. This has been attributed to the small concentration of Ti being located close to the alanate particle surface and hence invisible to X-ray diffraction or to the quasi-amorphous state of the transition-metal element. After cycling, evidence was found for a solid solution $Al_{1-x}Ti_x$ ($x \sim 0.07$). No F-containing phase was identified [26].

A more complete understanding of the nature of the additives, down to the nanometer scale, should play an important role for improving the kinetic and thermodynamic properties of alanates used in hydrogen-storage applications. The number of electron-microscopy studies on alanates has been limited due to the low stability and air sensitivity of these materials. Scanning electron microscopy (SEM) and energy-dispersive X-ray spectroscopy (EDS) have been used to study Ti-doped $NaAlH_4$ after 17 cycles [5] and some work has been done examining the structure of dehydrogenated Ti-doped $NaAlH_4$ using transmission electron microscopy (TEM) combined with EDS [24].

The alanates release hydrogen through a series of decomposition–recombination reactions given by

$$NaAlH_4 \leftrightarrow 1/3Na_3AlH_6 + 2/3Al + H_2, \quad (1)$$

$$1/3Na_3AlH_6 \leftrightarrow NaH + 1/3Al + 1/2H_2, \quad (2)$$

$$NaH \leftrightarrow Na + 1/2H_2. \quad (3)$$

The first two reactions give a theoretical reversible hydrogen-storage capacity of 5.6 wt. %. The third reaction occurs at too high a temperature to be practical for hydrogen-storage applications. $NaAlH_4$ is still considered to be the best candidate for a reversible hydrogen-storage material [7].

Some of the apparent inconsistent studies of Ti-doped $NaAlH_4$ reported earlier appear to be due to the lack of comparison between as-milled samples and those obtained after a few cycles. In

✉ Fax: +47-73-59-77-10, E-mail: randi.holmestad@phys.ntnu.no

this paper, TEM and SEM in conjunction with EDS have been used to examine the microstructure of $NaAlH_4$ containing 2% TiF_3 additive, after the ball-milling process and after 15 cycles. The effect of the additive on particle morphology, grain size and distribution of the phases, particularly with respect to the mixing and the distribution of Ti, has been examined.

2 Experimental

$NaAlH_4$ (Albemarle Corp.) was after recrystallization from THF/pentane, ball milled with 2 mol % TiF_3 (Aldrich Chemicals Inc.) additives in a Fletscher 7 planetary ball mill at 350 rpm for 30 min. The ball to sample mass ratio was approximately 20 : 1. The cycling was carried out by desorption at 160 °C for 3 h and absorption at 120 °C and 110 bar for 12 h.

Electron-microscope samples are prepared by spreading the dry powder on a holey carbon film supported on a copper grid. All handling of the samples was done in Ar atmosphere in a glove box to minimize reaction with moisture and oxygen. Samples are mounted in the TEM sample holder and transferred from the glove box to the TEM using a vacuum transfer container. The sample holder is exchanged into the TEM by means of a removable glove-bag device, which maintains an Ar overpressure during the transfer process. For SEM, a simple sealed transfer container has been developed that allowed the sample to be placed directly into the SEM air-lock entry chamber while still

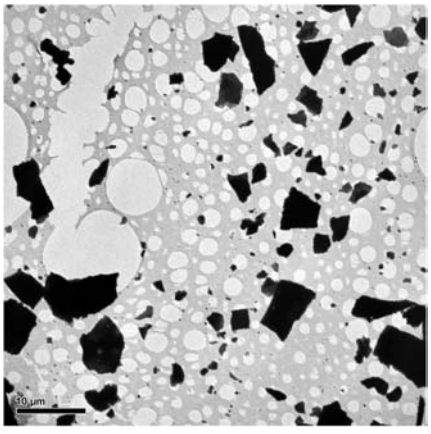

FIGURE 1 Low-magnification TEM bright-field image of $NaAlH_4$ with 2% TiF_3 after initial ball milling

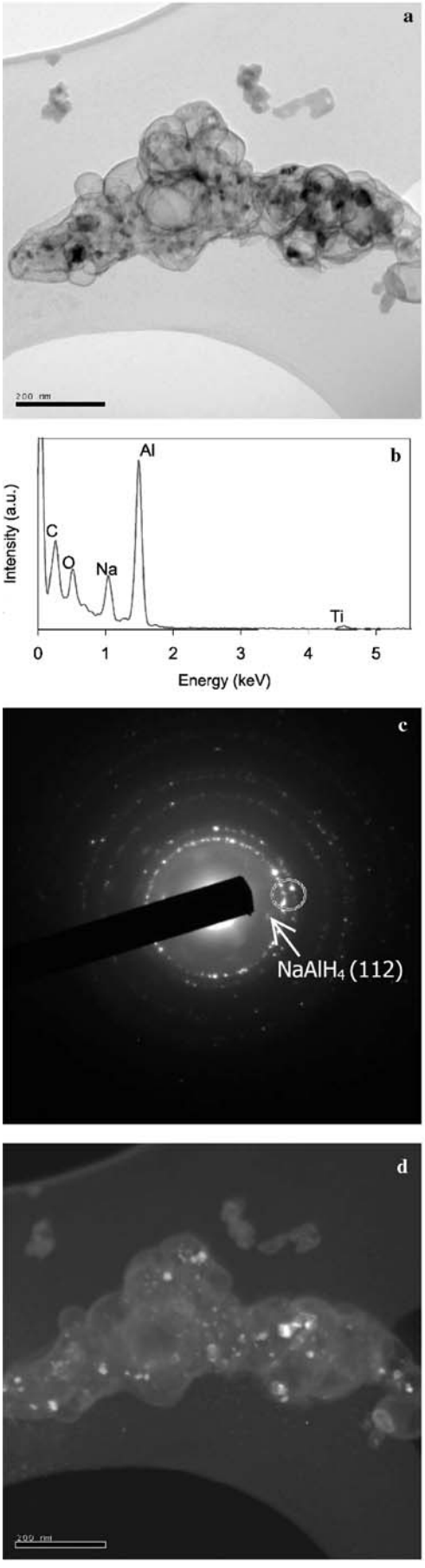

FIGURE 2 TEM bright-field image (**a**), EDS spectrum (**b**), SAD pattern (**c**) and dark-field image (**d**) made from the spots indicated in (**c**) of a Na-, Al-rich particle after the initial ball milling

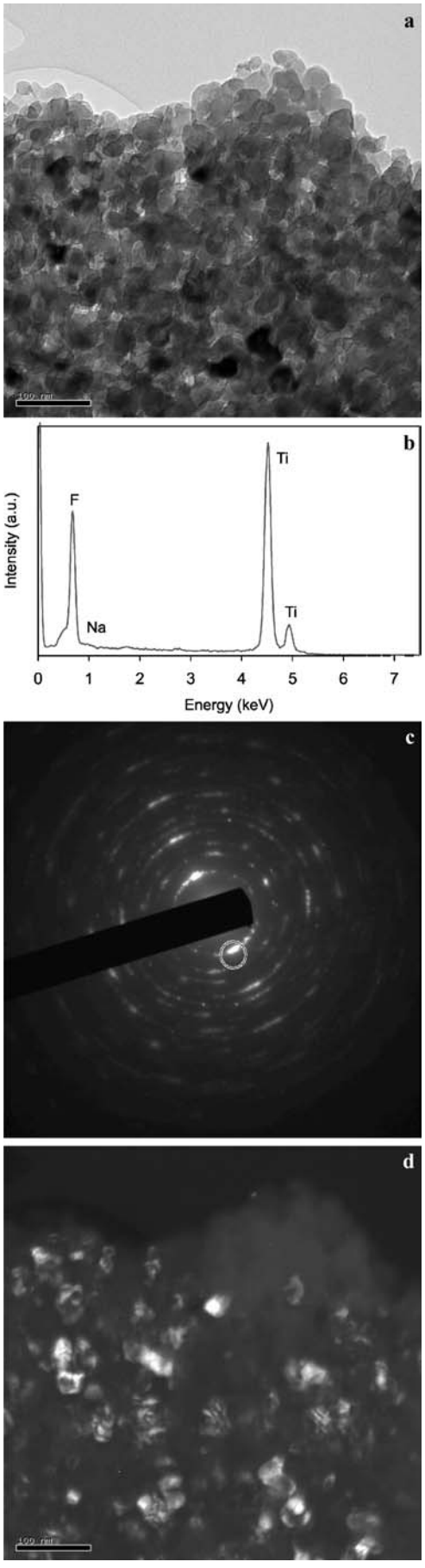

FIGURE 3 TEM bright-field image (**a**), EDS spectrum (**b**), SAD pattern (**c**) and dark-field image (**d**) made from the spots indicated in (**c**) of a Ti-, F-rich particle after the initial ball milling

under an inert Ar atmosphere. Electron-microscopy studies are performed with a Jeol 2010F field-emission-gun (FEG) TEM operated at 200 kV and a Hitachi S-4300SE SEM operated at 10 kV. Both the electron microscopes are equipped with an Oxford Inca EDS system.

3 Results and discussion

3.1 *After ball milling*

Figure 1 shows a TEM bright-field (BF) image of the $NaAlH_4$ sample with 2% TiF_3 directly after the ball-milling process showing the distribution of the particles on the carbon film at a very low magnification. The particles range in size from about 1 to 15 μm. After the ball-milling process, a clear separation of particles containing mostly Ti and F and particles rich in Al, Na and O is observed. A bright-field image of a single particle is shown in Fig. 2a. The EDS data from this particle indicates that Na, Al, O and a small quantity of Ti are present (Fig. 2b). Although samples were not exposed directly to the air, the O signal was present in all the alanate particles. Indexing of the selected-area diffraction (SAD) pattern (Fig. 2c) obtained from the particle showed that Al is the main crystalline phase contributing to the intensity of the pattern, although a few spots from the $NaAlH_4$ phase are also detected. The *d*-spacings measured from the diffraction pattern compared with powder X-ray diffraction (PXD) are listed in Table 1. The results are in qualitative agreement with the PXD data obtained earlier [26]. The presence of some oxygen is expected after ball milling from the identification of levels of Na_2O_2 during the earlier X-ray diffraction analysis. It is also possible that some further reaction of the alanate phase with oxygen occurred because of exposure to low levels of O during the sample-transfer procedures.

d-spacings (Å)	PXD data	Identification	*hkl*
3.150	3.011	$NaAlH_4$	112
2.415	2.337	Al	111
2.068	2.024	Al	200
1.456	1.431	Al	220
1.286	1.220	Al	311

TABLE 1 Index of the *d*-spacings of a Na-, Al-rich particle after the initial ball-milling process

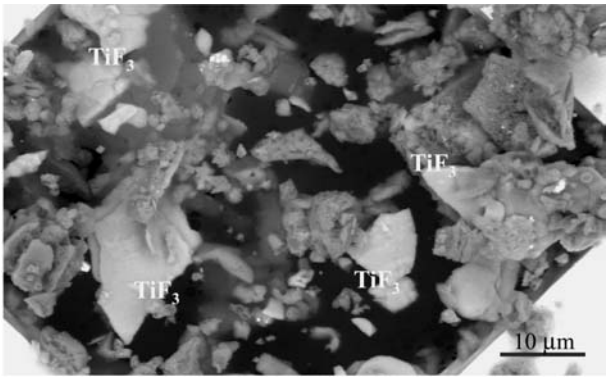

FIGURE 4 Backscattered electron (BSE) SEM image after the initial ball milling showing the particle distribution

Crystallographic studies of the alanate phase were limited. This is due to the weak diffraction signal obtained from the light-element phases and possible sensitivity of the crystal structure to the electron beam.

A dark-field (DF) image made from the indicated sections of rings in the SAD pattern is shown in Fig. 2d. Each grain in the image represents a single crystal of a particular phase that is lying in a favorable orientation to give diffraction intensity in the image. Measuring the size of the grains giving contrast in a number of DF images of the alanate particles gives a typical value of 11 nm. Based on the diffraction pattern, most of the grains visible in the dark-field image are metallic aluminium.

A significant number of particles are found by EDS to contain predominantly Ti and F. These particles have a different morphology than the alanate-phase particles, forming a porous polycrystalline agglomerate as shown in Fig. 3a. The composition is shown by the EDS analysis of Fig. 3b. Al and Na are only present at very low levels in this particle. The *d*-spacings from the diffraction pattern (Fig. 3c) match very well with the TiF_3 phase, as shown in Table 2.

d-spacings (Å)	PXD data	Identification	*hkl*
3.915	3.846	TiF_3	012
2.781	2.741	TiF_3	104
2.379	2.316	TiF_3	113
1.977	1.923	TiF_3	024
1.761	1.731	TiF_3	116
1.595	1.566	TiF_3	214
1.313	1.300	TiF_3	1010

TABLE 2 Index of the *d*-spacings of a Ti-rich particle after the initial ball-milling process

Oxygen is almost absent in the EDS spectrum from the Ti- and F-rich particle. The measured TiF_3 grain sizes within the particles measured from DF images (Fig. 3d) are found to be about 26 nm, significantly higher than in the alanate particles. One can suggest that prior ball milling of the dopant precursor might produce small grains, which are desirable for the improvement of the kinetics.

A SEM image taken with backscattered electrons (BSEs) from the sample after ball milling also indicates variations in the composition (Fig. 4). The brighter particles (higher average atomic number) with a smooth, plate-like, morphology were all found to be rich in Ti and F, while the majority, with rougher, irregular shape, were the Na-, Al- and O-containing alanate particles.

Neither TiF_3 particles nor any other Ti compounds were detected after the ball milling by earlier X-ray studies [26]. We show clearly here by SEM BSE, TEM and EDS analysis that the TiF_3 phase contains most of the Ti that is present in the material after ball milling and that the degree of mixing of TiF_3 with the alanate phase is low. This suggests that the initial influence of the additives is due to a very small proportion of the Ti being incorporated into the alanate phase.

To study the structure of the TiF_3 phase in finer detail, high-resolution TEM (HRTEM) experiments were performed on a Ti-rich particle. Figure 5a shows the atomic structure of a single grain. A measured lattice spacing of $d_{012} = 3.83$ Å corresponds to the TiF_3 (012) plane. The confirmation of the TiF_3 phase in HR mode was done by comparing the experimental images with simulated images based on the known structure. A coherent twin boundary, possibly due to strain, is observed in the detailed structure visible in Fig. 5b.

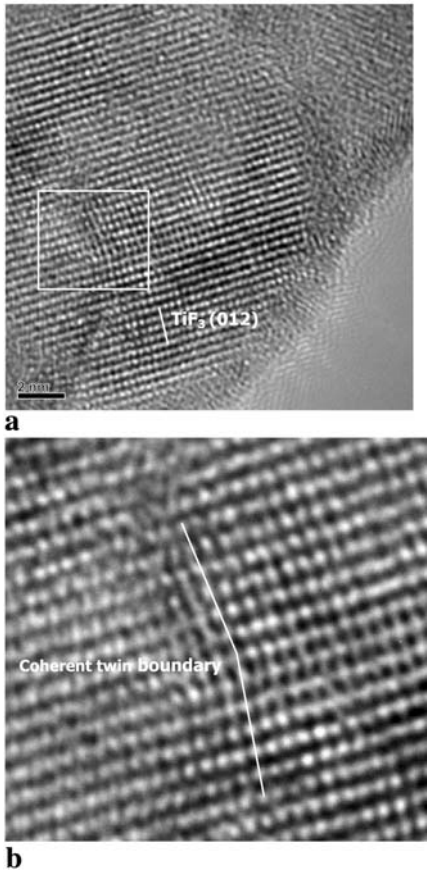

FIGURE 5 **a** High-resolution image of a TiF_3 grain. Indicated lattice planes are indexed as TiF_3 (012). The *rectangle* marked is enlarged in Fig. 5b. **b** HRTEM image showing a coherent twin boundary in the TiF_3 phase

Scanning TEM (STEM) EDS mapping was performed on a Ti-rich particle in order to investigate the correlation between elements and to establish their distribution within individual particles. In Fig. 6 we see a correlation of Ti and F maps, which is consistent with the observation above that the original ball-milling process did not decompose the TiF_3 phase into metallic Ti. Al, along with Na, is concentrated only in the middle of the two-dimensional projected image, suggesting that a small discrete amount of the alanate phase is lying on the surface of the particle or at its center. The O signal is present at a low level everywhere in the particle, but it is strongest where the alanate phase is present, suggesting that some aluminium oxide or sodium oxide has

been formed. Even though the acquisition time for EDS maps was longer than 40 min, the particle was stable under the electron beam over this period of time.

While the EDS measurements suggest that some Ti is incorporated into the alanate phase, it is clear that most of the additive is present as an unmodified, separate TiF_3 phase, which shows a very low degree of mixing with the alanate phase.

A negative correlation between Al and Ti is noticed in a number of EDS maps (not shown here). The concentration of Al is highest where the Ti signal is weakest in the particle. Similar observations are established in Li alanates after the ball-milling process [27].

3.2 *After 15 cycles*

After 15 cycles the sample consists of very large particles ranging in size from 10 to 60 μm as indicated in Fig. 7. Useful information is obtained only from the thin areas at the edge of the particles. A BF image is shown in Fig. 8a. The same area is presented in the DF image (Fig. 8b) made from reflections indicated in the corresponding SAD pattern (Fig. 8c). All the measured reflections correspond to crystalline Al. The grain size for an Al-rich particle is found to be about 13 nm and therefore has not changed significantly upon cycling. There is some indication of clustered particles, which probably are formed by agglomeration of the starting material. This is consistent with the results of Thomas et al. [28].

A BSE SEM image showing the distribution of the particles is presented in Fig. 9a. Particles up to 500 nm, with brighter contrast, showed a Ti EDS signal while Na, Al and O were measured in the remaining, majority of particles. Due to their small size, the EDS signal from the Ti-containing particles was weak; however, close examination suggests that they are distributed over the surface of the alanates as shown in Fig. 9b and that they have a clear spherical or hemi-spherical morphology.

STEM EDS mapping of a single particle at higher spatial resolution is shown in Fig. 10. Na is uniformly distributed in the particles; oxygen is again associated with the alanate phase. Electron energy loss spectra (EELS) confirmed the existence of Al_2O_3 in the material (to be reported elsewhere). There is a lack of O and Na where the Ti is present. The F signal was generally weak in all the particles and absent in the acquired EDS map. The spherical Ti-rich region at the upper left surface of the particle is approximately 150 nm in size and correlates with Ti-rich features observed in the SEM image. Comparison of the Ti and Al EDS maps suggests that some Al is correlated with Ti. This is in contrast to the situation in the material directly following the ball-milling

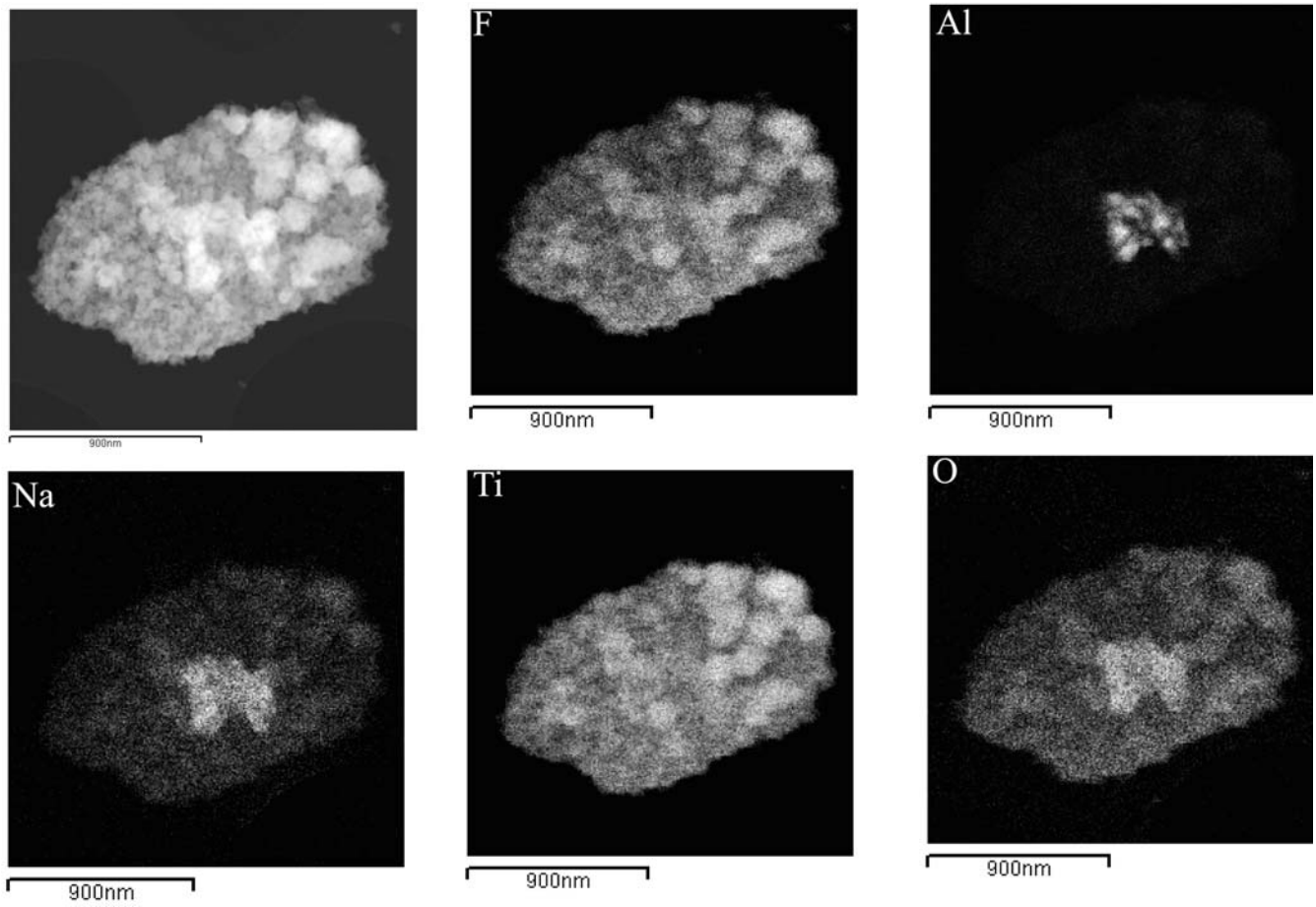

FIGURE 6 EDS maps from a particle after the ball-milling process showing the distribution of the elements. Al and Na are concentrated in the middle of the particle

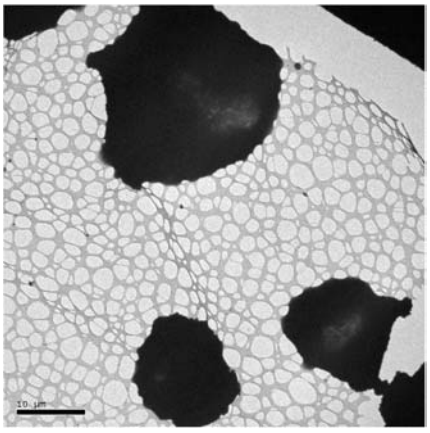

FIGURE 7 Low-magnification TEM bright-field image of $NaAlH_4$ with 2% TiF_3 after 15 cycles

process, where Ti and Al show no correlation.

In this paper, we have studied the differences in the material from freshly ball milled to 15 cycles. From the earlier studies of this material, it is known that the kinetics are unchanged [5, 7]. However, we observe quite big changes in the microstructure of these two conditions. We are therefore led to think that the role of Ti is not associated with any of the large phases (TiF_3 in the freshly ball milled and Ti–Al correlation in the cycled). The speculation could therefore be that the Ti can work directly, either by enhancing H_2 dissociation or by improving the H mobility, which is suggested by simulations [29]. On the other hand, preliminary unpublished diffraction line-shape analysis [30] indicates that Ti may function indirectly, as a grain refiner, keeping the grain size small through the cycling process, modifying the grain boundaries or controlling the surface properties of the alanate. Further experiments are planned to explore these possibilities.

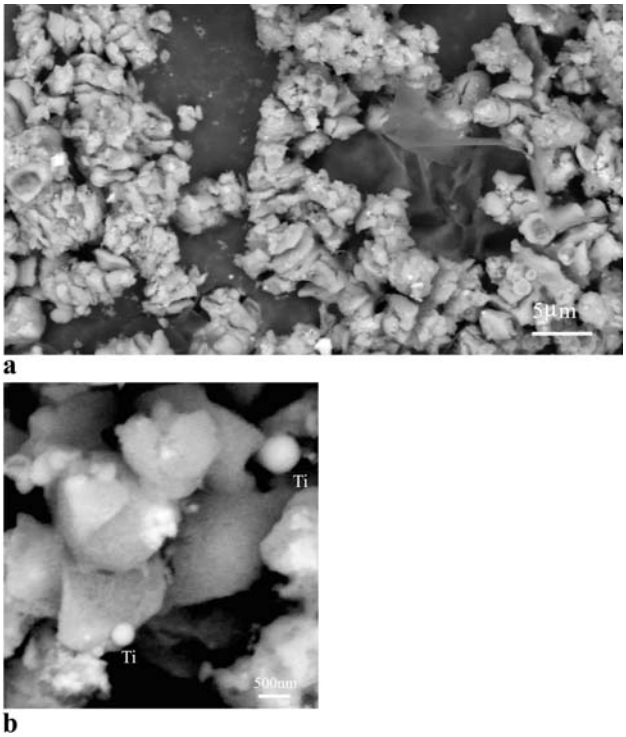

FIGURE 9 **a** Backscattered electron (BSE) SEM image after 15 cycles. **b** Higher-magnification BSE image showing the particle distribution after 15 cycles

4 Conclusions

The microstructure of $NaAlH_4$ with TiF_3 additive has been studied after the initial ball-milling process and after 15 cycles, using a combination of TEM, SEM and EDS. Electron microscopy provides information about the distribution of Ti within the material that has not been accessible by other techniques. After the initial ball-milling process, little mixing between the TiF_3 additive phase and alanate phase was found. TiF_3 particles, which account for most of the Ti, are shown clearly by SEM BSE, TEM and EDS analysis. The EDS maps of alanate-phase particles showed no correlation between the distribution of Al and Ti after the initial ball-milling process. TEM BF and DF images were used to measure the size of the grains and the particles. The measured grain size for TiF_3 was found to be significantly larger in comparison with alanate particles. In the latter, most of the diffraction contrast comes from metallic Al. In the initial state, the influence of Ti is clearly achieved with a very low level of Ti incorporated into the alanate.

There is no significant change in the Al grain size within the alanate particles between the sample after ball milling and after 15 cycles. The particle size has increased possibly by agglomer-

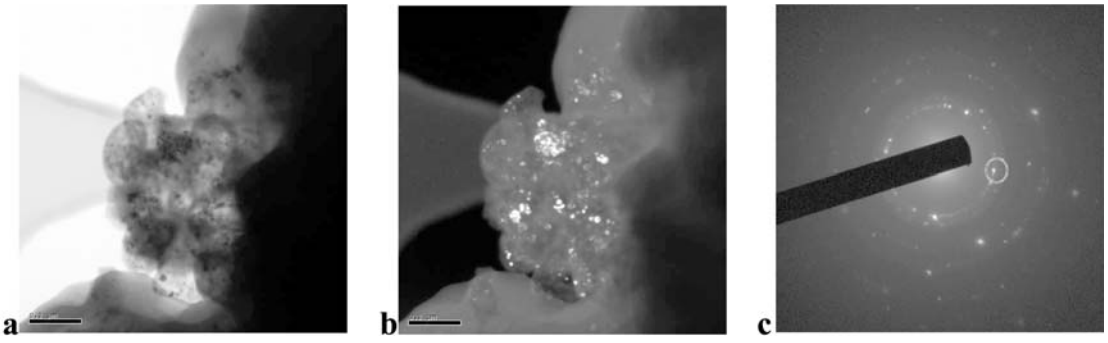

FIGURE 8 TEM bright-field image (**a**), dark-field image (**b**) and SAD pattern (**c**) of a particle after 15 cycles

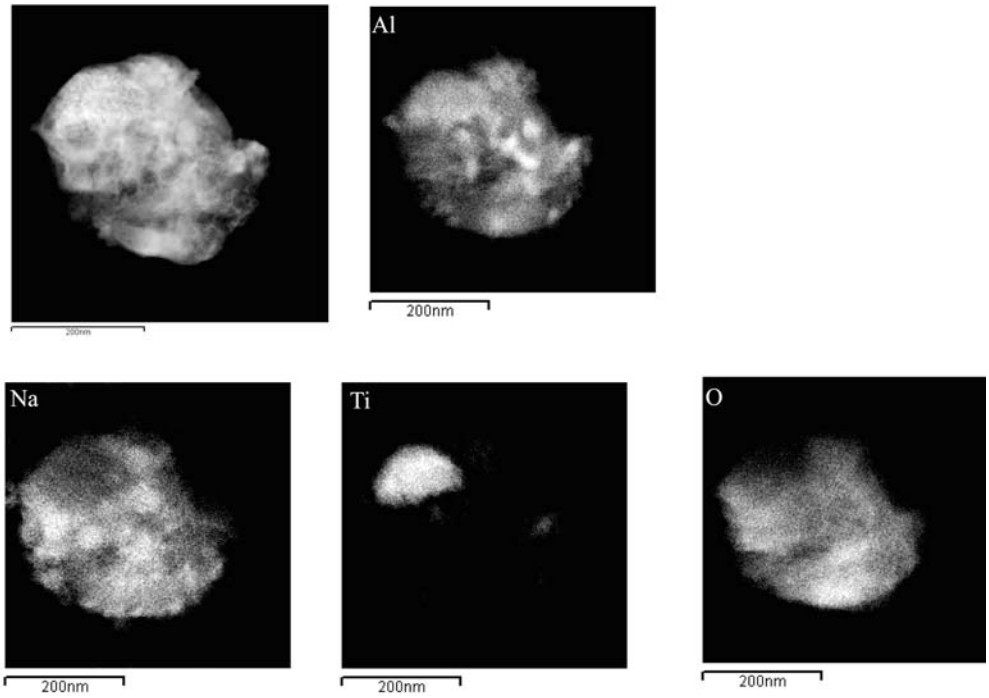

FIGURE 10 EDS maps from a particle after 15 cycles showing the distribution of the elements. A correlation between Al and Ti is seen

ation into large clusters. Evidence of a higher degree of mixing and decomposition of the original TiF_3 phase is observed. The levels of F, measured by EDS, are uniformly low throughout the material. BSE SEM imaging showed that Ti-rich particles are distributed over the alanate phase. More detailed examination evidence, produced by STEM EDS mapping, shows some correlation between Al and Ti.

ACKNOWLEDGEMENTS The Norwegian Research Council is gratefully acknowledged for financial support. CMJ gratefully acknowledges financial support received from the Office of Hydrogen, Fuel Cells, and Infrastructure Technologies of the US Department of Energy. The authors want to thank Calin Marioara for TEM high-resolution expertise and Ole Martin Løvvik for fruitful discussions.

REFERENCES

1 B. Bogdanovic, M. Schwickardi: J. Alloys Compd. **253**, 1 (1997)
2 B. Bogdanovic, M. Schwickardi: International Patent WO97/03919 (1997)
3 C.M. Jensen, R.A. Zidan, N. Mariels, A.G. Hee, C. Hagen: Int. J. Hydrogen Energy **23**, 461 (1999)
4 R.A. Zidan, S. Takara, A.G. Hee, C.M. Jensen: J. Alloys Compd. **285**, 119 (1999)
5 B. Bogdanovic, R.A. Brand, A. Marjanovic, M. Schwickardi, J. Tolle: J. Alloys Compd. **302**, 36 (2000)
6 A. Zaluska, L. Zaluski, J.O. Strom-Olsen: J. Alloys Compd. **298**, 125 (2000)
7 C.M. Jensen, K.J. Gross: Appl. Phys. A **72**, 213 (2001)
8 K.J. Gross, G.J. Thomas, C.M. Jensen: J. Alloys Compd. **330**, 683 (2002)
9 G. Sandrock, K. Gross, G. Thomas, C. Jensen, D. Meeker, S. Takara: J. Alloys Compd. **330**, 696 (2002)
10 G.P. Meisner, G.G. Tibbetts, F.E. Pinkerton, C.H. Olk, M.P. Balogh: J. Alloys Compd. **337**, 254 (2002)
11 G. Sandrock, K. Gross, G. Thomas: J. Alloys Compd. **339**, 299 (2002)
12 D.L. Anton: J. Alloys Compd. **356**, 400 (2003)
13 T. Kiyobayashi, S.S. Srinivasan, D. Sun, C.M. Jensen: J. Phys. Chem. **423**, (2003)
14 E.H. Majzoub, K.J. Gross: J. Alloys Compd. **356**, 363 (2003)
15 K.J. Gross, E.H. Majzoub, S.W. Spangler: J. Alloys Compd. **356**, 423 (2003)
16 P. Wang, C.M. Jensen: J. Alloys Compd. **379**, 99 (2004)
17 S.S. Srinivasan, H.W. Brinks, B.C. Hauback, D. Sun, C.M. Jensen: J. Alloys Compd. **377**, 283 (2004)
18 K.J. Gross, S. Guthrie, S. Takara, G. Thomas: J. Alloys Compd. **297**, 270 (2000)
19 D. Sun, T. Kiyobayashi, H.T. Takeshita, N. Kuriyama, C.M. Jensen: J. Alloys Compd. **337**, L8 (2002)
20 B.C. Hauback, H.W. Brinks, C.M. Jensen, K. Murphy, A.J. Maeland: J. Alloys Compd. **358**, 142 (2003)
21 M.P. Balogh, G.G. Tibbetts, F.E. Pinkerton, G.P. Meisner, C.H. Olk: J. Alloys Compd. **350**, 136 (2003)
22 B. Bogdanovic, M. Felderhoff, M. Germann, M. Hartel, A. Pommerin, F. Schuth, C. Weidenthaler, B. Zibrowius: J. Alloys Compd. **350**, 246 (2003)
23 D. Sun, S.S. Srinivasan, T. Kiyobayashi, N. Kuriyama, C.M. Jensen: J. Phys. Chem. B **107**, 10 176 (2003)
24 M. Felderhoff, K. Klementiev, W. Grunert, B. Spliethoff, B. Tesche, J.M. Bellosta von Colbe, B. Bogdanovic, M. Hartel, A. Pommerin, F. Schuth, C. Weidenthaler: Phys. Chem. **6**, 4369 (2004)
25 J. Iniguez, T. Yildirim, T.J. Udovic, M. Sulic, C.M. Jensen: Phys. Rev. B **70**, 60 101 (2004)
26 H.W. Brinks, C.M. Jensen, S.S. Srinivasan, B.C. Hauback, D. Blanchard, K. Murphy: J. Alloys Compd. **376**, 215 (2004)
27 C.M. Andrei, J. Walmsley, H.W. Brinks, R. Holmestad, B.C. Hauback, G.A. Botton: submitted to J. Phys. Chem. B
28 G.J. Thomas, K.J. Gross, N.Y.C. Yang, C. Jensen: J. Alloys Compd. **330**, 702 (2002)
29 O.M. Løvvik, S. Opalka: submitted to Phys. Rev. B
30 M. Pitt: personal communications

Synchrotron X-ray Studies of $Al_{1-y}Ti_y$ Formation and Re-hydriding Inhibition in Ti-Enhanced $NaAlH_4$

Hendrik W. Brinks,*,† Bjørn C. Hauback,† Sesha S. Srinivasan,‡ and Craig M. Jensen‡

Institute for Energy Technology, P. O. Box 40, Kjeller, NO-2027 Norway, and Department of Chemistry, University of Hawaii, Honolulu, Hawaii 96822

Received: March 1, 2005; In Final Form: May 9, 2005

$NaAlH_4$ samples with Ti additives ($TiCl_3$, TiF_3, and $Ti(OBu)_4$) have been investigated by synchrotron X-ray diffraction in order to unveil the nature of Ti. No crystalline Ti-containing phases were observed after ball milling of $NaAlH_4$ with the additives, neither as a solid solution in $NaAlH_4$ nor as secondary phases. However, after cycling, a high-angle shoulder of Al is observed in the same position with 10% $TiCl_3$ as that with 2% $Ti(OBu)_4$, but with considerably higher intensity−indicating that the shoulder is caused by Ti. After prolonged reabsorption, there is only a small fraction of free Al phase left to react with Na_3AlH_6, whereas the shoulder caused by $Al_{1-y}Ti_y$ is dominating. The Ti-containing phase causing the shoulder therefore contains less Ti than Al_3Ti, and the aluminum in this phase is too strongly bound to react with Na_3AlH_6 to form $NaAlH_4$. The composition of the $Al_{1-y}Ti_y$ phase is estimated from quantitative phase analysis of powder X-ray diffraction data to be $Al_{0.85}Ti_{0.15}$. Formation of this phase may explain the reduction of capacity beyond the theoretical reduction from the dead weight of the additive and the reaction between the additive and $NaAlH_4$.

1. Introduction

The development of lightweight, high reversible capacity hydrogen storage materials is of central importance to the actualization of practical hydrogen-powered vehicles. In 1997, Bogdanovic and Schwickardi[1] reported that the elimination of hydrogen from solid $NaAlH_4$ is markedly accelerated and rendered reversible under moderate conditions upon mixing the hydride with a few mole percent of selected transition metal complexes. Since that time, aluminum-based complex hydrides, "alanates", have been regarded as a highly promising group of materials for onboard hydrogen-storage applications. Hydrogen cycling capacities of 3−4 wt % have been achieved for Ti-doped $NaAlH_4$ at 120−160 °C with relatively good kinetics.[2−5]

$NaAlH_4$ decomposes according to the three sequential steps seen in eqs 1−3. The first two reactions, releasing in total 5.6 wt % hydrogen, are regarded as useable for reversible hydrogen storage at moderately low temperatures. Two-thirds of this hydrogen is released in the first reaction.

$$NaAlH_4 = {}^1/_3Na_3AlH_6 + {}^2/_3Al + H_2 \quad (1)$$

$${}^1/_3Na_3AlH_6 = NaH + {}^1/_3Al + {}^1/_2H_2 \quad (2)$$

$$NaH = Na + {}^1/_2H_2 \quad (3)$$

Ti can be introduced into the hydride either by mixing $NaAlH_4$ with the Ti-based additive (often titanium halides) in a dispersion[1] or by ball milling.[6] Samples prepared in these ways have been studied, and partial results on the state of Ti have been achieved. For the former technique, hydrogen evolution during the reaction was determined in accordance with reduction of $Ti^{III/IV}$ to Ti^0 without changing the valence of Al.[7] ^{57}Fe Mössbauer spectroscopy investigations confirm formation of bcc Fe from addition of both $Ti(OBu)_4$ and $Fe(OEt)_2$ to $NaAlH_4$ and suggest formation of an Fe−Al alloy during dehydrogenation.[7]

For samples prepared by ball milling, recent X-ray absorption studies indicate Ti^0, at least after cycling of $NaAlH_4$ with Ti additives.[8−10] Thorough powder X-ray diffraction (PXD) studies of fresh and cycled $NaAlH_4$ samples with different additives do not indicate any significant bulk solid solution of Ti in Na or Al sites from precise determination of the unit-cell dimensions.[11,12] Neutron diffraction data, with intensities strongly dependent on an eventual solid solution of Ti in $NaAlD_4$, are in line with that.[11] No crystalline Ti-containing phases were detected in samples that were ball-milled but not cycled.[11,12] However, after cycling at least part of the Ti is forming a phase with Al after cycling with a lower Ti-content than Al_3Ti.[11] The content of this Ti−Al phase has been reported to increase with increasing Ti additive.[13] Similar observations were made in studies of the synthesis of $TiAl_3$ from a suspension of $TiCl_3$ and $LiAlH_4$ in mesitylene heated to 550 °C.[14] In this study, Al was detected by PXD in the precipitate before heating, but neither Ti nor any Ti−Al alloy were detected at this point. The main part of the Ti compounds added to $NaAlH_4$ is probably reduced to Ti^0 in the ball-milling process and forms an Al-rich Ti−Al alloy after the heat treatment during cycling. The fact that Ti−Al alloys can be prepared by ball milling of the elements[15−21] supports this hypothesis. However, still the mechanism of the enhancement of the kinetics is not revealed.

To further unveil the nature of the titanium species that arises from ball milling $NaAlH_4$ with titanium additives and perhaps hence extend the knowledge of the mechanism of the action of the additives, cycled samples with $TiCl_3$, TiF_3, and $Ti(OBu)_4$ additives were analyzed in detail by synchrotron radiation PXD (SR-PXD).

* To whom correspondence should be addressed. Telephone: +47 63 80 64 99. Fax: +47 63 81 09 20. E-mail: hwbrinks@ife.no.
† Institute for Energy Technology.
‡ University of Hawaii.

10.1021/jp051031p CCC: $30.25
Published on Web 00/00/0000 PAGE EST: 6.2

TABLE 1: Mole Fractions (%) of the Phases Based on Rietveld Refinements

sample no.	additive	no.of cycles	% $NaAlH_4$	% Na_3AlH_6	% $Al/Al_{1-y}Ti_y$	% NaCl
1	10% $TiCl_3$	0	58.9		22.4	18.7
2	10% $TiCl_3$	3	14.4	14.2	46.8	24.5
3[a]	10% TiF_3	0	59.0	4.4	36.6	
4	2% $Ti(OBu)_4$	101	71.9	5.9	19.8	2.0

[a] NaF was not observed.

TABLE 2: Unit-Cell Dimensions Determined by Rietveld Refinements of Synchrotron Radiation PXD Data of the Ti-Enhanced $NaAlH_4$ Samples

	$NaAlH_4$		Na_3AlH_6	Al	$Al_{1-y}Ti_y$
sample no.	*a* (Å)	*c* (Å)	*V* (Å^3)	*a* (Å)	*a* (Å)
1	5.0237(1)	11.3507(2)		4.0489(1)	
2	5.0234(1)	11.3514(2)	232.34(1)	4.0493(1)	4.0368(1)
3	5.0235(1)	11.3500(2)	232.50(2)	4.0493(1)	
4	5.0237(1)	11.3503(1)	232.39(1)	4.0490(-)	4.0344(4)

[a] Estimated standard deviations are given in parentheses. For comparison, the values for the pure phases determined at the same instrument are as follows: $a = 5.0232(1)$ Å and $c = 11.3483(1)$ Å for $NaAlH_4$, $V = 232.50(2)$ Å for Na_3AlH_6, and $a = 4.0490$ Å for Al.[3]

2. Experimental Section

All reactions and operations were performed under argon in a glovebox or using standard Schlenk techniques with oxygen and water free solvents. $NaAlH_4$ was purchased from Albemarle Corp. and recrystallized with THF/pentane before use. $TiCl_3$ and TiF_3 were purchased from Aldrich Chemicals Inc. and used without further purification. $TiCl_3$ and TiF_3 were added to $NaAlH_4$ by ball milling 30 and 60 min, respectively, in a Fritsch pulverizette 7 at 350 rpm. The ball to sample mass ratio was approximately 20:1.

The cycled samples with $TiCl_3$ were dehydrided at 160 °C against 1 bar pressure for 3 h and hydrided at 115 bar at 120 °C for 12 h. The $NaAlH_4$ with $Ti(OBu)_4$ additive was cycled 100 cycles with the same conditions (same sample as in ref 3), and the last rehydrogenation (cycle 101) was carried out at 85 bar and 120 °C for 65 h.

SR-PXD data at 22 °C were collected at the Swiss−Norwegian beam line (station BM1B) at the European Synchrotron Radiation Facility (ESRF) in Grenoble, France. The samples were kept in rotating 0.5 mm boron-silica-glass capillaries. Intensities were measured in steps of $\Delta(2\theta) = 0.004$ and 0.005°. The wavelength of 0.49956 Å was obtained from a channel-cut Si(111) monochromator.

Rietveld refinements were carried out using the program Fullprof (version 2.80).[22] X-ray form factors were taken from the Fullprof library. Thompson−Cox−Hastings pseudo-Voigt profile functions were used, and backgrounds were modeled by interpolation between manually chosen points. Information of the microstructure was obtained from isotropic broadening effects included in the Rietveld refinements. The instrumental resolution was determined with a LaB_6 standard.

3. Results

The samples that were analyzed by SR-PXD were $NaAlH_4$ with 10 mol % $TiCl_3$, uncycled (sample 1) and after 3 cycles (sample 2), and 10 mol % TiF_3 uncycled (sample 3) and 2 mol % $Ti(OBu)_4$ (sample 4) after 101 cycles. The mole fractions of each phase present in the samples and selected unit-cell dimensions from the Rietveld refinements are shown in Tables 1 and 2, respectively.

The unit-cell dimensions of the samples do not deviate from the pure samples of $NaAlH_4$ and Na_3AlH_6. This is in line with earlier observations[11] and indicates that there is no significant solid solution of Ti in the alanate. In addition, no Ti-containing phases were observed in the uncycled samples. Hence, no conclusions can be drawn from SR-PXD on the state of Ti directly after ball milling. The fit of the Rietveld refinement of the uncycled sample 1 is shown in Figure 1.

The addition of $TiCl_3$ results in formation of crystalline Al and NaCl. The SR-PXD reflections from NaCl are very broad after ball milling, but after cycling they are significantly sharper; cf. Figure 2. On the basis of microstructural analysis of the SR-PXD data, the broadening was found to originate both from strain and small crystallite size. The crystallite size was estimated to increase from 11 nm after ball milling until 270 nm after 3 cycles. Hence, the heat treatment in the cycling process results in a considerable increased crystallite size for NaCl. Al is formed in the same reaction, but the reflections are much sharper and the change in half-width of the reflections during cycling is less pronounced. The crystallite sizes of Al and $NaAlH_4$ were estimated to 56 and 170 nm after ball milling, and the sizes increase during cycling. More details on the microstructure of Ti-enhanced $NaAlH_4$ will be given in a forthcoming paper.

The reaction can be assumed to be

$$NaAlH_4 + 0.1TiCl_3 = 0.7NaAlH_4 + 0.3NaCl + 0.3Al + 0.1\text{“Ti”}_{(am)} + 0.6H_{2(g)} \quad (4)$$

After normalization, the expected mole percent of the crystalline phases for this reaction is 53.8% $NaAlH_4$, 23.1% NaCl, and 23.1% Al. The refined values based on the SR-PXD data for sample 1 are 58.9, 18.7, and 22.4%, respectively. This indicates that eq 4 is a good approximation of the reaction when $NaAlH_4$ is ball-milled with 10% $TiCl_3$.

For the TiF_3-enhanced $NaAlH_4$ (sample 3), crystalline NaF is not formed as expected by analogy to eq 4. This was earlier observed for 6% TiF_3,[11] and even 10% is not enough to observe any NaF. The reason for this may be that the crystallite size is even smaller than for NaCl and it becomes below the detection limit of SR-PXD. The background is slightly elevated around the expected positions for the NaF reflections. Furthermore, preliminary in-situ SR-PXD experiments indicate that NaF is formed upon heating in a vacuum and that the reflections gradually sharpen by heating.

Small amounts of Na_3AlH_6 were observed after ball milling with TiF_3 (sample 3). By assuming the reaction

$$NaAlH_4 + 0.1TiF_3 = 0.7NaAlH_4 + 0.3Al + 0.3\text{“NaF”}_{(am)} + 0.1\text{“Ti”}_{(am)} + 0.6\,H_{2(g)} \quad (5)$$

and furthermore allowing partial thermal decomposition during ball milling according to eq 1, the amounts of the resulting phases can be estimated. Rietveld refinements of the SR-PXD data gave 4.4 mol % Na_3AlH_6. From eqs 5 and 1 this corresponds to 56.8 and 38.8 mol % of $NaAlH_4$ and Al, respectively. This fits very well with the observed values of

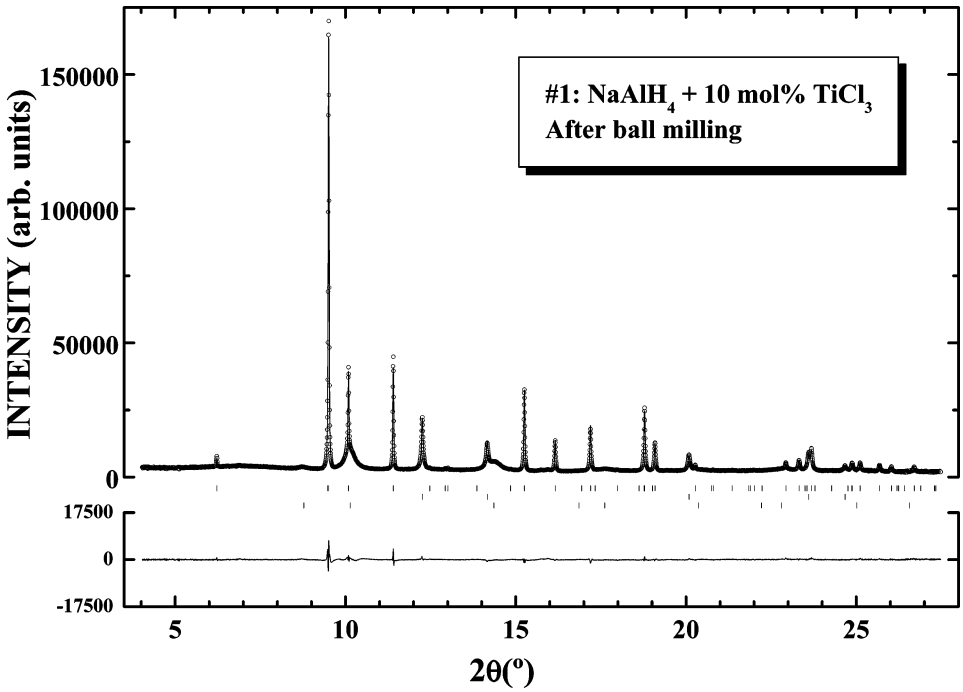

Figure 1. Observed intensities (circles) and calculated intensities from Rietveld refinements (upper line) of $NaAlH_4$ with 10 mol % $TiCl_3$ added ball milling, measured at 22 °C at BM1B, ESRF. Positions of Bragg reflections are shown with bars for $NaAlH_4$, Al, and NaCl (from top). The difference between observed and calculated intensity are shown with the bottom line.

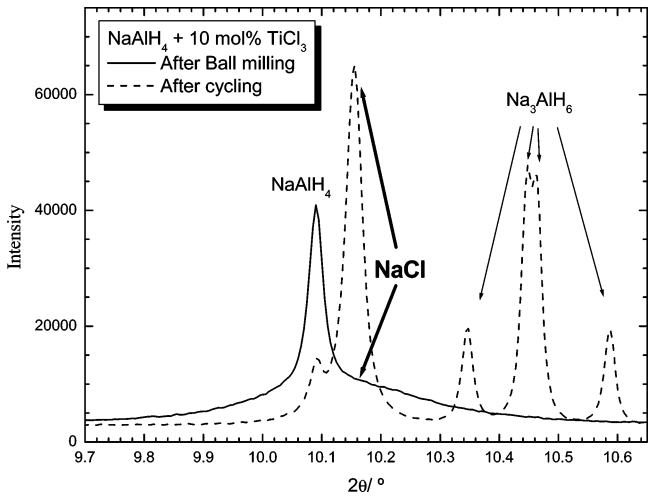

Figure 2. Comparison of the peak shape of NaCl in $NaAlH_4$ with 10 mol % $TiCl_3$ after ball milling and after cycling.

59.0 ($NaAlH_4$) and 36.6 mol % (Al). Hence, the "crystalline part" of eq 5 is confirmed, and the consumption of TiF_3 is fairly complete.

Quantitative phase analysis of the cycled sample of $NaAlH_4$ with 10 mol % $TiCl_3$ (sample 2), which was rehydrided in the final cycle, indicates equal amounts of $NaAlH_4$ and Na_3AlH_6; cf. Table 1. On the basis of eqs 4 and 1, the phase fractions can be estimated to be 13.5 ($NaAlH_4$), 13.5 (Na_3AlH_6), 50.0 (Al), and 23.0% (NaCl). These are close to the observed values: 14.4, 14.2, 46.8, and 24.5%, respectively. After cycling, including rehydrogenation, only 14.4% $NaAlH_4$ is formed compared to the theoretical capacity of 53.9% (eq 4). This means that, even after correction for NaCl and Al formed during ball milling, the rehydrogenation is only 27% of the theoretical capacity of the first step for $NaAlH_4/Na_3AlH_6$ (eq 1), whereas the rehydrogenation of the second step (eq 2; Na_3AlH_6/NaH) is complete, because no NaH is observed. This interesting observation demands further investigation.

There is certainly enough Na_3AlH_6 available for reaction with Al. Generally, long diffusion paths, e.g. through a $NaAlH_4$ product layer, may reduce the effective capacity. However, a closer look at the Al reflections reveals that this is not the main reason in this case; cf. Figure 3. All Al reflections are split in two—a low-intensity reflection at low angles and a reflection with a significantly higher intensity at higher angles. In the earlier study with only 2 mol % $Ti(OBu)_4$, there was a shoulder at the high-angle side that was interpreted as $Al_{1-y}Ti_y$. On the basis of the unit-cell volume, y was estimated to 0.07.[11]

The low-angle reflections at 12.27 and 14.17° are in line with pure Al (a = 4.0490 Å). Only a small amount of pure Al is left in sample 2. If the unlikely options of amorphous or evaporated aluminum are rejected, the only reasonable possibility left is that most of the Al is chemically bonded in the phase which gives reflections at the high angle side of pure Al. Unless there is an oxygen impurity, a reaction with Ti is most likely. The extra peaks are also observed with two different additives and with increasing intensities with an increasing amount of additive.

This phase has a slightly lower unit-cell dimension than Al (4.0368 compared to 4.0490 Å) and has the same relative intensities as fcc Al. Al with small substitutions of Ti results in a smaller unit-cell dimension,[23] and the unit-cell dimensions of both the stable $D0_{22}$ and the metastable $L1_2$ modification of Al_3Ti are smaller.[18] These are indications of an Al-rich Al—Ti intermetallic phase in this case. The unit-cell volume per atom increases at the Ti-rich side of Al_3Ti to a higher value than pure Al,[18] but if the present phase had a lower Al content than Al_3Ti, then there would have been free Al both from the ball-milling reaction (eq 4) and from the fraction of Al after eq 4 which still has not reacted with Na_3AlH_6. This is not observed. Hence, the data from a sample with high additive level proves unequivocally that an $Al_{1-y}Ti_y$ phase with $y < {}^1/_4$ is formed. If no Ti—Al phase were formed at all, an excess of Al should be

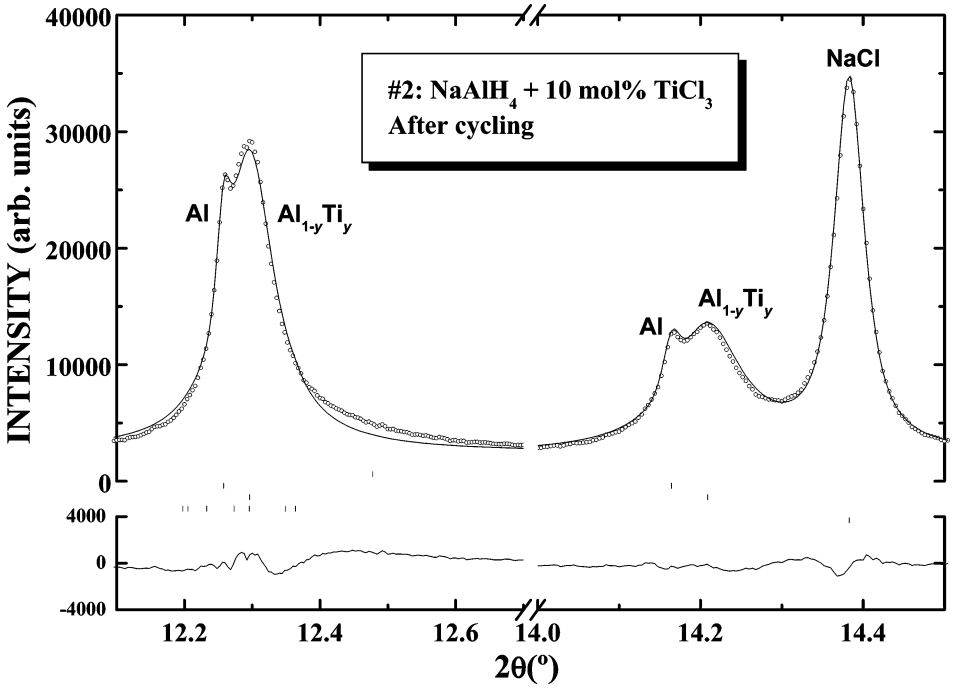

Figure 3. Observed intensities (circles) and calculated intensities from Rietveld refinements (upper line) of $NaAlH_4$ with 10 mol % $TiCl_3$ after 3 cycles, measured at 22 °C at BM1B, ESRF. Positions of Bragg reflections are shown with bars for $NaAlH_4$, Al, $Al_{1-y}Ti_y$, Na_3AlH_6, and NaCl (from top). The differences between observed and calculated intensities are shown with the bottom line.

present at this additive level and probably a predominant amount of Na_3AlH_6 would react.

There is no stable phase between Al and Al_3Ti according to the phase diagram,[18] and reports on fast quenching from melt results in phase separation into Al_3Ti and $Al_{0.998}Ti_{0.002}$.[23] On the other hand, there are several reports on attempts on mechanical alloying in this composition range. A continuous change in the unit-cell dimension of the Al-richer phase with milling time from Al to approximately the unit-cell dimension of Al_3Ti has been reported.[15] Furthermore, disappearing of Ti-reflections by PXD after ball milling has been reported.[20,21] On the basis of the quantitative phase analysis above, there is probably not much of the Al that reacts with Ti during ball milling even though the phases are formed in the same reaction (eq 4) and should be in close proximity in the sample. This could be due to relatively short ball-milling times used for reversible hydrogen storage in alanates compared to studies on mechanical alloying of Al−Ti intermetallics. But after a few cycles, probably because of the elevated temperature, at least a partial reaction takes place.

Apparently, the $Al_{1-y}Ti_y$ phase is so stable that Al is trapped and will not react with Na_3AlH_6. This will reduce the reversible storage capacity beyond the reduction in capacity from the dead weight from the additive and the reaction of the additive with $NaAlH_4$ during ball milling. The total reaction of the initial ball milling reaction and the formation of $Al_{1-y}Ti_y$ with $y < {}^1/_4$ during cycling could be formulated like

$$NaAlH_4 + xTiCl_3 = (1 - kx)NaAlH_4 + 3xNaCl + (x/y)Al_{1-y}Ti_y + lxNa_3AlH_6 + (2k - 3l)xH_2 \quad (6)$$

with

$$k = (3 - 6y)/2y \quad \text{and} \quad l = (1 - y)/2y - {}^3/_2$$

This equation is based on a complete consumption of all Ti in order to form a homogeneous $Al_{1-y}Ti_y$ phase. The excess Al

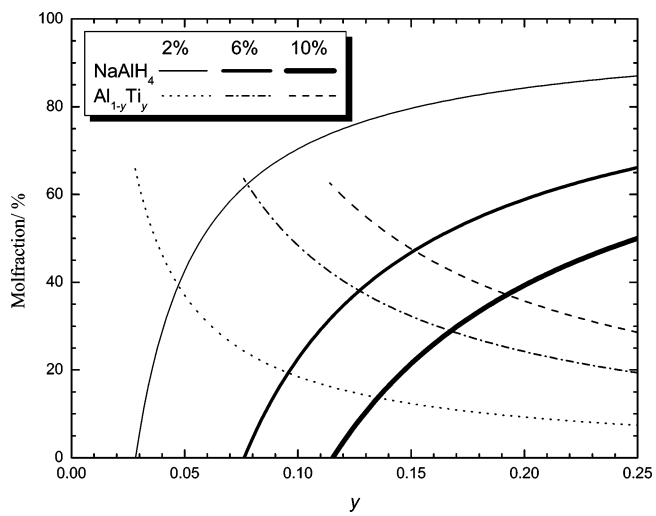

Figure 4. Mole fractions of $NaAlH_4$ and $Al_{1-y}Ti_y$ based on eq 4 for different amounts of $TiCl_3$ additive.

(compared to $y = 0.25$) is taken from $NaAlH_4$, and the amount of Na_3AlH_6, with Na:Al = 3:1, is balanced to give the same amounts of Al and Ti on both sides of the equation.

A more Al-rich phase (lower y) leads to less regenerated $NaAlH_4$, as shown for 2, 6, and 10% additive level in Figure 4, and reduced capacity on the first stage of $NaAlH_4$. These curves may be used to estimate y based on the phase composition. The estimated y value is then used in the Rietveld refinements to generate new and more accurate phase compositions. By this recursive procedure a value for y is obtained. Similarly, the reduced capacities during cycling in Sieverts-type apparatus may also be used to estimate y−on the assumptions that all free Al is reacted with Na_3AlH_6 and that Na_3AlH_6 is completely dehydrided in the experimental conditions chosen for the cycling. However, reduced capacity due to reasons other than $Al_{1-y}Ti_y$ formation will lead to an underestimation of y.

The present data were used for the estimation of y. After corrections for assumed complete reaction of free Al (5.5 mol

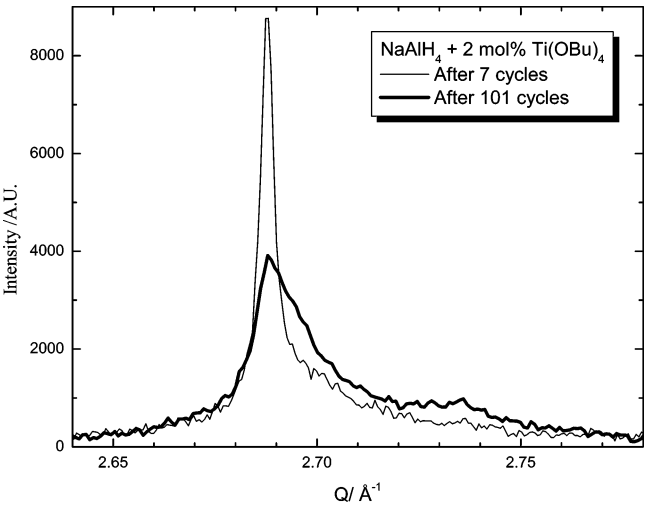

Figure 5. SR-PXD data around the strongest Al reflection for a reabsorbed sample after 7 and 101 cycles, showing that there is less free Al (left reflection) after 101 than after 7 cycles.

%) with Na_3AlH_6 (reversed eq 1), the remaining phase composition (to be compared to eq 6) is 22.7% $NaAlH_4$, 11.5% Na_3AlH_6, and 41.3% $Al_{1-y}Ti_y$, and the remaining is NaCl. From Figure 4, the mole fractions of $NaAlH_4$ and $Al_{1-y}Ti_y$ were used separately to estimate y values of 0.153 and 0.173. A similar curve for Na_3AlH_6 gave a y value of 0.138. The quantitative phase analysis points to the existence of $Al_{0.85}Ti_{0.15}$ in the cycled $NaAlH_4$ sample with 10% $TiCl_3$ additives. The unit-cell dimension of this Al "shoulder" is the same as that for the cycled $NaAlH_4$ sample with 2% $Ti(OBu)_4$,[11] and the composition is probably similar. The present quantitative phase analysis, based on SR-PXD, give a more accurate composition estimate than the rough estimation from linear unit-cell volume intrapolation between Al and Al_3Ti with the $L1_2$ structure−in particular for samples with high amounts of additive. The asymmetric profile of the first $Al_{1-y}Ti_y$ reflection in Figure 3 may indicate that the composition of this phase is not completely homogeneous throughout the sample.

$NaAlH_4$ with 2 mol % $Ti(OBu)_4$ (sample 4) was in the 101th cycle re-hydrogenated at 120 °C and 86 bar pressure in a Sieverts-type apparatus with excellent temperature stability for 65 h. Of the final absorption 84 and 92% are completed during the first 12 and 20 h, respectively.

The quantitative phase analysis of this sample resulted in 71.9 mol % $NaAlH_4$, 5.9 mol % Na_3AlH_6, and 19.8 mol % Al (15.1 mol % present as $Al_{1-y}Ti_y$). In addition the sample included 2 mol % NaCl impurity. By assuming that the additive destroys 8 mol % $NaAlH_4$ and forms crystalline Al and amorphous phases such as NaOBu and Ti, the phase fractions can from eq 1 be estimated to 74.3, 5.9, and 19.8 mol %, respectively. This corresponds to 81% complete re-hydrogenation in step 1 of $NaAlH_4$.

Compared to the SR-PXD data after 7 cycles for the same sample,[11] the peak widths of $NaAlH_4$ and Na_3AlH_6 for the sample after 101 cycles are similar. However, the Al peaks differ. In Figure 5, SR-PXD data around the strongest Al peak of the 7 and 101 cycle samples are compared after background subtraction and normalizing to the strongest peak from $NaAlH_4$. Because of the slightly different wavelengths of the experiments, the data are presented on the Q-scale ($2\pi/d$). After 101 cycles the content of free Al is clearly less than after 7 cycles, probably because of the extended re-hydrogenation time. This brings about better opportunities to examine the shoulder. There appear to be two shoulders: at $a = 4.038$ Å ($Q = 2.695$ Å^{-1}) and at $a = 4.018$ Å ($Q = 2.709$ Å^{-1}). Similar double shoulders are also observed at the high-angle side of the second strongest Al reflection. Both shoulders were included in the refinements for estimation of the fraction of $Al/Al_{1-y}Ti_y$. A possibility is that, by extended cycling, aluminum and titanium may continue the reaction and several types of Al-rich intermetallics are formed.

In the dehydrided sample after 100 cycles, the mole fractions were estimated to be 54.6, 8.7, and 35.3% Al, Na_3AlH_6, and NaH, respectively.[11] This corresponds to a 59% complete desorption of Na_3AlH_6. Since the mol fractions after the next absorption corresponds to 81%, the capacity could, as a first approximation, be estimated from the capacities of the two reaction steps to be 3.8 wt %. Corrected for the prolonged absorption in the last reabsorption, the estimation from quantitative phase analysis is close to the observed values for the last cycles, which is approximately 3.4 wt %.

4. Discussion

Three different X-ray absorption studies near the Ti edge indicate reduction of Ti^{III} to Ti^0 after the ball-milling reaction, but the interpretation of the extended X-ray absorption fine structures deviate considerably.[8−10] A general drawback of this technique is that because the Ti^0 edge is at lower energy than the edge for higher Ti valences, a smaller amount of Ti in higher valences would be masked by the Ti^0 contribution. Nevertheless, it is clear that most of the titanium precursor is reduced to the metallic state by the ball milling with the reducing agent $NaAlH_4$.

Similar results were recently shown by pressure measurements during ball milling.[24] This study showed a pressure increase in accordance with complete reduction of $TiCl_x$ to Ti. But without PXD characterization of the product, it is still a possibility for partial thermal decomposition to Na_3AlH_6 during the prolonged milling. This would eventually affect the calculated number of hydrogens released per Ti considerably.

EPR experiments, which are sensitive to Ti^{III}, show traces of Ti^{III} after ball milling with $TiCl_3$ and larger amounts of Ti^{III} after ball milling with TiF_3.[25] In both cases, Ti^{III} are replaced by signals for Ti^0 after a few cycles. This is interpreted as unreacted additive that is consumed during cycling.

The present study using quantitative phase analysis of SR-PXD data shows that ball milling of $NaAlH_4$ with $TiCl_3$ and TiF_3 leads to close to complete reaction of the Ti precursors with $NaAlH_4$, such that NaCl and Al are formed. Neither Na nor Al are found to be replaced by Ti. This implies that Ti^{III} is reduced, either partially to e.g. TiH_x or $Ti_{1-y}Al_yH_x$ or completely to Ti^0 (Ti or a Ti-rich Ti−Al alloy). Because no crystalline Ti-containing phases are found, it is not possible to conclude from SR-PXD the state of Ti directly after ball milling with $NaAlH_4$.

Recent experiments with 0.915 Ti + 0.085 Al in methanol indicate removal of pure Al within 4 h of ball milling and formation of an amorphous phase, which may contain hydrogen, after 12 h.[26] It has been reported that stable Ti−Al phases with up to 45% Al may be hydrided,[27] and metastable phases achieved by mechanical alloying up to 65% Al may be hydrided.[28] A considerable Al content would have caused a shift in the Al:NaCl ratio, which in the present work is shown to be in close agreement with eq 4 for sample 1. Similarly, a large hydrogen content in the Ti-containing phase is expected to give a shift in the near-edge X-ray absorption compared to Ti^0. These considerations indicate formation of amorphous titanium, possibly with small amounts of Al and H, after ball milling. In a recent report, a wide feature in the PXD diagram measured

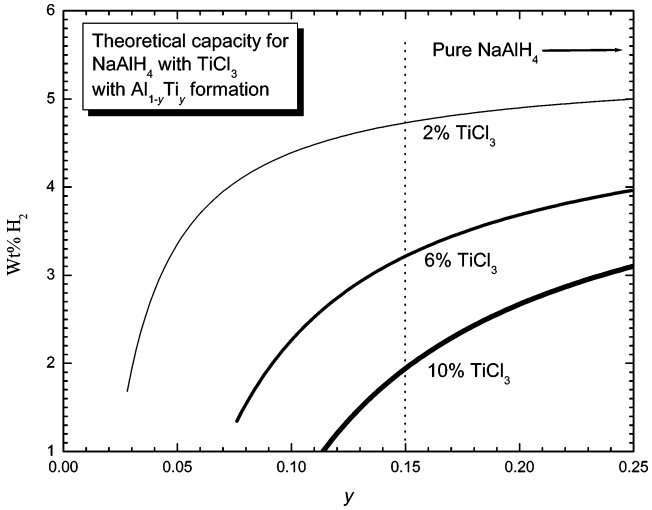

Figure 6. Theoretical hydrogen storage capacity of $NaAlH_4$ with different amounts of $TiCl_3$ additive as a function of the Ti content in $Al_{1-y}Ti_y$.

directly after ball milling is interpreted as an amorphous Ti−Al phase of undefined composition.[29]

The present results show that, after cycling a metastable phase with a composition between Al_3Ti and Al is formed. This phase is formed for Ti additions as high as 10 mol %. Estimations from the quantitative phase analysis give a composition of $Al_{0.85}$-$Ti_{0.15}$, and this phase is characterized by a unit-cell dimension of approximately 4.0365 Å, both with the $Ti(OBu)_4$ and the $TiCl_3$ additive. This phase can account for more than 80% of the Ti introduced into the sample. Furthermore, the positions of Al and Ti have been shown to be correlated in a cycled $NaAlH_4$ with TiF_3 additive from energy-dispersive X-ray analysis in a recent transmission electron microscopy study.[30]

The effect of $Al_{0.85}Ti_{0.15}$ on the kinetics of the sodium alanate system is at the moment not clear. There is always a possibility that a minor fraction of Ti is causing the improvement, whereas the major fraction is detected by PXD and other techniques. Nevertheless, after cycling Ti-enhanced $NaAlH_4$, most of the Ti is present as a solid solution in Al, and it is a reasonable possibility that Ti from this phase is of importance to the enhanced kinetics. At the moment, it is not clear whether the composition of the Al−Ti phase is constant during desorption and absorption.

When $Al_{1-y}Ti_y$ is formed during cycling, this reduces the storage capacity of the first step of $NaAlH_4$ because of insufficient Al for the reaction with Na_3AlH_6. Combined with the capacity loss from the dead weight of the additive and reaction of the additive according to eq 4, the hydrogen storage capacity of $NaAlH_4$ with $TiCl_3$ additive as a function of y in $Al_{1-y}Ti_y$ is shown in Figure 6. A decreasing y leads to a considerable loss of capacity; e.g. formation of $Al_{0.85}Ti_{0.15}$ in a sample with 2 mol % $TiCl_3$ will give a maximum storage capacity of 4.73 wt %, whereas with 10 mol % only 1.94 wt % may be maintained.

Certainly, additional decreased capacity due to long diffusion paths and resulting incomplete reaction may be important. Bogdanovic et al.[13] did observe Na_3AlH_6 after absorption, and ball milling of this sample did not remove Na_3AlH_6 completely, but excess Al added by ball milling at this stage did. This could also be interpreted on the basis of the present model, because it is reasonable to believe that ball milling does not release free Al from $Al_{1-y}Ti_y$, which probably was present in the sample after cycling. Introduction of free Al, however, may consume the remaining Na_3AlH_6.

There are literature data available on cycling capacities for $NaAlH_4$. Bogdanovic's original data with 2 mol % $TiCl_3$ give 4.2 wt %,[1] which indicates $y = 0.10$, assuming no limitations in diffusion. Sandrock et al. studied the storage capacity as a function of additive level[2] and found a reduced capacity which corresponds to $y = 0.18$ in the frame of eq 6. These results are in the same range as the present estimation based on quantitative phase analysis.

By ball milling, it is possible to induce a variety of chemical reactions without reaching the thermodynamically most stable state; e.g. ball milling of $LiAlD_4$ and 2NaH recently has been shown to partly react to $NaAlD_4$ and LiH, which after heat treatment under pressure further reacts to $Na_2LiAlD_4H_2$.[31] Present and earlier experimental evidence indicate that mainly a redox reaction to Al^0, Ti^0, and NaCl happens during ball milling of $NaAlH_4$ and $TiCl_3$. This reaction is subsequently, during the heat treatment in the cycling, followed by another thermodynamically favorable (see e.g. ref 18) reaction: from Al and Ti to an Al-rich $Al_{1-y}Ti_y$.

Metastable Al−Ti phases are relatively stable at elevated temperature after mechanical alloying, but there is a possibility that cycling at a different temperature could give a different composition of $Al_{1-y}Ti_y$ and hence different capacity than achieved at 160 °C in the present report. The capacity of $NaAlH_4$ + 2 mol % $Ti(OBu)_4$ has, though, been shown to be quite stable at 3.5−4.0 wt % during many cycles.[3]

Acknowledgment. The skilful assistance from the project team at the Swiss−Norwegian Beam Line, ESRF, is gratefully acknowledged. S.S.S. and C.M.J. gratefully acknowledge financial support received from the Office of Hydrogen, Fuel Cells and Infrastructure Technologies of the U.S. Department of Energy.

References and Notes

(1) Bogdanovic, B.; Schwickardi, M. *J. Alloys Compd.* **1997**, *253*, 1−9.
(2) Sandrock, G.; Gross, K.; Thomas, G. *J. Alloys Compd.* **2002**, *339*, 299−308.
(3) Srinivasan, S. S.; Brinks, H. W.; Hauback, B. C.; Sun, D.; Jensen, C. M. *J. Alloys Compd.* **2004**, *377*, 283−289.
(4) Fichtner, M.; Fuhr, O.; Kircher, O.; Rothe, J. *Nanotechnology* **2003**, *14*, 778−785.
(5) Wang, P.; Jensen, C. M. *J. Phys. Chem. B* **2004**, *108*, 15827−15829.
(6) Jensen, C. M.; Zidan, R.; Mariels, N.; Hee, A.; Hagen, C. *Int. J. Hydrogen Energy* **1999**, *24*, 461−465.
(7) Bogdanovic, B.; Brand, R. A.; Marjanovic, A.; Schwickardi, M.; Tolle, J. *J. Alloys Compd.* **2000**, *302*, 36−58.
(8) Graetz, J.; Reilly, J. J.; Johnson, J.; Ignatov, A. Y.; Tyson, T. A. *Appl. Phys. Lett.* **2004**, *85*, 500−502.
(9) Léon, A.; Kircher, O.; Rothe, J.; Fichtner, M. *J. Phys. Chem. B* **2004**, *108*, 16372−16376.
(10) Felderhoff, M.; Klementiev, K.; Grunert, W.; Spliethoff, B.; Tesche, B.; von Colbe, J. M. B.; Bogdanovic, B.; Hartel, M.; Pommerin, A.; Schuth, F.; Weidenthaler, C. *Phys. Chem. Chem. Phys* **2004**, *6*, 4369−4374.
(11) Brinks, H. W.; Jensen, C. M.; Srinivasan, S. S.; Hauback, B. C.; Blanchard, D.; Murphy, K. *J. Alloys Compd.* **2004**, *376*, 215−221.
(12) Weidenthaler, C.; Pommerin, A.; Felderhoff, M.; Bogdanovic, B.; Schuth, F. *Phys. Chem. Chem. Phys* **2003**, *5*, 5149−5153.
(13) Bogdanovic, B.; Felderhoff, M.; Germann, M.; Hartel, M.; Pommerin, A.; Schuth, F.; Weidenthaler, C.; Zibrowius, B. *J. Alloys Compd.* **2003**, *350*, 246−255.
(14) Haber, J. A.; Crane, J. L.; Buhro, W. E.; Frey, C. A.; Sastry, S. M. L.; Balbach, J. J.; Conradi, M. S. *Adv. Mater.* **1996**, *8*, 163−166.
(15) Zhang, F.; Lu, L.; Lai, M. O. *J. Alloys Compd.* **2000**, *297*, 211−218.
(16) Klassen, T.; Oehring, M.; Bormann, R. *Acta Mater.* **1997**, *45*, 3935−3948.
(17) Klassen, T.; Oehring, M.; Bormann, R. *J. Mater. Res.* **1994**, *9*, 47−52.

(18) Oehring, M.; Klassen, T.; Bormann, R. *J. Mater. Res.* **1993**, *8*, 2819−2829.

(19) Oehring, M.; Yan, Z. H.; Klassen, T.; Bormann, R. *Phys. Stat. Solidi A* **1992**, *131*, 671−689.

(20) Choi, J. H.; Moon, K. I.; Kim, J. K.; Oh, Y. M.; Suh, J. H.; Kim, S. J. *J. Alloys Compd.* **2001**, *315*, 178−186.

(21) Fan, G. J.; Gao, W. N.; Quan, M. X.; Hu, Z. Q. *Mater. Lett.* **1995**, *23*, 33−37.

(22) Rodríguez-Carvajal, J. *Physica B* **1993**, *192*, 55−69.

(23) Tonejc, A.; Bonefacic, A. *Scr. Metall.* **1969**, *3*, 145−147.

(24) Bellosta von Colbe, J. M.; Bogdanovic, B.; Felderhoff, M.; Pommerin, A.; Schuth, F. *J. Alloys Compd.* **2004**, *370*, 104−109.

(25) Jensen, C. M.; Sun, D.; Srinivasan, S. S.; Wang, P.; Murphy, K.; Wang, Z.; Eberhard, M.; Naghipour, A. Unpublished results.

(26) Morales-Hernández, J.; Velázquez-Salazar, J.; García-González, L.; Espinoza-Beltrán, F. J.; Berceinas-Sánchez, J. D. O.; Munoz-Saldana, J. *J. Alloys Compd.* **2005**, *388*, 266−273.

(27) Hashi, K.; Ishikawa, K.; Aoki, K. *Met. Mater. Korea* **2001**, *7*, 175−179.

(28) Hashi, K.; Ishikawa, K.; Suzuki, K.; Aoki, K. *Mater. Trans.* **2002**, *43*, 2734−2740.

(29) Haiduc, A. G.; Stil, H. A.; Schwarz, M. A.; Paulus, P.; Geerlings, J. J. C. *J. Alloys Compd.* **2005**, *393*, 252−263.

(30) Andrei, C. M.; Walmsley, J. C.; Brinks, H. W.; Holmestad, R.; Srinivasan, S. S.; Jensen, C. M.; Hauback, B. C. *Appl. Phys. A: Mater. Sci. Process.* **2005**, *80*, 709−715.

(31) Brinks, H. W.; Hauback, B. C.; Jensen, C. M.; Zidan, R. *J. Alloys Compd.* **2005**, *392*, 27−30.

Characterization of titanium dopants in sodium alanate by electron paramagnetic resonance spectroscopy

Meredith T. Kuba
Department of Chemistry, University of Hawaii, Honolulu, Hawaii 96822
Sandra S. Eaton
Department of Chemistry and Biochemistry, University of Denver, Denver, Colorado 80208
Christine Morales and Craig M. Jensen[a)]
Department of Chemistry, University of Hawaii, Honolulu, Hawaii 96822

(Received 1 August 2005; accepted 2 August 2005)

Electron paramagnetic resonance (EPR) spectra were obtained for samples of Ti-doped $NaAlH_4$ subjected to different numbers of cycles of dehydrogenation/re-hydrogenation. Ti is observed to evolve from its initial Ti(III) state through a series of Ti(0) species during the first 5 cycles. Although the conversion of Ti(III) to Ti(0) occurs much more readily for $TiCl_3$-doped samples than those prepared with TiF_3, in both cases the evolution of Ti follows the same sequence that involves 3 distinguishable Ti(0) species and ends in the predominance of the same single Ti(0) species. The spectrum of a sample of $NaAlH_4$ containing 2 mol% of cubic Al_3Ti is distinctly different than any of those observed for the Ti(0) species that arise during the hydrogen cycling of the hydride. The major changes in the nature of the predominant Ti species have little if any effect on the dehydrogenation kinetics, which strongly suggests that the profoundly enhanced hydrogen cycling kinetics of Ti-doped $NaAlH_4$ are due to a Ti species present in only a relatively minor amount.

I. INTRODUCTION

The commercialization of fuel cell powered vehicles is a technological challenge of great current importance and interest. One of the most significant obstacles to reaching this goal is the development of a practical means of onboard hydrogen storage. Metal hydrides have long been utilized as hydrogen carriers. However, commercial vehicular applications impose very stringent demands on hydrogen absorbing materials. Crucial criteria include a high available hydrogen weight percentage, rapid hydrogen cycling kinetics, a suitable hydrogen plateau pressure at moderate temperature, sufficient cycling lifetimes, and low cost. No hydrogen absorbing metal or alloy has been discovered that meets all of these criteria. In 1997, Bogdanovic and Schwickardi reported that the hydrogen could be reversibly evolved from solid $NaAlH_4$ under moderate conditions upon doping the hydride with a few mole percent of selected transition metal complexes.[1] This was a seminal discovery in the area of metal hydrides as hydrogen cycling at moderate temperatures was unprecedented for saline hydrides. Subsequent efforts toward the development of Ti-doped $NaAlH_4$ by ourselves and others[2–14] have given rise to materials that undergo dehydrogenation and re-hydrogenation at temperatures and times that are adequate for practical applications. Recently, it has been found that the phenomenon of kinetic enhancement upon transition metal doping extends to the reversible dehydrogenation of $LiNH_2$[15,16] and $LiBH_4/MgH_2$.[17]

Despite this progress, several problems have persisted. The reversible dehydrogenation of doped $NaAlH_4$ is known to proceed by the sequence of reactions seen in Eqs. (1) and (2).

$$NaAlH_4 \longrightarrow 1/3\ Na_3AlH_6 + 2/3\ Al + H_2 \qquad (1)$$

$$Na_3AlH_6 \longrightarrow 3\ NaH + Al + 3/2\ H_2 \qquad (2)$$

Although these equations predict that 5.6 wt% hydrogen should be available from this system, studies have shown that the only 3–4 wt% can be cycled under conditions that are relevant to the practical operation of an onboard PEM fuel cell.[12] Also, sodium and mixed sodium-lithium are the only alanates that have been found to undergo largely reversible dehydrogenation under moderate conditions upon doping.[1] Moreover, the kinetic enhancement achieved by standard Ti doping of other materials

[a)]Address all correspondence to this author.
e-mail: jensen@gold.chem.hawaii.edu
DOI: 10.1557/JMR.2005.0404

falls far short of the requirements for practical applications.[17] The fundamental basis of the kinetic enhancement of hydrogen cycling that arises upon doping remains an enigma. Clearly, an understanding of this novel solid-state chemistry would be invaluable to the effort to develop alanates and related high-capacity, high-performance hydrogen-storage materials. As a probe of this phenomenon, we have carried out electron paramagnetic resonance (EPR) studies of Ti-doped $NaAlH_4$.

II. EXPERIMENTAL

A. Materials

Titanium(III) chloride ($TiCl_3$) and titanium(III) fluoride (TiF_3) were obtained from Aldrich Chemical Inc. (Milwaukee, WI) and used as received. Sodium aluminum hydride ($NaAlH_4$) was obtained from Albemarle Corp. (Baton Rouge, LA) Cubic Al_3Ti was prepared according to the literature procedure.[18]

B. Purification of $NaAlH_4$

The purification procedure was carried out in a glove box under nitrogen. The aluminum present in the commercially obtained $NaAlH_4$ was removed by filtration following dissolution of the hydride in a minimal amount of tetrahydrofuran (THF). Analytically pure $NaAlH_4$ was precipitated upon the addition of pentane to the THF solution. The hydride was isolated by filtration, washed with several portions of pentane, and dried overnight under high vacuum. EPR spectra of samples of the purified, undoped hydride contained only extremely weak organic radical signals that were detectable only slightly above the baseline near $g \sim 2.002$.

C. Doping procedure

The hydride was doped in a glove box under nitrogen. $NaAlH_4$ (~2.00 g) was charged with a prescribed amount of $TiCl_3$ or TiF_3 and loaded into a tungsten carbide bowl (12 ml) with seven 7-mm-diameter tungsten carbide balls (ball-to-powder ratio varied between 30:1 to 40:1). The capped and sealed bowl was then transferred to a Fritsch (Idar-Oberstein, Germany) 7 planetary mill and ball milled for 30 min at a speed of 300 rpm.

D. Kinetic measurements

The dehydrogenation studies were carried out using an automated Sieverts' type apparatus (LESCA Co., Osaka, Japan), which allowed for the accurate volumetric determination of the amount of hydrogen evolved. Rapid heating of the sample to the desired temperature was accomplished by immersing the sample reactor into a silicon oil bath (accuracy of ±1 K) preheated to a given temperature. Dehydrogenation was performed against a back pressure of 0.1 MPa in a fixed volume.

E. Electron paramagnetic resonance studies

X-band (9.228 GHz) continuous wave (CW) EPR spectra were recorded at room temperature on a Varian (Palo Alto, CA) E-9 spectrometer interfaced to a PC. Spectrometer parameters were 100 KHz magnetic-field modulation frequency, 4 G modulation amplitude, 1024 data points, 4 min scan time, and 2 scans signal averaged. Two magnetic field ranges were examined. To characterize signals with g values near 2.0, 400-G scans centered at 3300 were obtained with a microwave power of 5 mW. At this power, signals with $g \sim 1.99$ were in the linear response range. Scans from 0 to 8000 G were obtained with a microwave power of 80 mW, which was in the linear response region for the broad signals that were detected in most of the samples.

III. RESULTS

Two sets of samples of Ti-doped $NaAlH_4$ were prepared for the EPR spectroscopic studies. The first was doped through mechanical milling with 2 mol% TiF_3. As seen in Fig. 1(a) , the 8000-G wide EPR of the uncycled, doped hydride is dominated by a sharp signal with $g = 1.976$ and $\Delta B_{pp} \sim 90$ G. This g value is within the range observed for Ti(III) species in a variety of environments.[19–24] Therefore, we propose that the sharp signal is due to the presence of a major population of magnetically dilute $S = 1/2$ Ti(III) sites in the $NaAlH_4$ lattice. After 3 cycles of dehydrogenation the integrated intensity of the Ti(III) signal is only about 73% of that in sample before cycling. As seen in Fig. 1(b), a broader signal with $\Delta B_{pp} \sim 1500$ G can also be discerned thus indicating the presence of a multi-spin Ti species. After 5 cycles [Fig. 1(c)], the Ti(III) and $\Delta B_{pp} \sim 1500$ G signals disappear, and the spectrum is dominated by a broad signal with $g = 2.01$ and $\Delta B_{pp} \sim 650$ G and also contains a signal near zero-field. After 10 cycles [Fig. 1(d)], the height of the signal with $\Delta B_{pp} \sim 650$ G is similar to that after 5 cycles, but the signal near zero-field has largely disappeared.

The series of samples doped with 2 mol% $TiCl_3$ also revealed a series of changes in the dominant population of titanium through the first 10 cycles. However, as seen in Fig. 1(e), the spectrum of the sample of uncycled, $NaAlH_4$ doped with 2 mol% $TiCl_3$ is dominated by a broad signal near zero-field and contains only a minor sharp Ti(III) signal with $g \sim 1.97$. The spectrum of the sample which has undergone 3 cycles [Fig. 1(f)], contains only a minor Ti(III) signal at $g = 1.97$, and the broader signal with $\Delta B_{pp} \sim 1500$ G has evolved in shape. The spectrum [Fig. 1(g)] of the $TiCl_3$ doped sample that was cycled 5 times is very similar to that of TiF_3 doped hydride after 5 cycles and features a signal $g = 2.01$ and $\Delta B_{pp} \sim 650$ G plus a signal near zero field. The analogy with the TiF_3 doped materials extends to the 10 cycle $TiCl_3$ sample [Fig. 1(h)] in which the signal $g = 2.01$

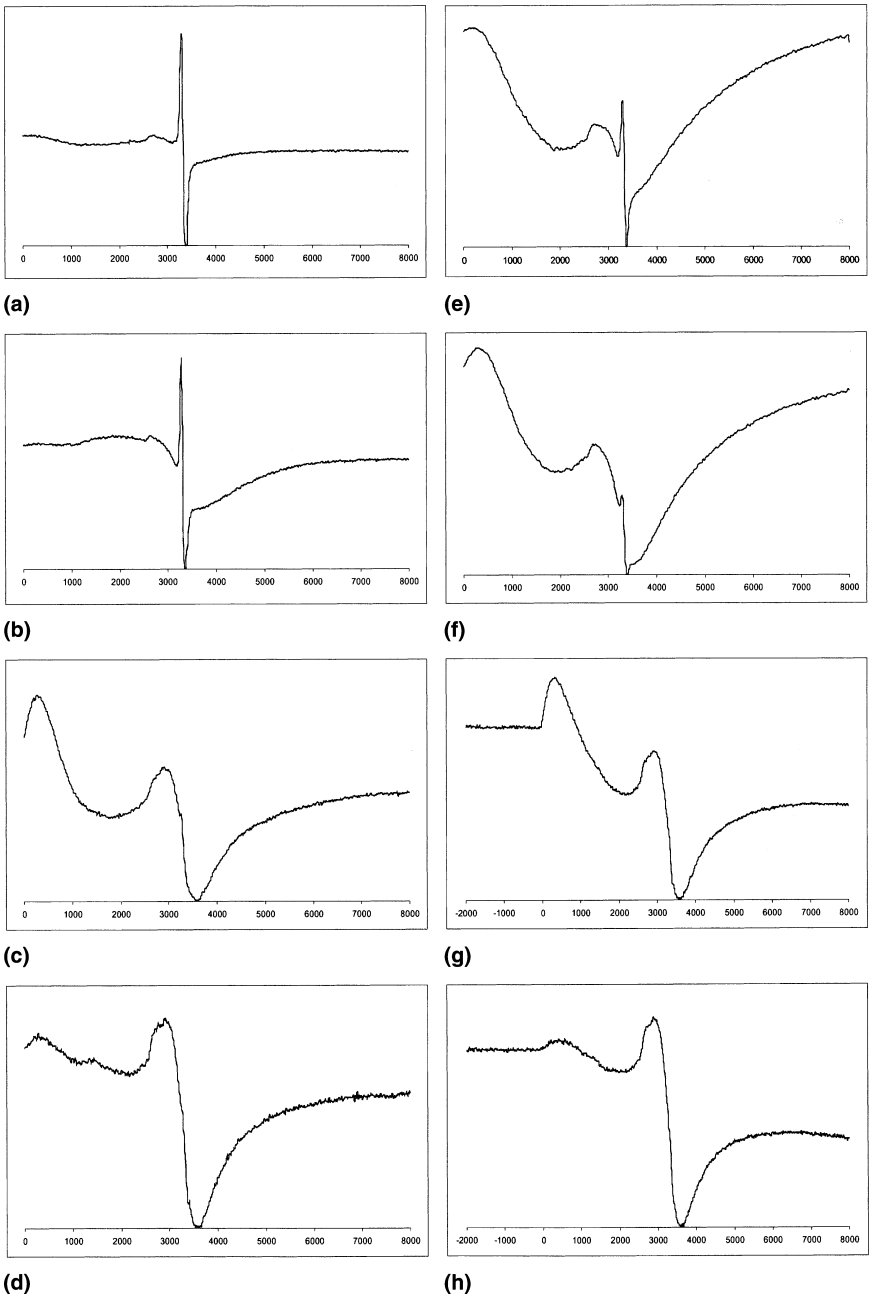

FIG. 1. EPR spectrum of (a) 2 mol% TiF_3 doped $NaAlH_4$, uncycled; (b) 2 mol% TiF_3 doped $NaAlH_4$, after 3 cycles; (c) 2 mol% TiF_3 doped $NaAlH_4$, after 5 cycles; (d) 2 mol% TiF_3 doped $NaAlH_4$, after 10 cycles; (e) 2 mol% $TiCl_3$ doped $NaAlH_4$, uncycled; (f) 2 mol% $TiCl_3$ doped $NaAlH_4$, after 3 cycles; (g) 2 mol% $TiCl_3$ doped $NaAlH_4$, after 5 cycles; and (h) 2 mol% $TiCl_3$ doped $NaAlH_4$, after 10 cycles.

and $\Delta B_{pp} \sim 650$ G is slightly more intense than the 5 cycle sample, and the zero field signal has disappeared.

In an attempt to identify the multi-spin Ti species that were observed in these studies, a sample of $NaAlH_4$ was prepared which contained 2 mol% of cubic Al_3Ti. As seen in Fig. 2, the EPR signal observed for the alloy has components near zero-field analogous to those for some of the Ti species, but the overall shape and the component near $g = 2$ is distinctly different than any of the signals observed for the 3 different species that arise during the hydrogen cycling of the doped hydride.

IV. DISCUSSION

Our results clearly indicate that the majority of titanium is transformed from Ti(III) to Ti(0) species during early cycles of dehydrogenation/re-hydrogenation. Recent electron microscopy studies of TiF_3 doped $NaAlH_4$ have confirmed that TiF_3 is present in the mechanically

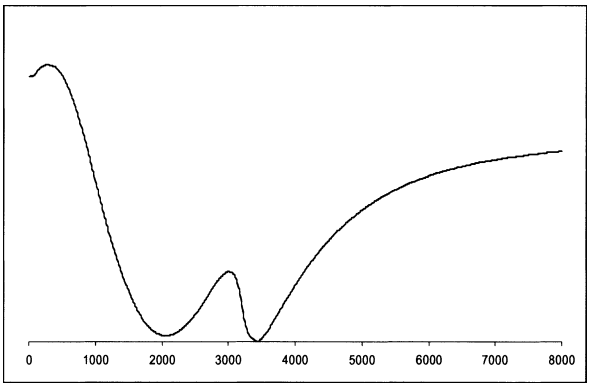

FIG. 2. EPR spectrum of $NaAlH_4$, mechanically milled with 2 mol% cubic Al_3Ti.

milled material prior to cycling and that the Ti becomes correlated with Al after 15 cycles.[25] Our findings are also in agreement with synchrotron x-ray studies of cycled samples which established that increasing amounts of a solid solution with an approximate composition of $Al_{0.93}Ti_{0.07}$ form over the course of repeated cycling.[26] Apparently, $TiCl_3$ is a more active dopant precursor as the Ti(III) signal has largely disappeared in the chloride doped sample even prior to the first dehydrogenation and Ti(0) species arise much earlier in the course of cycling the hydride.

Several studies have probed the valence and local structure of titanium in samples of $NaAlH_4$ that were doped using the $TiCl_3$ precursor through Ti K-edge x-ray absorption (XANES).[27–29] Although the investigators have uniformly determined that a Ti(0) species predominates in these materials, there has been some disagreement as to its nature. Graetz et al. conclude that "Al_3Ti forms immediately on doping with $TiCl_3$ and oxidation state is nearly invariant during hydrogen cycling"[27] while Fichtner and co-workers found that "the formation of an alloy with Al or TiH_2 is not supported by EXAFS data."[28] Our observation of the presence of three different Ti(0) species over the course of the 5 cycles of dehydrogenation/re-hydrogenation serves to resolve the apparent conflict in the conclusions of the XANES studies. We infer that in addition to the number of cycles and the dopant precursor employed, the nature of the predominant Ti(0) in Ti-doped $NaAlH_4$ is sensitive to slight variations in the conditions utilized during the mechanical milling process.

We have previously observed only a relatively minor change in the dehydrogenation kinetics during the first 5 cycles of a sample of $NaAlH_4$ doped with 2 mol% of TiF_3.[12] It is remarkable that the observed change in the oxidation state of the predominant titanium species results in only a minor change in the dehydrogenation kinetics. Furthermore, despite the radical difference in the relative amounts of Ti(III) and Ti(0) in the TiF_3 and $TiCl_3$ doped samples, nearly identical kinetics have been found to result from these dopant precursors.[30] Therefore, our studies, in combination with the earlier EXAFS results, strongly suggest that the enhanced hydrogen cycling kinetics of Ti-doped $NaAlH_4$ are due to a minority Ti species and that the majority of the Ti is in a catalytically inactive, resting state. This conclusion is supported by our finding that all known TiAl alloys are ineffective in promoting the dehydrogenation/re-hydrogenation kinetics of $NaAlH_4$.[31]

V. CONCLUSIONS

The majority of the Ti in doped $NaAlH_4$ has been observed to evolve from Ti(III) through a series of Ti(0) species during the first 5 cycles of dehydrogenation/re-hydrogenation. Although the conversion of the initial Ti(III) species to Ti(0) occurs much more readily for $TiCl_3$ than TiF_3, the evolution of Ti species follows the same sequence and ends in the same Ti(0) species regardless of which dopant precursor is used. At no point do the signals for the Ti dopants resemble those observed for cubic-Al_3Ti. The observed changes in the predominant Ti species during hydrogen cycling are remarkable in view of the relatively stable dehydrogention kinetics. We conclude that the profoundly enhanced hydrogen cycling kinetics of Ti-doped $NaAlH_4$ are due to a Ti species that is present in only a relatively minor amount.

ACKNOWLEDGMENT

We gratefully acknowledge the financial support for this research from the Office of Hydrogen, Fuel Cells, and Infrastructure Technologies of the United States Department of Energy.

REFERENCES

1. B. Bogdanovic and M. Schwickardi: Ti-doped alkali metal aluminium hydrides as potential novel reversible hydrogen-storage materials. *J. Alloys Compd.* **253,** 1 (1997).
2. C.M. Jensen, R. Zidan, N. Mariels, A. Hee, and C. Hagen: Advanced titanium doping of sodium aluminum hydride: Segue to a practical hydrogen storage material? *Int. J. Hydrogen Energy* **24,** 461 (1999).
3. R. Zidan, S. Takara, A. Hee, and C. Jensen: Hydrogen cycling behavior of zirconium and titanium–zirconium-doped sodium aluminum hydride. *J. Alloys Compd.* **285,** 119 (1999).
4. C.M. Jensen and R.A. Zidan: Hydrogen storage materials and method of making by dry homogenation. U.S. Patent No. 6 471 935 (2002).
5. B. Bogdanovic, R. Brand, A. Marjanovic, M. Schwickardi, and J. Tolle: Metal-doped sodium aluminium hydrides as potential new hydrogen-storage materials. *J. Alloys Compd.* **302,** 36 (2000).
6. C.M. Jensen and K.J. Gross: Development of catalytically enhanced sodium aluminum hydride as a hydrogen-storage material. *Appl. Phys. A* **72,** 213 (2001).

7. B. Bogdanovic and M. Schwickardi: Ti-doped $NaAlH_4$ as a hydrogen-storage material—Preparation by Ti-catalyzed hydrogenation of aluminum powder in conjunction with sodium powder. *Appl. Phys. A* **72,** 221 (2001).
8. G. Sandrock, K. Gross, G. Thomas, C. Jensen, D. Meeker, and S. Takara: Engineering considerations in the use of catalyzed sodium alanates for hydrogen storage. *J. Alloys Compd.* **330–332,** 696 (2002).
9. K.J. Gross, G.J. Thomas, and C.M. Jensen: Catalyzed alanates for hydrogen storage. *J. Alloys Compd.* **330–332,** 683 (2002).
10. G. Sandrock, K. Gross, and G. Thomas: Effect of Ti-catalyst content on the reversible hydrogen storage properties of the sodium alanates. *J. Alloys Compd.* **339,** 299 (2002).
11. M. Fichtner, O. Fuhr, O. Kircher, and J. Rothe: Small Ti clusters for catalysis of hydrogen exchange in $NaAlH_4$. *Nanotechnology* **14,** 778 (2003).
12. S.S. Srinivasan, H.W. Brinks, B.C. Hauback, D. Sun, and C.M. Jensen: Long term cycling behavior of titanium doped $NaAlH_4$ prepared through solvent mediated milling of NaH and Al with titanium dopant precursors. *J. Alloys Compd.* **377,** 283 (2004).
13. P. Wang and C.M. Jensen: Preparation of Ti-doped sodium aluminum hydride from mechanical milling of NaH/Al with off-the-shelf Ti powder. *J. Phys. Chem. B* **108,** 15829 (2004).
14. P. Wang and C.M. Jensen: Method for preparing Ti-doped $NaAlH_4$ using Ti powder: Observation of an unusual reversible dehydrogenation behavior. *J. Alloys Compd.* **379,** 99 (2004).
15. T. Ichikawa, S. Isobe, N. Hanada, and H. Fujii: Lithium nitride for reversible hydrogen storage. *J. Alloys Compd.* **365,** 271 (2004).
16. T. Ichikawa, N. Hanada, S. Isobe, H. Leng, and H. Fujii: Mechanism of novel reaction from $LiNH_2$ and LiH to Li_2NH and H_2 as a promising hydrogen storage system. *J. Phys. Chem. B* **108,** 7887 (2004).
17. J. Vajo, S. Skeith, and F. Mertens: Reversible storage of hydrogen in destabilized $LiBH_4$. *J. Phys. Chem. B* **109,** 3719 (2005).
18. P. Bhattacharya, P. Bellon, R.S. Averback, and S.J. Hales: Nanocrystalline TiAl powders synthesized by high-energy ball milling: Effects of milling parameters on yield and contamination. *J. Alloys Compd.* **368,** 187 (2004).
19. J.L. Atwood, G.K. Barker, J. Holton, W.E. Hunter, M.F. Lappert, and R. Pearce: Silylmethyl and related complexes. 5 metalhlocene bis(trimethylsilyl) methyls and benzyldryls of early transition metals $[M(\eta^5 - C_5H_5)_2R]$ (M = Ti or V) and $[M(\eta^5 - C_5H_5)_2(x)R]$ (M = Zr or Hf and x = Cl or R) and the crystal and molecular structures of $[M(\eta^5 - C_5H_5)_2\ (CHPh_2)_2]$ (m = Zr or Hf). *J. Am. Chem. Soc.* **99,** 6645 (1977).
20. G. Corradi, I.M. Zaritskii, A. Hofstaetter, K. Polgar, and L.G. Rakitina: Ti^{3+} on Nb site: A paramagnetic Jahn–Teller center in vacuum-reduced $LiNbO_3$:Mg:Ti single crystals. *Phys. Rev. B: Cond. Mater. Mater. Phys.* **58,** 8329 (1998).
21. T.C. DeVore and W. Weltner, Jr.: Titanium difluoride and titanium trifluoride molecules: Electron spin resonance spectra in rare-gas matrices at 4 K. *J. Am. Chem. Soc.* **99,** 4700 (1977).
22. V.V. Lagula, M.D. Glinchuk, R.O. Kuzian, S.N. Nokhrin, I.P. Bykov, L. Jastrabik, and J. Rosa: Electron spin resonance of Ti^{3+} in $KTa_{0.9}Nb_{0.1}O_3$. *Solid State Commun.* **122,** 277 (2002).
23. A.M. Prakash, H.M. Sung-Suh, M. Hyung, and L. Kevan: Electron spin resonance evidence for isomorphous substitution of titanium into titanosilicate TiMCM-41 mesoporous molecular sieve. *J. Phys. Chem. B* **102,** 857 (1988).
24. R.C. Wilson and R.J. Myers: Electron paramagnetic resonance spectrum and spin relaxation for $Ti(H_2O)$ in aqueous solution and in frozen glass. *J. Chem. Phys.* **64,** 2208 (1976).
25. C.M. Andrei, J. Walmsley, H.W. Brinks, R. Homestad, S.S. Srinivasan, C.M. Jensen, and B.C. Hauback: Electron-microscopy studies of $NaAlH_4$ with TiF_3 additive: Hydrogen-cycling efffects. *Appl. Phys. A* **80,** 709 (2005).
26. H.W. Brinks, C.M. Jensen, S.S. Srinivasan, B.C. Hauback, D. Blanchard, and K. Murphy: Synchotron x-ray and neutron diffraction studies of $NaAlH_4$ containing Ti additives. *J. Alloys Compd.* **376,** 215 (2003).
27. J. Graetz, J.J. Reily, J. Johnson, A.Y. Ingatov, and T.A. Tyson: X-ray absorption study of Ti-activated sodium aluminum hydride. *Appl. Phys. Lett.* **85,** 500 (2004).
28. A. Leon, O. Kircher, J. Rothe, and M. Fichtner: Chemical state and local structure around Ti atoms in $NaAlH_4$ doped with $TiCl_3$ using x-ray absorption spectroscopy. *J. Phys. Chem. B* **108,** 16372 (2004).
29. M. Felderhoff, K. Klementiev, W. Grunert, B. Spliethoff, B. Tesche, J.M.B. von Colbe, B. Bogdanovic, M. Hartel, A. Pommerin, F. Schuth, and C. Weidenthaler: Correlative TEM-EDX and XAFS studies of Ti-doped sodium alanate. *Phys. Chem. Chem. Phys.* **6,** 4369 (2004).
30. D.L. Anton: Hydrogen desorption kinetics in transition metal modified $NaAlH_4$. *J. Alloys Compd.* **356–357,** 400 (2003).
31. C.M. Jensen, M. Kuba, M. Sulic, K. Morales, C. Brown, W. Langley, and T. Dalton: Catalytically enhanced hydrogen storage systems, in *Proceedings of the 2005 US DOE Hydrogen Annual Program Review*, Washington DC, May 2004, available at: www.hydrogen.energy.gov/pdfs/review05/st3_jensen.pdf.

Department of Energy
Golden Field Office
1617 Cole Boulevard
Golden, Colorado 80401-3305

April 12, 2007

TO: Dean Olson, Director, Office of Finance and Accounting, CF-10

FROM: Tim Rea, Finance Team Leader

COPY TO: James T. Campbell, Deputy CFO
Judy Penry, CFO, Oak Ridge

SUBJECT: Inter-Entity Work Orders / Development and & Implementation of the Proposed Department of Energy – Payment and Collection (DOE-PAC) System/Process.

As you know, Inter-Entity Transactions and the Inter-Entity transaction backlog were identified in FY 2006 by the CFO Tiger Team as an area in need of attention. A Sub-team was formed among HQ-EFASC and a number of Field Offices. Much was accomplished and the transaction backlog was reduced, but the work was not completed.

Two major open issues are the ongoing need for clear guidance on use of and correct STARS entries for Fund 0911 and Fund 0912; and for a standard Work for Others Descriptive Flexfield structure for Inter-Entity Work Orders. The Sub-team's recommendations for the flexfield have been forwarded to and discussed with EFASC and I believe formal guidance is forthcoming.

Another major issue is the ongoing volume of outstanding receivables and payables between DOE organizations, the work involved in managing these, and the fact that DOE and its Integrated Contractors are moving cash through various methods to pay each other – all within a single agency. Prior to the DOE consolidation into a single Agency Location Code, this practice was more defensible, but that is no longer the case. The Oak Ridge members of the original Inter-entity sub-team have proposed the use of a new approach (DOE-PAC) to address and automate the Billings and Collections. This approach would resemble the current Inter-Agency system of IPACs but would be used solely within DOE and solely by DOE and DOE Integrated Contractors.

On January 23, 2007, ORFSC and HQ staff held a meeting in Germantown to review the initial DOE-PAC Plan. In response to your request at the meeting, Oak Ridge has developed a Cost Benefit and Efficiency Analysis summary for the proposed process. This analysis supports the recommendation for the Department of Energy to proceed with the development and implementation of an automated and integrated DOE-PAC System to replace the current Inter Entity Cash process. DOE-PAC is intended to provide an automated tool for use by EFASC, ORFSC, and integrated contractors in performing their current payment, collection, and reconciliation responsibilities.

We have held meetings and teleconferences with various DOE and Integrated Contractor Financial community representatives. The Team requested input from EFASC, ORFSC, and several DOE Integrated Contractors. Comparison data on the current Cash process and proposed DOE-PAC process was requested and provided by ORFSC, EFASC, UT- Battelle, ORISE, and BWXT-Y12. Specifically, the data was used to develop a level of effort analysis of estimated hours per month for the current and new A/R and A/P processes. Data was compared, leveled, and extrapolated to arrive at an annualized projection of hours of effort required to function under the current versus new processes. A consistent standard hourly rate using the average mid-point range of the Rest of U.S. and D.C. Areas for a GS-12 or $35.35 per hour was applied to both current and new hours of processing time to arrive at the annualized cost savings.

The following table summarizes the results:

Summary Results of Cost Benefit and Efficiency					
Organization	**Function**	**Current DOE Process**	**DOE-PAC Process**	**Estimated Dollar Savings**	**Estimated DOE-PAC Percent Efficiency/ Gain**
DOE	Accounts Payable	$176.75 Per Invoice	$60.09 Per Invoice	$116.66 Per Invoice	66%
	Accounts Receivable	$17.68 Per Billing	$3.54 Per Billing	$14.14 Per Billing	80%
Integrated Contractors	Accounts Payable	$247,780 Per Year	$187,443 Per Year	$60,337 Per Year	24%
	Accounts Receivable	$453,369 Per Year	$249,999 Per Year	$206,371 Per Year	45%
A/P Combined Percent Efficiency Estimate				**45%**	
A/R Combined Percent Efficiency Estimate				**63%**	

While this analysis is not intended to be comprehensive for the Department, I believe it demonstrates that the proposed DOE-PAC system would result in significant savings in labor, processing and rework. Several other benefits seem clear from developing and adopting the proposed DOE-PAC process.

- Quality control of periodic Confirmation of Billings and Collections is not consistently performed under the current processes. Quality control is automated within the DOE-PAC process, creating efficiency and virtually eliminating the current confirmation issue under the current process.

- The DOE-PAC system will eliminate the need to track numerous collections within the Treasury Cash-Link System by the DOE and Integrated Contractor community.

- The real-time recording of payments and collections with DOE-PAC issuance will eliminate much of the year-end confirmation process.

- The automated posting of entries for both ORFSC and EFASC will eliminate significant data entry time and expense.

- The ability to expand system use to activity between DOE Integrated Contractors can bring about even greater savings.

The incremental cost of the DOE-PAC System development will be absorbed by virtue of using existing ORFSC in-house resources and support services. Some costs can be anticipated from the DOE and the Integrated Contractor implementations similar to those incurred with the existing inter-entity process. Implementation is estimated to require a lead time of approximately 60 days. We are seeking your support and approval to proceed with development. The next steps in development and implementation would be:

- Secure representation from the DOE financial community to assure system design meets user's needs.
- Develop a Plan of Actions and Milestones (POAM) for phased implementation
- Provide instructions and timelines to field offices for corrective action to the inter-entity work orders descriptive flexfield.

We recognize this project will require an extensive education of all parties involved in the process. On-line tutorials, written procedures, and briefings are planned to aid in implementation.

I would like to discuss this with you and the appropriate HQ & EFASC staff at the upcoming HQ/Field CFO meeting in order to obtain CFO support and approval to proceed with development and implementation of the DOE-PAC system.

Journal of Alloys and Compounds 390 (2005) 305–313

Journal of ALLOYS AND COMPOUNDS

www.elsevier.com/locate/jallcom

Effects of milling, doping and cycling of $NaAlH_4$ studied by vibrational spectroscopy and X-ray diffraction

S. Gomes[a], G. Renaudin[a], H. Hagemann[b], K. Yvon[a,*], M.P. Sulic[c], C.M. Jensen[c]

[a] *Laboratoire de Cristallographie, Université de Genève, 24 quai E. Ansermet, CH-1211 Geneva 4, Switzerland*
[b] *Département de Chimie Physique, Université de Genève, 30 quai E. Ansermet, CH-1211 Geneva 4, Switzerland*
[c] *Department of Chemistry, University of Hawaii, Honolulu, HI 96822, USA*

Received 15 August 2004; accepted 24 August 2004

Abstract

The effects of milling and doping $NaAlH_4$ with $TiCl_3$, TiF_3 and $Ti(OBu^n)_4$, and of cycling doped $NaAlH_4$ have been investigated by infrared (IR) and Raman spectroscopy and X-ray powder diffraction. Milling and doping produce similar effects. Both decrease the crystal domain size (∼900 Å for milled and ∼700 Å for doped, as compared to ∼1600 Å for unmilled and undoped $NaAlH_4$) and increase anisotropic strain (by a factor >2.5, mainly along *c*). They also influence structure parameters such as the axial ratio *c*/*a*, cell volume and atomic displacement amplitudes. They show IR line shifts by ∼15 cm^{-1} to higher frequencies for the Al–H asymmetric stretching mode ν_3, and by ∼20 cm^{-1} to lower frequencies for one part of the H–Al–H asymmetric bending mode ν_4, thus suggesting structural changes in the local environment of the $[AlH_4]^-$ units. The broad ν_3 bands become sharpened which suggests a more homogeneous local environment of the $[AlH_4]^-$ units, and there appears a new vibration at 710 cm^{-1}. The Raman data show no such effects. Cycling leads to an increase in domain size (1200–1600 Å), IR line shifts similar to doped samples (except for TiF_3: downward shift by ∼10 cm^{-1}) and a general broadening of the ν_3 mode that depend on the nature of the dopants. These observations support the idea that some Ti diffusion and substitution into the alanate lattice does occur, in particular during cycling, and that this provides the mechanism through which Ti-doping enhances kinetics during re-crystallisation.

Keywords: Hydrogen storage materials; Infrared and Raman spectroscopy; X-ray diffraction; Alanates

1. Introduction

Doping of sodium tetrahydrido aluminate ($NaAlH_4$) with titanium based catalysts such as $Ti(OBu^n)_4$, $TiCl_3$ and TiF_3 improves its hydrogen release properties [1–6]. The doping process usually consists of milling the alanate in the presence of few mole percent of catalysts. However, several studies indicate that milling $NaAlH_4$ in the absence of catalysts also improves hydrogen release [7–9]. Furthermore, there appears to exist an optimum milling time to introduce the dopant into the hydride, extended milling times leading to a spontaneous hydrogen loss [9]. Up to now, the mechanism of action of the Ti dopants has not been established. In particular, the location of titanium dopants has been a subject of a great deal of speculation and controversy. One school of thought has held that the remarkable enhancement of the hydrogen cycling kinetics in Ti doped $NaAlH_4$ is due to surface-localized catalytic species consisting of elemental titanium or a Ti–Al alloy [1,4,6,10]. Alternatively, it has been hypothesized that doping involves the substitution of titanium into the bulk of the hydride [11–13]. The present work represents an attempt to measure possible structural and microstructural changes in $NaAlH_4$ induced by milling, doping and cycling. For this purpose various samples of untreated, doped, milled and cycled hydrides and deuterides were investigated by using

* Corresponding author. Tel.: +41 22 379 62 31; fax: +41 22 379 68 64.
E-mail address: klaus.yvon@cryst.unige.ch (K. Yvon).

0925-8388/$ – see front matter © 2004 Elsevier B.V. All rights reserved.
doi:10.1016/j.jallcom.2004.08.036

vibration spectroscopy (IR and Raman) and X-ray powder diffraction.

2. Experimental

2.1. Preparation, milling, doping and cycling

Sodium aluminium hydride was obtained from Albemarle Corp. and recrystallized from tetrahydrofuran prior to use (samples 1–3 called "pure", see experiment Nos. 1–4 in Tables 1 and 4). The deuteride $NaAlD_4$ (>99% D, sample 4, see experiment No. 5 in Table 1) was synthesized by the literature method [14]. X-ray powder diffraction (XPD) analysis (see Table 1) indicated that the hydride samples were single phase while the deuteride sample contained ∼5 wt.% NaF and ∼25 wt.% metallic Al. Milling was performed by grinding the pure hydride and deuteride samples 2 and 4, respectively, in a ceramic mortar during 20 and 40 min in an argon filled glove-box (called "milled" samples thereafter, see experiment Nos. 6–9 in Tables 1 and 4). XPD analysis showed that these samples contained no new phases. Doping was performed by ball-milling the pure hydride samples 1 and 3 in the presence of $Ti(OBu^n)_4$ (2 and 6 mol%, Aldrich, purity 97%), $TiCl_3$ (2 mol%, Aldrich, purity 99.999%) and TiF_3 (6 mol%, Aldrich, purity 99%) as described in [2,15]. XPD analysis on these samples (called "doped" samples thereafter, see experiment Nos. 11–13 in Tables 1 and 4) revealed the presence of metallic Al (up to 7 wt.%) and TiF_3 (1 wt.%) for one doped sample (experiment No. 13). Cycling was performed on the 2 mol% doped sample 3 according to a dehydrogenation by heating at 160 °C for 5 h and a rehydrogenation upon standing under 100 bar of H_2 at 100 °C for 12 h (with three successive cycles). XPD analysis on these samples (called "cycled" samples thereafter, see experiment Nos. 14–16 in Tables 1 and 4) indicated the presence of the decomposition products Na_3AlH_6 (up to 35 wt.%), metallic Al (up to 12 wt.%) and NaCl (5 wt.%). Given the scarcity of spectroscopy literature on sodium hexahydrido-aluminate (only one reported Raman spectrum [16]) the compound was synthesized by the method of Huot et al. [17] and investigated by IR and Raman spectroscopy. The sample contained about 5 wt.% of NaH impurity. All measurements were performed within less than 1 month after sample preparation. Measurements performed a few months later confirmed that the samples changed their phase compositions over time, in particular the cycled ones for which the Na_3AlH_6 phase disappeared at the expense of metallic Al.

2.2. Raman and infrared spectroscopy

The Raman set-up used was the same as that described previously [18,19]. It consisted of an Argon ion laser (488 nm excitation wavelength) and a Kaiser Optical Holospec monochromator equipped with a liquid nitrogen cooled CCD camera. The spectral resolution was ∼3–4 cm^{-1}. Additional measurements were performed by using a Labram Raman microscope using 532 nm excitation. The samples were enclosed in sealed glass capillaries with a diameter Ø 1.0 mm by using a purified Ar filled glove-box. The Fourier transformation infrared (FT-IR) spectrometer used was a Paragon 1000 (Perkin-Elmer) equipped in attenuated total reflection (ATR) mode with the Golden Gate Single Reflection Diamond (P/N 10500 Graseby-Specac Series). The diamond crystal had a refractive index of 2.4 at 1000 cm^{-1}. The spectral resolution was 4 cm^{-1} and the spectral range 500–4400 cm^{-1}. The powder samples were pressed against the crystal with a calibrated strength in a purified Ar filled glove-box and protected by an airtight polyethylene film during measurement. Additional measurements in nujol suspension (prepared in a purified Ar filled glove-box and placed between two airtight NaCl plates) were done using a Bio-Rad Excalibur instrument, and KBr pellets (hand pressed in an inert atmosphere) using a Nicolet Nexus 470 FT-IR instrument. All spectra were recorded at room temperature. Both the Raman and infrared spectra were analysed by using the line fitting procedure with Lorentzian profile of the program SPECTRAW [20]. It should be noted that the Raman intensities observed for Na_3AlH_6 were much weaker than those for $NaAlH_4$.

2.3. X-ray powder diffraction (equipment and analysis)

The samples were analysed on a Huber Guinier Diffractometer 600 by using monochromatic Ge(1 1 1) Cu $K\alpha_1$ radiation. The system was equipped with a closed-cycle helium Helix Model 22 Refrigerator. The powders were mixed with an internal silicon standard and placed between two polyethylene terephtalate foils (Goodfellow) of 0.013 mm thickness. All manipulations were performed in a purified Ar filled glove-box. In view of the instability of the samples (especially the doped and cycled ones) and the long data acquisition times (>12 h) all measurements except one (experiment No. 4) were performed at 10 K (diffraction interval $10° < 2\theta < 100°$, step size $\Delta 2\theta = 0.02°$, counting time per step 10 s). Samples 1–3 were studied in order to check the reproducibility of the microstructural analysis, and one of these (sample 3) was investigated at room temperature in order to check if microstructural properties such as strain were intrinsic to the $NaAlH_4$ phase and not induced during cooling (experiment Nos. 3–4). The following microstructure parameters were extracted from the data by conventional Rietveld analyses (program Fullprof.2k [21]): average crystallite size and anisotropic strain from diffraction line broadening, and peak shift parameter Sh (related to stacking faults [21–23]) from the displacements of certain groups of reflections (see below). The diffraction profiles (both instrumental and sample intrinsic) were modelled by using a Thomson–Cox–Hastings pseudo-Voigt function [21] (convolutions between Gaussian and Lorentzian components having different full widths at half maximum, FWHM) to simulate the peak shapes of both $NaAlH_4$, Si and impurities phases when present. Structural

Table 1
Results of XPD analyses on pure, milled, doped and cycled alanate samples; strain anisotropy along *c*; pure $NaAlH_4$ refers to unmilled and undoped as-received samples; e.s.d.'s in parentheses

Experiment		Sample		Phase analysis	Structure analysis		Microstructure analysis		
No.	Temperature (K)	Sample	Treatment	Composition (wt.%)	*c*/*a*, *V* (Å^3)	Atomic displacements B_{Na} (Å^2), B_{Al} (Å^2)	Grain size (Å)	Strain (‰), anisotropy	Shift parameter Sh for (*h*,*k*,*l*), l = 4*n*
Pure alanates									
1	10	1	$NaAlH_4$, untreated	$NaAlH_4$ single phase	2.24231 (3), 279.116 (4)	4.08 (8), 3.77 (6)	1597 (1)	0.594, 0.062	−0.20 (2)
2	10	2	$NaAlH_4$, untreated	$NaAlH_4$ single phase	2.24222 (3), 279.258 (3)	4.37 (7), 3.87 (4)	1705 (1)	0.590, 0.142	−0.55 (2)
3	10	3	$NaAlH_4$, untreated	$NaAlH_4$ single phase	2.24239 (3), 279.142 (4)	4.17 (8), 3.92 (6)	1828 (1)	0.544, 0.128	0.07 (2)
4	295	3	$NaAlH_4$, untreated	$NaAlH_4$ single phase	2.25947 (3), 286.567 (3)	5.81 (7), 4.76 (5)	1770 (2)	0.439, 0.051	0.04 (2)
5	10	4	$NaAlD_4$, untreated	68 wt.% $NaAlD_4$, 27 wt.% Al, 5 wt.% NaF	2.24060 (8), 276.415 (7)	4.3 (2), 4.6 (1)	1038 (1)	0.883, 0.177	0.06 (4)
Milled alanates									
6	10	2	Milled 20 min	$NaAlH_4$ single phase	2.24315 (6), 279.228 (6)	4.7 (1), 4.25 (7)	918 (1)	1.676, 0.130	−0.07 (3)
7	10	2	Milled 40 min	$NaAlH_4$ single phase	2.24895 (9), 279.546 (8)	5.1 (1), 4.1 (1)	801 (1)	2.158, 0.255	0.19 (5)
8	10	4	Milled 20 min	68 wt.% $NaAlD_4$, 27 wt.% Al, 5 wt.% NaF	2.24114 (9), 276.394 (9)	5.0 (1), 4.6 (1)	767 (1)	1.587, 0.157	0.07 (5)
9	10	4	Milled 40 min	67 wt.% $NaAlD_4$, 28 wt.% Al, 5 wt.% NaF	2.2472 (2), 276.79 (2)	5.6 (3), 4.9 (2)	608 (1)	2.234, 0.459	−0.11 (6)
Doped alanates									
11	10	1	Doped, 6 mol% $Ti(OBu^n)_4$	$NaAlH_4$ single phase	2.24320 (6), 278.925 (6)	4.7 (1), 4.3 (1)	594 (1)	1.807, 0.105	−0.04 (4)
12	10	3	Doped, 2 mol% $TiCl_3$	93 wt.% $NaAlH_4$, 7 wt.% Al	2.24365 (6), 279.268 (6)	4.8 (1), 4.42 (7)	759 (1)	1.614, 0.249	−0.22 (3)
13	10	1	Doped, 6 mol% TiF_3	97 wt.% $NaAlH_4$, 2 wt.% Al, 1 wt.% TiF_3	2.24349 (8), 279.355 (9)	5.1 (2), 4.4 (1)	698 (1)	1.705, 0.185	−0.08 (5)
Cycled alanates									
14	10	3	Cycled, 2 mol% $Ti(OBu^n)_4$	56 wt.% $NaAlH_4$, 9 wt.% Al, 35 wt.% Na_3AlH_6	2.24295 (7), 279.130 (6)	3.1 (1), 6.1 (2)	1230 (2)	1.503, 0.091	−0.47 (3)
15	10	3	Cycled, 2 mol% $TiCl_3$	72 wt.% $NaAlH_4$, 12 wt.% Al, 11 wt.% Na_3AlH_6, 5 wt.% NaCl	2.24463 (6), 279.616 (6)	5.0 (1), 4.05 (7)	1124 (1)	0.931, 0.468	−0.35 (4)
16	10	3	Cycled, 2 mol% TiF_3	76 wt.% $NaAlH_4$, 9 wt.% Al, 15 wt.% Na_3AlH_6	2.24438 (5), 279.633 (5)	4.6 (1), 4.26 (7)	1606 (1)	1.601, 0.352	−0.09 (3)

parameters of the alanate structure were fixed at the values reported by Hauback et al. [24]: space group $I4_1/a$, Na in 4*a* (0, 1/4, 1/8), Al in 4*b* (0, 1/4, 5/8) and H in 16*f* (0.2372, 0.3836, 0.5469). This procedure was justified because subsequent refinements on milled, doped and cycled samples gave no evidence for significant changes in atom positions. The deconvolution by FullProf.2k allowed extracting the intrinsic line profile from the observed one provided the instrumental resolution function is known (from the adding of internal Si in each sample). Any increase of FWHM in the observed diffraction profile with respect to the instrumental FWHM was considered to be intrinsic to the sample. Isotropic average crystallite size and anisotropic strain effects were then separated and refined due to the distinct angular dependences of the Lorentzian and Gaussian components of the intrinsic line broadening. All samples have shown strain mainly directed along *c*. The peak shift parameter Sh was refined according to the expression $2\theta_{\text{shifted}} = 2\theta_{\text{Bragg}} + 2\text{Sh}\, d^2 \tan\theta \times 10^{-2}$ for reflections (*h*,*k*,*l*) with *l* = 4n. Although some values obtained during this work clearly differed from zero and thus provided evidence for the existence of stacking faults [21–23] this parameters will not be discussed in the text. The results (cell parameters, atomic displacement parameters, grain size, strain, Sh parameter) are summarized in Table 1.

3. Results and discussion

3.1. Pure $NaAlH_4$ and $NaAlD_4$

3.1.1. Structure

The cell parameters at 10 K and room temperature are consistent with those reported in previous work [11,14,24–28]. However, they show small but significant differences among the samples (up to 30 e.s.d.'s) that presumably reflect effects due to the sample preparation. For the hydride samples the cell volumes at 10 K vary between V = 279.12 (No. 1) and 279.26 Å^3 (No. 2) while the axial ratios vary between c/a = 2.2422 (No. 2) and 2.2424 (No. 3). The latter are bigger than for the deuteride sample (No. 5: c/a = 2.2406) and tend to increase with temperature (No. 4: c/a = 2.2595 at 295 K), i.e. the lattice expands mainly along *c*. As to the metal atom displacements they are clearly overestimated (B_{Na} = 4.1–4.4 Å^2, B_{Al} = 3.8–3.9 Å^2) but their relative values ($B_{\text{Na}} > B_{\text{Al}}$) are consistent with those reported (except for 8 K neutron data $B_{\text{Na}} < B_{\text{Al}}$ [24]) and increase as expected with temperature. The microstructural parameters change only little as a function of temperature. The average grain size of sample 3, for example, is slightly bigger at 10 K (1828 Å) than at room temperature (1770 Å), and its strain measured at 10 K (average value of 0.54‰ with an anisotropy of 0.13‰ mainly along *c*) is slightly bigger than that measured before at room temperature (average value of 0.44 ‰ with an anisotropy of 0.05‰). This suggests that cooling increases slightly strain and anisotropy. No literature data are available for comparison.

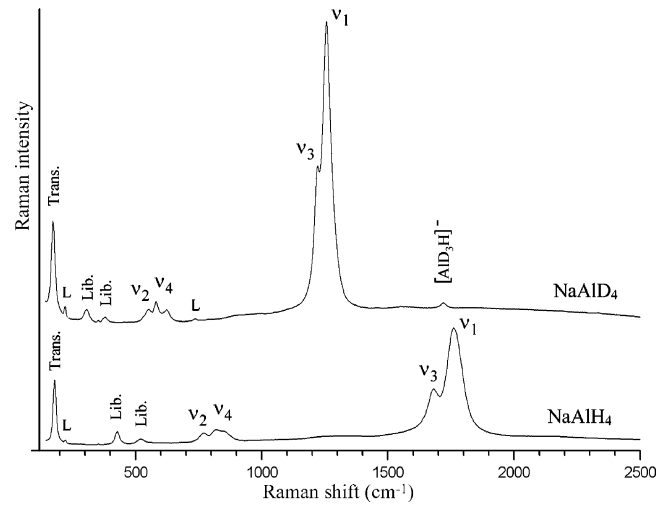

Fig. 1. Raman spectra at room temperature of $NaAlH_4$ and $NaAlD_4$. Lines labelled L are Laser plasma lines not belonging to the Raman spectrum; 'Trans.' and 'Lib.' indicate translation and libration modes, respectively.

3.1.2. Vibrations

The Raman and IR spectra are shown in Figs. 1 and 2, respectively, and compared with literature data on $NaAlH_4$ [29–33] and $NaAlD_4$ [30] in Tables 2 and 3. The Raman spectra of the hydride agree with those reported [29–32]. Those of deuteride reveal the expected isotope frequency shifts for the internal $[AlD_4]^-$ vibrations. The shifts for the external vibrations confirm recent [29] and previous assignments [31] to librational (429 and 521 cm^{-1}) and translational (180 cm^{-1}) modes. In addition, a weak band occurs at 1719 cm^{-1} that can be assigned to the Al–H stretching mode in a $[AlD_3H]^-$ moiety, indicating the presence of ca. 1–2% hydrogen impurity (relative to deuterium) in the deuterated sample. The occurrence of a single band in this region indicates the presence of a single Al–H bond length which is in agreement with the structural description of the $[AlH_4]^-$ moiety by a flattened tetrahedral polyhedron having S_4 site symmetry and a single H site [24].

The IR spectra are shown in Fig. 2 and the observed frequencies are collected in Table 3. All pure untreated samples gave exactly the same spectra (for this reason no indication about sample number are given). They are similar for preparations in KBr pellets and nujol mulls and agree with literature data [31–33]. The stretching bands around 1700 cm^{-1} are extremely broad (about 270 cm^{-1} with a large shoulder at the left). While their maximum can be assigned to the ν_3 $[AlH_4]^-$ asymmetric stretching band one should be aware that the spectra in this region may be complicated by a series of possible contributions. There are site and factor group splittings: the degenerate ν_3 mode of F_2 symmetry for the free ion (point group T_d) is split into $B + E$ contributions (site group S_4) which transform as $A_u + B_g + E_g + E_u$ in C_{4h} (factor group of the crystal). In addition, by analogy with observations for the analogous $[BH_4]^-$ ion [34], one can expect the presence of Fermi resonances involving overtones and combination bands of the lower frequency modes observed

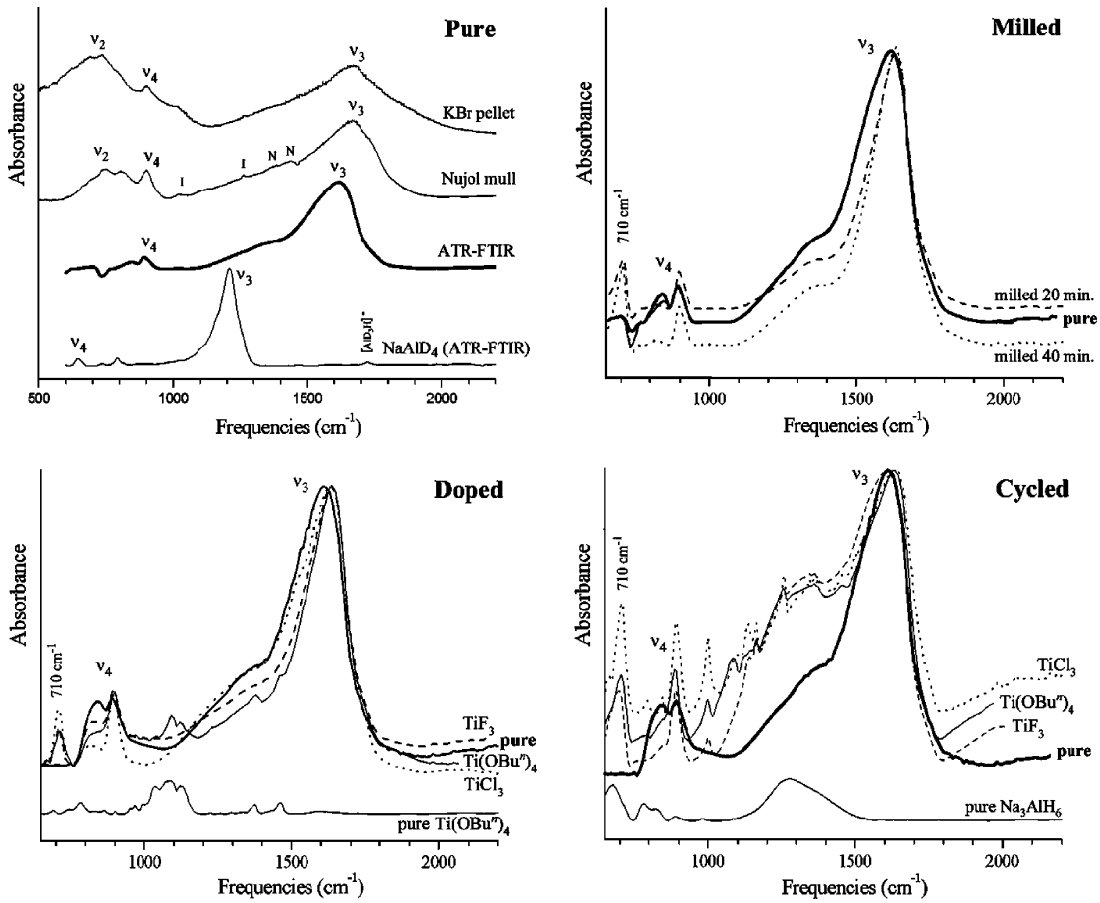

Fig. 2. Infrared spectra at room temperature. Top left: pure $NaAlH_4$ from different infrared spectrometers and comparison with $NaAlD_4$. Top right: milled $NaAlH_4$ (experiment Nos. 1, 6 and 7, ATR FT-IR mode). Bottom left: $NaAlH_4$ doped with various Ti-catalysts (experiment Nos. 1, 10–13, ATR FT-IR mode) and comparison with pure $Ti(OBu^n)_4$. Samples doped with 2 and 6 mol% $Ti(OBu^n)_4$ show the same spectra. Bottom right: cycled $NaAlH_4$ doped with various Ti-catalysts (experiment Nos. 1, 14–16, ATR FT-IR mode) and comparison with pure Na_3AlH_6.

Table 2
Raman frequencies (ω_i in cm^{-1}) of pure $NaAlH_4$ (sample 1) and $NaAlD_4$ (sample 4) at room temperature; ratio ω_i^H/ω_i^D calculated from data of this work (estimated errors $\pm 2\,cm^{-1}$)

ω_i	Pure $NaAlH_4$					Pure $NaAlD_4$		Ratio (ω_i^H/ω_i^D)
	[29]	[32]	[31]	[30]	This work	[30]	This work	
Translation	107	–	117	–	–			
	116	–	126	–	–			
	174	–	182	–	180		174	1.03
Libration	419	–	427	–	429	–	306	1.40
	511	–	520	–	521	–	379	1.37
ν_2	765	767	767	–	770	–	550	1.40
ν_4	812	824	816	772	817	572	582	1.40
	847	–	845	–	848	–	624	1.36
Combination bands	–	–	~1300	–	~1300	–	~940	1.38
	–	–	1520	–	–			
ν_3	1680	1686	1680	1665	1681	1208	1222	1.38
	–	–	1770	–	–	–	–	
ν_1	1769	1763	1815 (Sh)	1730	1762	1245	1257	1.40
$[AlD_3H]^-$						–	1719	

Sh: shoulder.

Table 3
Infrared frequencies (ω_i in cm^{-1}) of pure $NaAlH_4$ and $NaAlD_4$ at room temperature (estimated errors $\pm 2\,cm^{-1}$)

ω_i	Pure $NaAlH_4$						Pure $NaAlD_4$			Ratio (ω_i^H/ω_i^D)		
	Literature			This work			This work			This work		
	[32][a]	[31][b]	[33][a]	KBr pellet	Nujol mull	ATR	KBr pellet	Nujol mull	ATR	KBr pellet	Nujol mull	ATR
ν_2	688	–	680	690	690	–	500	–	–	1.38	–	–
	752	720	730	735	735		555	–	–	1.32	–	–
n.a.	–	800 (Sh)	–	800 (Sh)	805 (Sh)	–		–	–			
ν_4	–	–	–	–	–	845	–	–	–	–	–	–
	901	910	900	900	900	895	645	640	640	1.40	1.41	–
n.a.							740	740	735			
n.a.							790	795	790			
Combination bands	–	1000 (Sh)	–	∼1010 (Sh)	–	∼1250 (Sh)	–	–	–	–	–	
	–	–	–	∼1370 (Sh)	–	∼1370 (Sh)	–	–	∼1105 (Sh)	–	–	1.24
n.a.	–	–	–	–	–	–	–		∼1150 (Sh)			
ν_3	1678	∼1680	1680	1670	1675	1615	1225	1225	1210	1.37	1.37	1.33
n.a.	–	–	–	1850 (Sh)	1730 (Sh)	1730 (Sh)	–	1305 (Sh)	–	–	1.33	–
$[AlD_3H]^-$							1725	1725	1725			

Sh: shoulder; n.a.: unassigned bands.
[a] Nujol mull.
[b] KBr pellet.

between 680 and 900 cm^{-1}. The assignment of these lower frequency modes is not straightforward: there appear four bands at 690, 735, 800 (shoulder) and 900 cm^{-1}, while only three bands are expected ($A_u + E_u$) for ν_4, and A_u for ν_2. For these reasons, the assignments proposed in Tables 2 and 3 should be considered as tentative.

Surprisingly, the IR spectra obtained using the ATR set-up are quite different as they reveal a prominent shift of the ν_3 $[AlH_4]^-$ stretching band from 1670–1675 to 1615 cm^{-1}. It should be stressed that all samples were prepared in the same way. In view of our previous ATR FT-IR measurements on alkali borohydrides [18,19,34] that have always produced spectra comparable to those in the literature our sampling technique presumably did not lead to sample decomposition. There are two possible explanations for the frequency shift of ν_3:

(a) The complex permittivity at infrared frequencies of $NaAlH_4$ generates differences in ATR and transmission measurements [35].
(b) There occurs a high-pressure phase transition. High-pressure phases were theoretically predicted for $NaAlH_4$ (above 64.3 kbar [36]), experimentally found for the lithium analogue $LiAlH_4$ (tetragonal above 70 kbar and 373–673 K, and orthorhombic above 70 kbar and 773 K [37]). The latter showed a downward shift of the ν_3 $[AlH_4]^-$ stretching band. No such phases were observed for $NaAlH_4$ under similar conditions. Given that the samples in our ATR experiments were subjected to pressures of up to 3 kbar attempts were made to reduce the applied pressure by setting the dynamometric screw to a minimum estimated pressure of 500 bar. This value was in the upper range of typical pressures applied to prepare KBr pellets, but afterwards the pressure was released to obtain a free pellet for IR transmission measurements. However, the only apparent effect on the spectra was a change of intensity (the higher the value of the setting, the stronger the intensity) and no frequency shift could be established.

Since neither one of these two possibilities can be excluded at present, the ATR data will be considered separately from the other IR measurements.

3.2. Milled $NaAlH_4$

3.2.1. Structure

After 40 min of milling the axial ratios and cell volumes measured at 10 K increase significantly for both the hydride (experiment No. 7: c/a = 2.2490, V = 279.55 Å^3) and the deuteride (experiment No. 9: c/a = 2.2472, V = 276.79 Å). No literature data are available for comparison as yet. Interestingly, the displacement amplitudes of the metal atoms increase by up to 30% for Na and 7% for Al (B_{Na} = 5.6 and 4.3 Å^2, B_{Al} = 4.9 and 4.6 Å^2 for milled and unmilled deuteride, respectively, and B_{Na} = 5.1 and 4.4 Å^2, B_{Al} = 4.1 and 3.9 Å^2 for milled and unmilled hydride, respectively). Furthermore, the crystallite size decrease by a factor of ∼2 (800 Å for milled as compared to 1700 Å for unmilled $NaAlH_4$), while the strain increases by a factor of ∼3 (0.59‰) for pure $NaAlH_4$; 2.16‰ for 40′ milled $NaAlH_4$ (experiment Nos. 2, 6, 7 for hydride samples and Nos. 5, 8, 9 for deuteride sample). The anisotropy of strain increases weakly in a first step and strongly after extended milling time (from an average of 0.11‰ for the three pure samples to 0.13‰ for 20′ milled and 0.25‰ for 40′ milled $NaAlH_4$).

Table 4
Infrared frequencies (ω_i in cm^{-1}, measured with ATR FT-IR mode) of pure, milled, doped and cycled alanate samples (estimated errors $\pm 2\,cm^{-1}$); full width at half maximum (FWHM) are indicated for the ν_3 $[AlH_4]^-$ stretching band

	Experiment No.											
	1	6	7	10	11	12	13	14	15	16
	Sample 1 pure	Sample 2 milled 20 min	Sample 2 milled 40 min	Sample 3 doped, 2 mol% $Ti(OBu^n)_4$	Sample 1 doped, 6 mol% $Ti(OBu^n)_4$	Sample 3 doped, 2 mol% $TiCl_3$	Sample 1 doped, 6 mol% TiF_3	Sample 3 cycled, 2 mol% $Ti(OBu^n)_4$	Sample 3 cycled, 2 mol% $TiCl_3$	Sample 3 cycled, 2 mol% TiF_3
New vibration	–	710	710	710	710	710	710	705	710	700
ν_4	845	820	815	805	810	–	810	845	845	845
	895	895	895	895	895	895	895	890	890	890
Combination bands	~1250 (Sh)	~1250 (Sh)	~1250 (Sh)	~1250 (Sh)	~1250 (Sh)	~1250 (Sh)	~1250 (Sh)	–[a]	–[a]	–[a]
	~1370 (Sh)	~1370 (Sh)	~1370 (Sh)	~1370 (Sh)	~1370 (Sh)	~1370 (Sh)	~1370 (Sh)	–[a]	–[a]	–[a]
ν_3	1615	1630	1635	1630	1640	1635	1635	1635	1635	1605
	~1730 (Sh)	~1730 (Sh)	~1730 (Sh)	~1730 (Sh)	~1730 (Sh)	~1730 (Sh)	~1730 (Sh)	~1730 (Sh)	~1730 (Sh)	~1730 (Sh)
FWHM of ν_3 (cm^{-1})	270	200	180	180	160	240	180	210	220	250

Sh: shoulder.
[a] Unresolved bands due to presence of vibrations from secondary phases.

3.2.2. Vibrations

The ATR FT-IR spectra shown in Fig. 2 reveal an upward shift of the ν_3 $[AlH_4]^-$ stretching mode from 1615 to 1635 cm^{-1} (see Table 4). In addition one notices the appearance of a new band around 710 cm^{-1}, and a downward shift of one component of the ν_4 $[AlH_4]^-$ bending band (from 845 to ~820 cm^{-1}) with a decrease of its intensity. At the same time the broadening of the ν_3 $[AlH_4]^-$ stretching line decreases by about 30% (FWHM from 270 cm^{-1} for pure $NaAlH_4$ to 200 cm^{-1} for 20′ milled $NaAlH_4$ and 180 cm^{-1} for 40′ milled $NaAlH_4$). The upward shift of the ν_3 $[AlH_4]^-$ stretching band presumably correlates with the observed anisotropic cell expansion on milling and the slight modification of the sodium coordination of the $[AlH_4]^-$ units. Similar effects, although of smaller amplitude, were observed for the milled deuteride sample (not shown here). FT-IR measurements of pure $NaAlH_4$ in KBr pellets present a similar upward displacement of the ν_3 $[AlH_4]^-$ stretching band upon milling (as well as upon Ti-doping) by about 15 cm^{-1} (from ca. 1670 to 1685 cm^{-1}) as in the ATR measurement.

The Raman spectra show no significant changes upon milling. Due to the reduced particle size the elastic light scattering of the samples increases, thus yielding stronger laser plasma lines and weaker Raman spectra. Line fitting analyses suggest that the position and width of the ν_3 band at 1681 cm^{-1} remains unchanged within experimental error. In principle, one would expect IR and Raman spectra to be correlated, i.e. to observe similar shifts for the ν_3 band in both experiments. The fact that this is not the case here could be related to the very broad Al–H stretching bands that suggest the presence of strong couplings with low frequency (translational?) lattice modes. This allows for the possibility that in IR and Raman experiments we do observe different components (irreducible representations) stemming from the same ν_3 vibration but coupled by symmetry to a different low frequency mode, which in turn may behave differently upon milling, including perturbations generated by strain and surface modes that become increasingly important for nanocrystalline particles.

3.3. Doped and cycled $NaAlH_4$

3.3.1. Effects of doping

Doping leads to small but significant changes in cell parameters, atomic displacement amplitudes and microstructure. The axial ratio at 10 K generally increases (up to c/a= 2.2437 for $TiCl_3$, experiment No. 12) while the cell volume decreases for $Ti(OBu^n)_4$ (experiment No. 11: V = 278.93 Å^3) and increases for TiF_3 (experiment No. 13, V = 279.36 Å^3) and $TiCl_3$ (experiment No. 12, V = 279.27 Å^3). The increase of c/a is similar to that after milling, while the decrease in cell volume for $Ti(OBu^n)_4$ doping is opposite to that after milling. Only few literature data are available for comparison, such as those reported by Brinks et al. [25] (c/a = 2.2592 and V = 287.35 Å^3 for pure $NaAlH_4$, c/a = 2.2592

and V = 286.33 Å^3 for $TiCl_3$ doped hydride, c/a= 2.2595 and V = 286.36 Å^3 for TiF_3 doped hydride from synchrotron data at room temperature), and Sun et al. [11] (c/a = 2.2592 and V = 286.95 Å^3 for pure $NaAlH_4$, c/a = 2.2596–2.2634 and V = 286.45–289.25 Å^3 for several $Ti(OBu^n)_4$ doped hydride from X-ray powder diffraction at room temperature) that show the same tendency for the axial ratio but not for the volume changes. The metal atom displacements increase as with milling but to a larger extent (14–24% for B_{Na} in doped samples compared to 16% for milled hydride, and 13–16% for B_{Al} in doped samples compared to 5% for milled hydride), while the crystallite size decreases (600–760 Å) and the strain increases (experiment Nos. 11–13: 1.6–1.8‰) similar to milling. Finally, contrary to milling, Ti-doping leads to the formation of secondary phases such as Al (up to 8 wt.%, see Table 1) which implies a partial loss of hydrogen.

The Raman spectra of the doped samples are quite similar to those of the milled samples except that the signal-to-noise ratios of the latter are significantly lower because of their grey appearance. The spectra of the $Ti(OBu^n)_4$ doped sample reveal weak bands corresponding to unreacted $Ti(OBu^n)_4$. The IR spectra which are less sensitive to colouring also show similar features as milled samples: an upward shift and sharpening of the main ν_3 $[AlH_4]^-$ stretching band (see Fig. 2 and Table 4), a downward shift of one component of the ν_4 $[AlH_4]^-$ bending band, and the appearance of a new vibration at 710 cm^{-1}. The $TiCl_3$-doped sample shows a surprisingly broad main ν_3 $[AlH_4]^-$ stretching band (close to the value of the pure $NaAlH_4$).

3.3.2. *Effects of cycling*

Cycling leads to rather heterogeneous effects with respect to structure and vibrations. While the axial ratio increases for the cycled $TiCl_3$ doped sample (experiment No. 15: c/a = 2.2446) and for the cycled TiF_3 doped sample (experiment No. 16: c/a = 2.2444), it decreases for the cycled $Ti(OBu^n)_4$ doped sample (experiment No. 14: c/a = 2.2430). The atomic displacement amplitudes do not much change except those of the $Ti(OBu^n)_4$-doped sample (experiment No. 14) that decrease anomalously for sodium (B_{Na} = 3.1 Å^2) and increase for aluminium (B_{Al} = 6.1 Å^2). As expected, the average crystallite size increases strongly for all samples (1100–1600 Å^3) and comes close to that of undoped and unmilled samples. While the strain remains relatively unchanged its anisotropy changes as a function of dopants, being not far from isotropic for $Ti(OBu^n)_4$ and rather anisotropic for $TiCl_3$ and TiF_3. The IR spectra (see Fig. 2 and Table 4) reveal a downward shift of the main ν_3 $[AlH_4]^-$ stretching band by ∼20 cm^{-1} in the TiF_3-doped sample (experiment No. 16) and a broadening of the ν_3 $[AlH_4]^-$ stretching band that is difficult to quantify because of the possible contribution of the broad ν_3 band of Na_3AlH_6 at its left shoulder. Interestingly, the IR spectra of the $Ti(OBu^n)_4$ cycled experiment No. 14 still show the presence of the unreacted dopant after the cycling process.

4. Conclusion

The present study suggests that doping $NaAlH_4$ with Ti-based catalysts and milling $NaAlH_4$ in the absence of catalysts have similar effects on its structure and dynamics vibrations. Both treatments tend to increase the axial cell parameter ratios, cell volumes, atomic displacement amplitudes and strain and to decrease grain size. They lead to IR line shifts by ∼15 cm^{-1} to higher frequencies for the ν_3 asymmetric stretching mode, and by ∼20 cm^{-1} to lower frequencies for one part of the ν_4 asymmetric bending mode, thus suggesting small structural changes in the local environment of the $[AlH_4]^-$ units. The broad ν_3 bands become sharpened which suggests a more homogeneous local environment of the $[AlH_4]^-$ units, and there appears a new vibration at 710 cm^{-1}. The Raman data show no such effects. The effects for the doped samples depend only little on the nature of the catalyst. The only significant difference between milling and doping is the formation of Al metal and titanium halides during the latter. Cycling leads to a general re-crystallization and a less uniform behaviour with respect to structure and vibrations. In contrast to milling and doping its effects depend on the nature of the dopants. Cycling leads to a general increase in domain size (1100–1600 Å) and to a slight decrease in strain while the strain anisotropy increases except for the $Ti(OBu^n)_4$ doped sample. The shifts of the ν_3 asymmetric stretching mode in the IR spectra of cycled samples are similar to those of the doped samples except for the TiF_3 sample that shows a decrease by ∼30 cm^{-1} compared to the uncycled samples and a decrease by ∼10 cm^{-1} compared to the pure samples. The broadening of the ν_3 mode also depends on the nature of the dopant. It is strongest for the TiF_3 sample and not visible for the $TiCl_3$ sample for which ν_3 was already quite broad after doping. Altogether these observations suggest that cycling leads to a less uniform local environment of the $[AlH_4]^-$ units. The broadening of ν_3 in particular is consistent with the presence of Ti in the local environment of some of the $[AlH_4]^-$ units. Note that such an effect is less (or not) apparent in uncycled (doped) samples. This supports the idea that titanium diffusion and some substitution into the alanate lattice does occur, in particular during cycling, and that this provides the mechanism through which Ti-doping enhances kinetics during re-crystallisation [10,12,13,38]. However, before reaching a final conclusion and a more quantitative assessment of the various effects more systematic studies of doping and cycling are needed. Such experiments are under currently way.

Acknowledgments

This work was supported by the Swiss National Science Foundation (subsidy Marie Heim-Vögtlin) and the Swiss Federal Office of Energy. MPS and CMJ gratefully acknowledge the financial support for this research from the Office

of Hydrogen, Fuel Cells, and Infrastructure Technologies of the US Department of Energy. GR thanks Dr. Radovan Cerny for useful discussions concerning the Rietveld refinement of microstructural features.

References

[1] B. Bogdanovic, M. Schwickardi, J. Alloys Compd. 1 (1997) 253–254.
[2] C.M. Jensen, R.A. Zidan, N. Mariels, A. Hee, C. Hagen, Int. J. Hydrogen Energy 24 (1999) 461.
[3] R.A. Zidan, S. Takara, A.G. Hee, C.M. Jensen, J. Alloys Compd. 285 (1999) 119.
[4] B. Bogdanovic, M. Felderhoff, M. Germann, M. Härtel, A. Pommerin, F. Schüth, C. Weidenthaler, B. Zibrowius, J. Alloys Compd. 350 (2003) 246.
[5] M. Fichtner, J. Engel, O. Fuhr, O. Kircher, O. Rubner, Mater. Sci. Eng. B 108 (2004) 42.
[6] J.M. Bellosta von Colbe, B. Bogdanovic, M. Felderhoff, A. Pommerin, F. Schüth, J. Alloys Compd. 370 (2004) 104.
[7] A. Zaluska, L. Zaluski, J.O. Strom-Olsen, J. Alloys Compd. 298 (2000) 125.
[8] M.P. Balogh, G.G. Tibbetts, F.E. Pinkerton, G.P. Meisner, C.H. Olk, J. Alloys Compd. 350 (2003) 136.
[9] D.L. Anton, J. Alloys Compd. (2003) 356–357.
[10] G.J. Thomas, K.J. Gross, N.Y.C. Yang, C.M. Jensen, J. Alloys Compd. 330–332 (2002) 702.
[11] D. Sun, T. Kiyobayashi, H.T. Takeshita, N. Kuriyama, C.M. Jensen, J. Alloys Compd. 337 (2002) 8.
[12] T. Kiyobayashi, S.S. Srinivasan, D. Sun, C.M. Jensen, J. Phys. Chem. A 107 (2003) 7671.
[13] J. Iniguez, T. Yildirim, T.J. Udovic, M. Sulic, C.M. Jensen, Phys. Rev. B 70 (2004) 60101.
[14] J.P. Bastide, J. El Hajri, P. Claudy, A. El Hajbi, Synth. React. Inorg. Met.-Org. Chem. 25 (7) (1995) 1037.
[15] C.M. Jensen, R.A. Zidan, US Patent 6,471,935 (2002).
[16] J.C. Bureau, Z. Amri, P. Claudy, J.M. Létoffé, Mater. Res. Bull. 24 (1989) 23.
[17] J. Huot, S. Boily, V. Guther, R. Schultz, J. Alloys Compd. 283 (1999) 304.
[18] S. Gomes, H. Hagemann, K. Yvon, J. Alloys Compd. 346 (2002) 206.
[19] H. Hagemann, S. Gomes, G. Renaudin, K. Yvon, J. Alloys Compd. 363 (2004) 126.
[20] D. Lovy, PROGRAM SPECTRAW, Version 1.40, Dépt. de Chimie Physique, University of Geneva, 1996.
[21] J. Rodriguez-Carvajal, PROGRAM Fullprof.2k, Version 2.45, Laboratoire Léon Brillouin (CEA-CNRS), France, July 2003 (Fullprof.2k manual available on http://www-llb.cea.fr/fullweb/fp2k/fp2k_divers.htm). See also J. Rodriguez-Carvajal, T. Roisnel, EPDIC-8, 23–26 May 2002. Trans. Tech. Publication Ltd., Uppsala, Sweden, Materials Science Forum 123 (2004) 443–444.
[22] E.J. Mittemeijer, P. Scardi (Eds.), Diffraction Analysis of the Microstructure of Materials' Springer Series in Materials Science, vol. 68, Springer-Verlag, Berlin, 2004.
[23] B.E. Warren, X-Ray Diffraction, Dover, New York, 1990.
[24] B.C. Hauback, H.W. Brinks, C.M. Jensen, K. Murphy, A.J. Maeland, J. Alloys Compd. 358 (2003) 142.
[25] H.W. Brinks, C.M. Jensen, S.S. Srinivasan, B.C. Hauback, D. Blanchard, K. Murphy, J. Alloys Compd. 376 (2004) 215.
[26] V. Ozolins, E.H. Majzoub, T.J. Udovic, J. Alloys Compd. 375 (2004) 1.
[27] V.K. Bel'skii, B.M. Bulychev, A.V. Golubeva, Russ. J. Inorg. Chem. 28 (1983) 1528.
[28] K.J. Gross, S. Gurthrie, S. Takara, G. Thomas, J. Alloys Compd. 297 (2000) 270.
[29] D.J. Ross, M.D. Halls, A.G. Nazri, R.F. Aroca, Chem. Phys. Lett. 388 (2004) 430.
[30] A.P. Kurbakova, L.A. Leites, V.V. Gavrilenko, Yu.N. Karaksin, L.I. Zakharkin, Spectrochim. Acta A 31 (1975) 281.
[31] J.C. Bureau, J.P. Bastide, B. Bonnetot, H. Eddaoudi, Mater. Res. Bull. 20 (1985) 93.
[32] A.E. Shirk, D.F. Shriver, J. Am. Chem. Soc. 95 (18) (1973) 5904.
[33] T.G. Adiks, V.V. Gavrilenko, L.I. Zakharkin, L.A. Ignat'eva, Z. Prikladnoi Spektroskopii 6 (6) (1967) 806.
[34] G. Renaudin, S. Gomes, H. Hagemann, L. Keller, K. Yvon, J. Alloys Compd. 375 (2004) 98.
[35] K. Yamamoto, H. Ishida, Vib. Spectrosc. 8 (1994) 1.
[36] P. Vajeeston, P. Ravindran, R. Vidya, H. Fjellvag, A. Kjekshus, Appl. Phys. Lett. 82 (14) (2003) 2257.
[37] B.M. Bulychev, V.N. Verbetskii, K.N. Semenenko, Russ. J. Inorg. Chem. 22 (11) (1977) 1611.
[38] K.J. Gross, E.H. Majzoub, S.W. Spangler, J. Alloys Compd. 423 (2003) 356–357.

Journal of Alloys and Compounds 377 (2004) 283–289

Journal of ALLOYS AND COMPOUNDS

www.elsevier.com/locate/jallcom

Long term cycling behavior of titanium doped $NaAlH_4$ prepared through solvent mediated milling of NaH and Al with titanium dopant precursors

Sesha S. Srinivasan [a], Hendrik W. Brinks [b], Bjorn C. Hauback [b], Dalin Sun [a,1], Craig M. Jensen [a,*]

[a] *Department of Chemistry, University of Hawaii, 2545 The Mall, Honolulu, HI 96822, USA*
[b] *Department of Physics, Institute for Energy Technology, P.O. Box 40, N-2027 Kjeller, Norway*

Received 6 January 2004; accepted 22 January 2004

Abstract

A simple and an efficient synthesis route, solvent mediated milling of NaH and Al with 2 mol% of the dopant precursor, $Ti(OBu)_4$ followed by hydrogenation, has been developed and employed to synthesize Ti-doped $NaAlH_4$. The long-term hydrogenation and dehydrogenation, up to 100 cycles were carried out systematically. Reversibility of about 3.4 wt.% hydrogen release was obtained during the first dehydrogenation (160 °C) run after the initial hydrogenation of Ti-doped (NaH + Al) at 150 °C; ∼11.4 MPa H_2 for 12 h. In the subsequent cycles, the storage capacity increased, reaching an optimum of 4.0 wt.%. This capacity was retained for 40 cycles with the dehydrogenation kinetic curves showing remarkable reproducibility. Comparison of the X-ray diffraction profiles of Ti-doped (NaH + Al) from initial and final stages of the cycling study reveals a growing resistance to the hydrogenation of Na_3AlH_6 to $NaAlH_4$.

Keywords: Hydrogenation; Dehydrogenation; Cycling stability; Solvent mediated milling; Hydrogen storage capacity; Sodium aluminum hydride; Hydrogen absorbing materials; Metal hydrides; Mechanochemical processing; Gas–solid reactions

1. Introduction

Alkali and alkaline earth metal based complex aluminum hydrides, $MAlH_4$ [M = Na, Li, K] and $Mg(AlH_4)_2$, have been found to have great potential as viable modes of storing hydrogen at moderate temperatures and pressures. These hydrides have been demonstrated to have higher hydrogen storage capacities at moderate temperatures and lower cost than conventional intermetallic metal hydride systems such as AB_5H_6, ABH_2, AB_2H_3, and A_2BH_{4-6} [1,2]. Among the various alkali based complex hydrides investigated in the recent years [3–38], titanium doped sodium aluminum hydride; $NaAlH_4$, has shown the greatest promise as a reversible hydrogen storage material.

The decomposition reactions of Ti-doped $NaAlH_4$ to $NaH + Al + 3/2H_2$ with intermediate stage $1/3Na_3AlH_6 + 2/3Al + H_2$ have been investigated extensively on the basis of structural phase determination [10,16,34–37] and the release of hydrogen [3–8,11,17–21,28,38]. However, fewer studies have focused on the hydrogenation of mixtures of Na/Al or NaH/Al to $NaAlH_4$. Ashby and co-workers [39–41], accomplished the synthesis of $NaAlH_4$ by reacting sodium under high hydrogen pressure (10–35 MPa) and temperature (140–160 °C) with an aluminum alkyl catalyst in the solvent, tetrahydrofuran (THF), for several hours. Dymova et al. [42] found that, in absence of solvent medium, a temperature of at least 280 °C and a hydrogen pressure of 17–18 MPa were necessary to accomplish this transformation. The high temperature was required to attain a liquid state of sodium. Bogdanovic and Schwickardi [43] successfully demonstrated the preparation of Ti-doped $NaAlH_4$ by hydrogenating (∼33 cycles) NaH powder and Al grindings with $Ti(OBu)_4$ as the dopant precursor. However, their synthesis process involves a complicated purification procedure

* Corresponding author. Tel.: +1-808-956-2769; fax: +1-808-956-5908.
E-mail address: jensen@gold.chem.hawaii.edu (C.M. Jensen).
[1] Present address: Department of Materials Science, Fudan University, 220 Handan Road, Shanghai 200433, PR China.

0925-8388/$ – see front matter © 2004 Elsevier B.V. All rights reserved.
doi:10.1016/j.jallcom.2004.01.044

of NaH and Al grindings and a catalyst doping mechanism prior to the hydrogenation. Recently, Majzoub and Gross demonstrated an *indirect Ti-doping method*, where $TiCl_2/TiCl_3$ dopant was pre-reacted with LiH by mechanical milling [44,45]. The resulting powder was then milled with 6 mol% of (NaH + Al) mixture. This method of producing $NaAlH_4$ adds extra weight to the sample due to the addition of LiH. Also, they did not report the long-term cycling behavior of the dopant precursors. For an ideal hydrogen storage material, the cycling stability and the overall weight of the sample must be evaluated, but work on these aspects is sparsely reported. Moreover, the role of titanium dopant on the cycling characteristics of $NaAlH_4$ is not easily intelligible.

We therefore have explored means of improving Bogdanovic's preparation of Ti-doped $NaAlH_4$ through simple milling of NaH and Al with $Ti(OBu)_4$. Our approach resembles Ashby's simple and efficient, solvent mediated hydrogenation of mixtures of NaH and Al, that is basis of the commercial manufacture of $NaAlH_4$ by Albemarle Corp. However, our process is mediated by the presence of only a minimal amount of solvent during milling with the dopant precursor and does not require an alkyl aluminum catalyst. The dehydrogenation performance in the first few cycles of the Ti-doped $NaAlH_4$ prepared through this process is markedly improved compared to the materials obtained through dry milling route. We have also carried out the hydrogenation and dehydrogenation up to 100 cycles and the kinetic features were correlated with the observed structural characteristics of Ti-doped (NaH + Al) in the initial and final stages of cycling.

2. Experimental details

2.1. Materials and method

Titanium butoxide $Ti(OBu)_4$, NaH (95% dry) and Al (99.95%, −200 mesh) were obtained from Aldrich Chemical Co. and used as received. Sodium hydride and aluminum (1:1 mole ratio) were loaded into a chrome–nickel stainless steel bowl (250 ml) with balls (10 mm) under nitrogen filled glove box. The weight ratio between the balls and the powder was 20:1. Approximately 100 ml of distilled pentane was injected into the bowl and the lid was covered tightly with foil. The assembly was then transferred to Fritsch Pulverisette 6 planetary mill. The milling was carried out at a speed of 300 rev/min with two rotations of forward and reverse directions for 30 min each, totaling 60 min. Immediately after the completion of milling, the bowl containing the milled sample was transferred to the glove box and filtered to separate the (NaH + Al) mixture from the solvent under nitrogen ambient. The yield of the milled sample obtained was ∼95% in the form of slurry. The successive step of adding and blending 2 mol% of $Ti(OBu)_4$ [called as Ti-doped hereafter] to the slurry, using a syringe, was carried out and this blended mixture was milled in a same manner described above for only 5 min. The Ti-doped (NaH + Al) mixture thus obtained was dried in the glove box and then loaded (0.5 g) in a stainless steel reactor for hydrogenation and dehydrogenation studies. For the dry milling process, (NaH + Al) mixture was blended with $Ti(OBu)_4$ and milled under a nitrogen atmosphere for 2 h with the same milling parameters mentioned above.

2.2. Hydrogenation and dehydrogenation cycling measurements

The hydrogenation and dehydrogenation cycling was performed using a Sieverts type volumetric apparatus [LESCA Co., Japan], which allowed for the accurate volumetric determination of the amount of hydrogen evolved. Rapid heating of the sample to the desired temperature was accomplished by immersing the sample reactor into a pre-heated silicon oil bath (accuracy of ±1 °C). The cycling studies were performed by repeated hydrogenation (150–120 °C, ∼11.5 MPa, 12 h) and dehydrogenation (160 °C, against 0.1 MPa for 3 h). The hydrogen capacity is presented in terms of wt.% and normalized to the weight of $NaAlH_4$ without including the weight of the catalyst.

2.3. Structural (PXD) characterization

The powder X-ray diffraction of Ti-doped (NaH + Al) before and after 100 cycles were performed using Swiss-Norwegian beam line (station BM1B) at the European Synchrotron Radiation Facility (ESRF), Grenoble, France. The sample was loaded in a 0.5 mm boron–silica–glass capillary. The wavelength of the X-ray used was 0.50024 Å at 22 °C from channel-cut Si(1 1 1) monochromator. The measurement of intensity was done with the step scan rate of $\Delta(2\theta) = 0.003$–$0.005°$. Rietveld refinement of the X-ray diffraction profiles of the Ti-doped (NaH + Al) was carried out using Fullprof software [46].

3. Results

3.1. Dehydrogenation kinetics and cycling stability

The experimental parameters, such as the pressure and temperature of hydrogenation and dehydrogenation temperature with the hydrogen capacity obtained, are listed in Table 1.

Fig. 1 represents the dehydrogenation kinetic curves of Ti-doped $NaAlH_4$, prepared from the solvent mediated milling and hydrogenation of Ti-doped (NaH + Al). These curves were plotted by calculating the total release of hydrogen in terms of weight percentage with respect to the dehydrogenation time. The release of hydrogen at 160 °C under 0.1 MPa corresponds to 3.4 wt.% during the initial dehydrogenation run. In the subsequent cycles, the hydro-

Table 1
Total released hydrogen capacity with ongoing hydrogenation and dehydrogenation cycling of Ti-doped $NaAlH_4$, prepared through solvent mediated milling and subsequent hydrogenation of Ti-doped (NaH + Al)

Cycle(s) number	Hydrogenation pressure (MPa)	Hydrogenation temperature (°C)	Dehydrogenation temperature (°C)	Hydrogen capacity (wt.%)
1–4	~11.50	150	160	3.74[a]
5–40	~11.40	120	160	4.0[a]
41–100	~11.35	120	160	3.5[a]

[a] Average value.

gen capacity increased attaining an optimum capacity of 4.0 wt.% in the fourth dehydrogenation run. This value corresponds to 70% of the hydrogen capacity calculated according to Eq. (1):

$$NaH + Al + 3/2H_2 \leftrightarrow NaAlH_4 \quad (1)$$

Also, the release of hydrogen occurs in two stages, which is represented by a bifurcated broken line as shown in Fig. 1. This clearly indicates that the dehydrogenation of (Ti-doped) $NaAlH_4$ follows the known two-step reactions given by Eq. (2):

$$NaAlH_4 \leftrightarrow 1/3Na_3AlH_6 + 2/3Al + H_2$$
$$\leftrightarrow NaH + Al + 3/2H_2 \quad (2)$$

The release of hydrogen in the first four-dehydrogenation runs of the Ti-doped $NaAlH_4$, obtained from the dry milling of Ti-doped (NaH + Al) is shown in Fig. 2. The dehydrogenation kinetics and the total release of hydrogen from the Ti-doped $NaAlH_4$ obtained from the solvent mediated milling process (see Fig. 1) was markedly improved compared to the material prepared through dry milling route (see Fig. 2).

The dehydrogenation kinetic curves of Ti-doped $NaAlH_4$ at 160 °C between the 5th and 40th cycles are shown in Fig. 3. It is interesting to note that the storage capacity of about 4.0 wt.% was maintained on an average in these cycles. This capacity was retained with dehydrogenation kinetic curves showing remarkable reproducibility. The two-step decomposition is indicated in Fig. 3 by a broken bifurcated line.

The amount of hydrogen discharged during the 100 cycles of these kinetic studies of Ti-doped $NaAlH_4$ is shown in Fig. 4. It is to be mentioned that the storage capacity of 3.4 wt.% was obtained in the very first dehydrogenation run and increased with increasing number of cycles. An optimum hydrogen capacity of about 4.0 wt.% was obtained

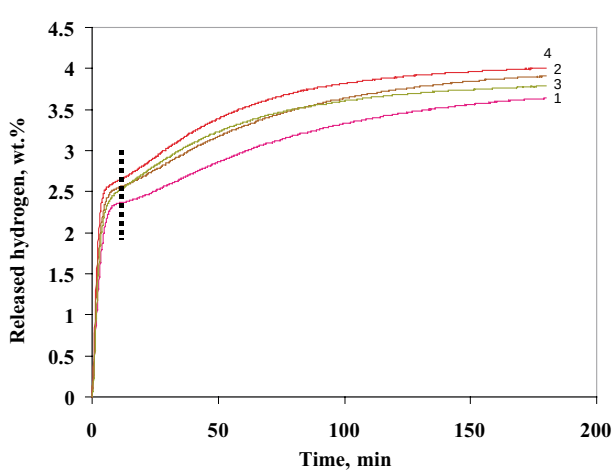

Fig. 1. The dehydrogenation kinetic curves of Ti-doped $NaAlH_4$ as prepared from the solvent mediated milling of Ti-doped (NaH+Al) at 160 °C, 0.1 MPa.

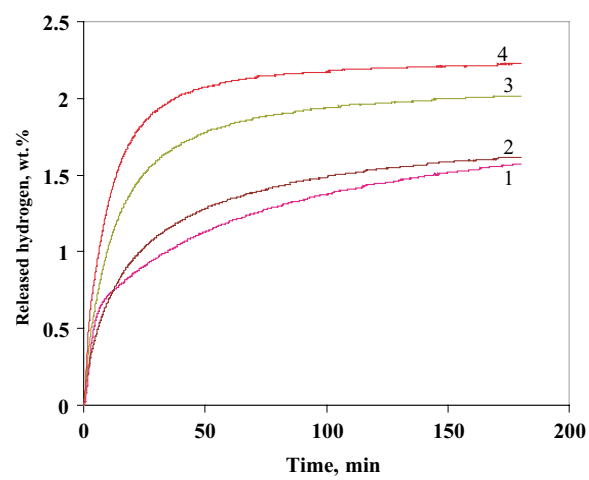

Fig. 2. The dehydrogenation kinetic curves of Ti-doped $NaAlH_4$ as prepared from the dry milling of Ti-doped (NaH + Al) at 160 °C, 0.1 MPa.

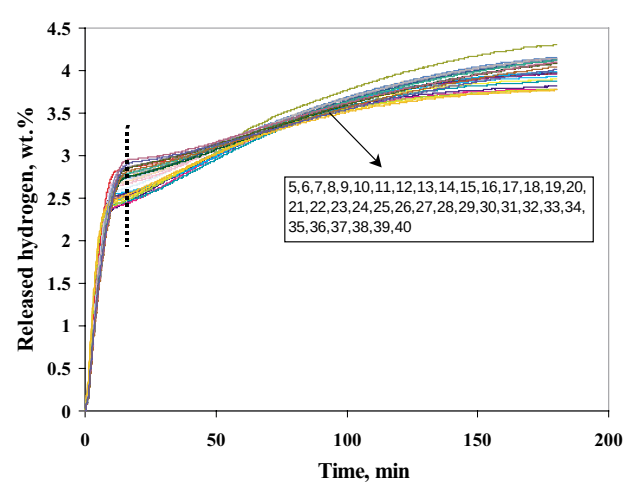

Fig. 3. The group of dehydrogenation kinetic curves of Ti-doped $NaAlH_4$ from 5 to 40 cycles at 160 °C, 0.1 MPa.

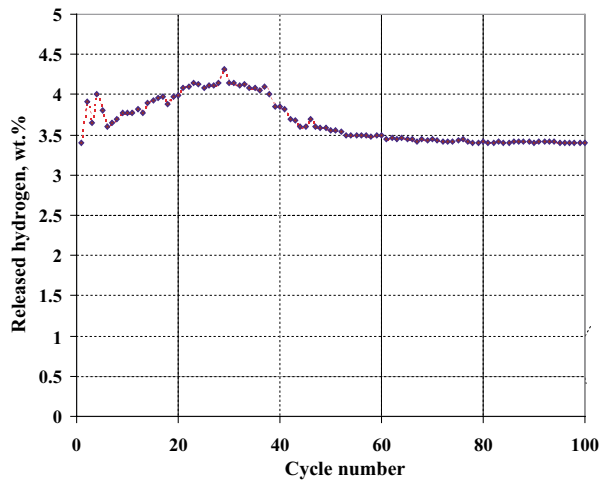

Fig. 4. The release of hydrogen (wt.%) vs. number of cycles.

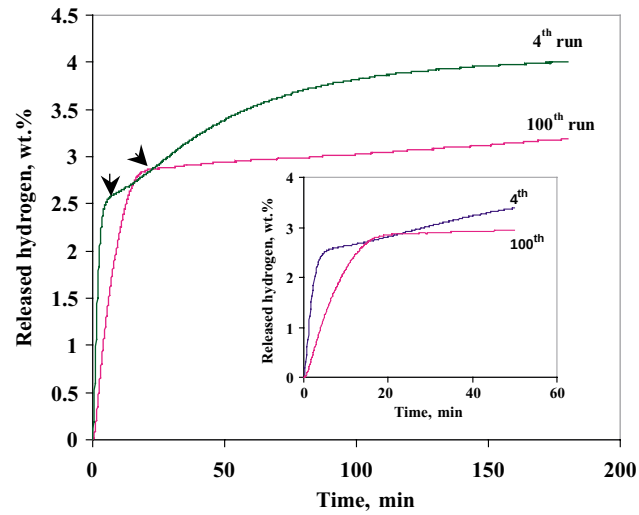

Fig. 5. Comparative kinetic curves of 4th and 100th dehydrogenation runs of Ti-doped $NaAlH_4$. The small scale drawing of the graph is represented in the inset.

in the fourth dehydrogenation run. A capacity of 4.3 wt.% was achieved in 29th cycle and an average total capacity of 4.0 wt.% was maintained up to 40 cycles. At the end of the 100th cycle, the hydrogen capacity was slightly reduced from 4.0 to 3.5 wt.%. Comparative dehydrogenation kinetic curves of 4th and 100th cycles are depicted in Fig. 5. The junction between the two-step dehydrogenation reactions for these extreme cycles was marked by an arrow and also shown with smaller scale in the inset of Fig. 5.

3.2. Structural (PXD) characterization

Powder X-ray diffraction characterizations using synchrotron radiation were carried out on the samples of Ti-doped (NaH + Al) before and after 100 cycles. Fig. 6 represents the PXD pattern of the Ti-doped (NaH + Al) before undergoing hydrogenation and dehydrogenation cycling experiments. The Rietveld profile fitting (refinement) was employed and the peaks were identified as NaH and Al. No other impurities or Ti/Ti–Al inflection peaks were traced out. The concentration, in mol%, of each phase and their corresponding lattice parameters obtained from the refinement are given in Table 2.

The PXD fitting profile of Ti-doped (NaH + Al) at the 100th dehydrogenation cycle is shown in Fig. 7. An addi-

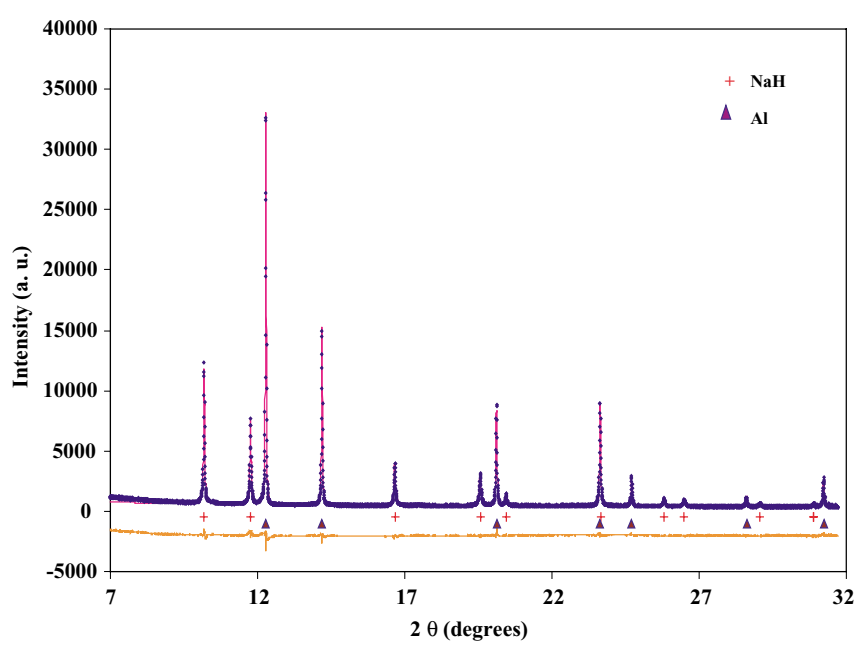

Fig. 6. PXD profile fitting of the Ti-doped (NaH + Al) mixture before hydrogenation–dehydrogenation cycling. The solid circle and the line are the observed and calculated intensities, respectively. The difference pattern is shown at the bottom.

Table 2
The phase composition in mol% and corresponding lattice constant values determined using synchrotron powder X-ray diffraction and Rietveld profile refinement

Sample	Concentration (mol%)				Lattice constants (Å)			
	NaH	Al	Na_3AlH_6	NaCl	NaH	Al	Na_3AlH_6[a]	NaCl
Ti-doped NaH + Al before cycling	57.1	42.9			4.88136	4.04991		
Ti-doped NaH + Al after 100 cycling	35.3	54.6	8.7	1.3	4.88003	4.04904	5.41014 5.53615 7.75615	5.64154

[a] Unit cell volume of Na_3AlH_6: 232.306 Å^3.

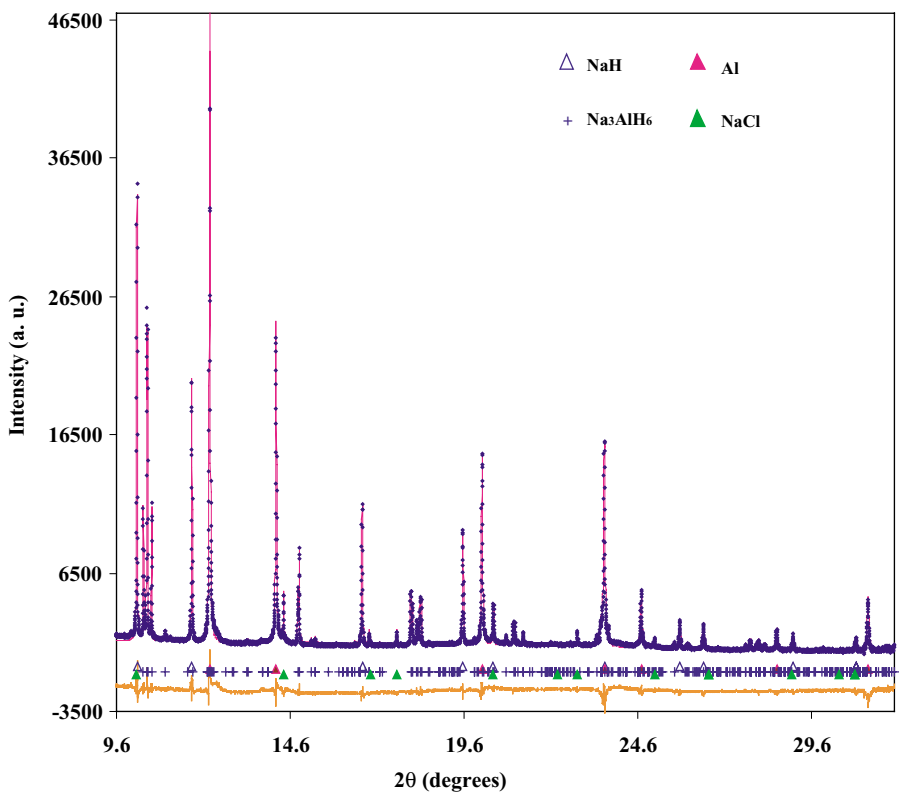

Fig. 7. PXD pattern of Ti-doped (NaH + Al) after the completion of 100 cycles.

tional reflection corresponds to Na_3AlH_6 and NaCl was observed in addition to NaH and Al. The amount of NaCl or NaCl-related structure was very small (less than 2 mol%), and hence it is negligible from the present discussion.

4. Discussion

The long term cycling studies of Ti-doped $NaAlH_4$ and its structural correlation were discussed in this section. The PXD pattern of the elemental mixture Ti-doped (NaH + Al) shows no extra reflections of impurities and ensures the correct stoichiometric ratio of NaH:Al (see Table 2). This mixture was hydrogenated under high-pressure and the cycling experiments were further carried out. The initial dehydrogenation of Ti-doped $NaAlH_4$ at 160 °C exhibits the fast kinetics of the first and second steps and the total hydrogen release estimated was 3.4 wt.% (Fig. 1). In the consecutive hydrogenation and dehydrogenation cycles, the capacity was increased and attained an optimum of 4.0 wt.% in the 40th cycle. The contribution of the second reaction as per Eq. (2), i.e. Na_3AlH_6 to NaH, to the total effective hydrogen capacity was found in these cycles (Fig. 3). The storage capacity decreased from 4.0 to 3.5 wt.%, between the 40th and 100th cycle (Fig. 4). This results from the partial reversibility of the two-step reaction, which is in accordance with the hypothesis proposed by Kiyobayashi et al. [38]. According to their theory, the delocalization of titanium catalyst may be the cause for the poor dehydrogenation rate of Na_3AlH_6, which in turn affects the overall hydrogen capacity. The comparative dehydrogenation curves of Fig. 5 reveal the following features: (i) the kinetics of the first step of dehydrogenation reaction has been reduced; (ii) the second dehydrogenation reaction proceeds to a significantly reduced extent. The PXD

studies of the Ti-doped (NaH + Al) after 100 cycles show the presence of an additional phase related to the Na_3AlH_6 structure besides the starting mixture (NaH + Al). The presence of Na_3AlH_6 indicates that the reaction of Eq. (2) is not complete and also supports the argument of Majzoub and Gross [44]. However, formation of crystalline Ti or $TiAl_3$ intermetallic phase was not observed in this 100-cycle measurement. This is in agreement with the recent finding that after 7 cycles, ∼ 1/3 of the Ti is present as $Al_{0.93}Ti_{0.07}$ and that the remainder of the Ti is apparently present in a highly dispersed fashion in the host lattice [47].

5. Conclusion

A simple and efficient synthesis method, solvent mediated milling and hydrogenation, was developed and employed in order to prepare Ti-doped $NaAlH_4$ from the basic materials, NaH and Al in the presence of $Ti(OBu)_4$. Unlike Bogdanovic's approach [43], this method does not involve complicated purification of NaH/Al and doping procedures prior to hydrogenation. Also our synthesis requires no precursor formation, which was earlier adopted by Gross et al. [45]. The dehydrogenation kinetic measurements of Ti-doped $NaAlH_4$, obtained from solvent mediated milling and subsequent hydrogenation of Ti-doped (NaH + Al) were carried out at a constant temperature of 160 °C under 0.1 MPa for up to 100 cycles. A release of 3.4 wt.% of hydrogen capacity was obtained in the very first dehydrogenation run. In the subsequent cycles, the capacity increased and optimum hydrogen storage of about 4.0 wt.% was achieved by the fourth dehydrogenation run. This capacity remained through 40 cycles. Significant decrease in the capacity from 4.0 to 3.5 wt.% was observed at the end of the 100th cycle. Synchrotron powder X-ray diffraction and Rietveld profile fitting analysis of Ti-doped (NaH + Al) after 100 cycles showed the presence of additional phases which are apparently linked to the observed diminishing dehydrogenation characteristics. Decreases in dehydrogenation kinetics and the total amount of released hydrogen over a number of cycles will be interpreted as follows: the appearance of the phase, Na_3AlH_6 in the prolonged cycling samples, indicates a reduced effectiveness of the Ti-dopant for the hydrogenation of Na_3AlH_6 to $NaAlH_4$. This may be due to delocalization of titanium dopant, which hinders the release of hydrogen from the hexahydride (Na_3AlH_6) phase. Further work is under progress to achieve the high hydrogen capacity with ongoing cycling by optimizing the experimental conditions and adopting new processing such as re-grinding and manipulating the dopant concentration.

Acknowledgements

We gratefully acknowledge support of this research from the Office of Hydrogen, Fuel Cells, and Infrastructure Technologies of the US Department of Energy and the New Energy and Industrial Technology Development Organization (NEDO) as a part of the International Clean Energy Network using Hydrogen Conversion (WE-NET) program with funding from the Ministry of Economy, Trade and industry of Japan.

References

[1] L. Schlapbach, A. Zuttel, Nature 414 (2001) 353.
[2] A.J. Maeland, Int. J. Hydrogen Energy 28 (2003) 821.
[3] B. Bogdanovic, M. Schwickardi, J. Alloys Comp. 253–254 (1997) 1.
[4] B. Bogdanovic, M. Schwickardi, International Patent, WO97/03919 (1997).
[5] C.M. Jensen, R.A. Zidan, N. Mariels, A.G. Hee, C. Hagen, Int. J. Hydrogen Energy 23 (1999) 461.
[6] R.A. Zidan, S. Takara, A.G. Hee, C.M. Jensen, J. Alloys Comp. 285 (1999) 119.
[7] B. Bogdanovic, R.A. Brand, A. Marjanovic, M. Schwickardi, J. Tolle, J. Alloys Comp. 302 (2000) 36.
[8] A. Zaluska, L. Zaluski, J.O. Strom-Olsen, J. Alloys Comp. 298 (2000) 125.
[9] V.P. Balema, K.W. Dennis, V.K. Pecharsky, Chem. Commun. (2000) 1665.
[10] K.J. Gross, S. Guthrie, S. Takara, G. Thomas, J. Alloys Comp. 297 (2000) 270.
[11] C.M. Jensen, K.J. Gross, Appl. Phys. A 72 (2001) 213.
[12] J. Chen, N. Kuriyama, Q. Xu, H.T. Takeshita, T. Sakai, J. Phys. Chem. B 105 (2001) 11214.
[13] J. Chen, N. Kuriyama, H.T. Takeshita, T. Sakai, Adv. Eng. Mater. 3 (9) (2001) 695.
[14] V.P. Balema, J.W. Wiench, K.W. Dennis, M. Pruski, V.K. Pecharsky, J. Alloys Comp. 329 (2001) 108.
[15] C.M. Jensen, R.A. Zidan, U.S. Patent 6,471,935 (2002).
[16] D. Sun, T. Kiyobayashi, H.T. Takeshita, N. Kuriyama, C.M. Jensen, J. Alloys Comp. 337 (2002) L8.
[17] K.J. Gross, G.J. Thomas, C.M. Jensen, J. Alloys Comp. 330–332 (2002) 683.
[18] G. Sandrock, K. Gross, G. Thomas, C. Jensen, D. Meeker, S. Takara, J. Alloys Comp. 330–332 (2002) 696.
[19] G.J. Thomas, K.J. Gross, N.Y.C. Yang, C. Jensen, J. Alloys Comp. 330–332 (2002) 702.
[20] G.P. Meisner, G.G. Tibbetts, F.E. Pinkerton, C.H. Olk, M.P. Balogh, J. Alloys Comp. 337 (2002) 254.
[21] G. Sandrock, K. Gross, G. Thomas, J. Alloys Comp. 339 (2002) 299.
[22] M. Fichtner, O. Fuhr, J. Alloys Comp. 345 (2002) 286.
[23] B. Bogdanovic, G. Sandrock, Mater. Res. Bull. 27 (2002) 712.
[24] B.C. Hauback, H.W. Brinks, H. Fjellvag, J. Alloys Comp. 346 (2002) 184.
[25] M. Fichtner, O. Fuhr, O. Kircher, J. Alloys Comp. 356–357 (2002) 418.
[26] H. Morioka, K. Kakizaki, S. Chung, A. Yamada, J. Alloys Comp. 353 (2003) 310.
[27] M. Fichtner, O. Fuhr, O. Kircher, J. Rothe, Nanotechnology 14 (2003) 778.
[28] D.L. Anton, J. Alloys Comp. 356–357 (2003) 400.
[29] S.M. Opalka, D.L. Anton, J. Alloys Comp. 356–357 (2003) 486.
[30] B. Bogdanovic, M. Felderhoff, S. Kaskel, A. Pommerin, K. Schlichte, F. Schuth, Adv. Mater. 15 (12) (2003) 1012.
[31] H.W. Brinks, B.C. Hauback, J. Alloys Comp. 354 (2003) 143.
[32] R. Genma, H.H. Uchida, N. Okada, Y. Nishi, J. Alloys Comp. 356–357 (2003) 358.
[33] A. Zuttel, S. Rentsch, P. Fischer, P. Wenger, P. Sudan, Ph. Mauron, Ch. Emmenegger, J. Alloys Comp. 356–357 (2003) 515.

[34] B.C. Hauback, H.W. Brinks, C.M. Jensen, K. Murphy, A.J. Maeland, J. Alloys Comp. 358 (2003) 142.
[35] M.P. Balogh, G.G. Tibbetts, F.E. Pinkerton, G.P. Meisner, C.H. Olk, J. Alloys Comp. 350 (2003) 136.
[36] B. Bogdanovic, M. Felderhoff, M. Germann, M. Hartel, A. Pommerin, F. Schuth, C. Weidenthaler, B. Zibrowius, J. Alloys Comp. 350 (2003) 246.
[37] D. Sun, S.S. Srinivasan, T. Kiyobayashi, N. Kuriyama, C.M. Jensen, J. Phy. Chem. B 107 (37) (2003) 10176.
[38] T. Kiyobayashi, S.S. Srinivasan, D. Sun, C.M. Jensen, J. Phys. Chem. A 107 (39) (2003) 7671.
[39] E.C. Ashby, French Patent 1,235,680, granted to Ethyl Corp., 30 May 1960.
[40] E.C. Ashby, G.J. Brendel, H.E. Redman, Inorg. Chem. 2 (3) (1963) 499.
[41] E.C. Ashby, P. Kobetz, Inorg. Chem. 5 (1966) 1615.
[42] T.N. Dymova, N.G. Eliseeva, S.I. Bakum, Y.M. Dergachev, Dokl. Akad. Nauk. SSSR 215 (1974) 1369.
[43] B. Bogdanovic, M. Schwickardi, Appl. Phys. A 72 (2001) 221.
[44] E.H. Majzoub, K.J. Gross, J. Alloys Comp. 356–357 (2003) 363.
[45] K.J. Gross, E.H. Majzoub, S.W. Spangler, J. Alloys Comp. 356–357 (2003) 423.
[46] J. Rodriguez-Carvajal, Physica 192 (1993) 55.
[47] H.W. Brinks, C.M. Jensen, S.S. Srinivasan, B.C. Hauback, D. Blandchard, K. Murphy, J. Alloys Comp. (2004) in press.

ELSEVIER

Journal of Alloys and Compounds xxx (2004) xxx–xxx

Journal of ALLOYS AND COMPOUNDS

www.elsevier.com/locate/jallcom

Synthesis and crystal structure of Na_2LiAlD_6

H.W. Brinks[a,*], B.C. Hauback[a], C.M. Jensen[b], R. Zidan[c]

[a] *Department of Physics, Institute for Energy Technology, P.O. Box 40, Kjeller NO-2027, Norway*
[b] *Department of Chemistry, University of Hawaii, Honolulu, HI 96822, USA*
[c] *Savanna Res Technol Ctr, Aiken, SC 29808, USA*

Received 2 September 2004; accepted 13 September 2004

Abstract

Na_2LiAlD_6 was synthesized by ball milling of $NaAlD_4$ and $LiAlD_4$ with subsequent heat treatment under D_2 pressure. The compound has an ordered perovskite-type structure with Li and Al in octahedral positions. The $[LiD_6]^{3-}$ and $[AlD_6]^{3-}$ complex anions are ordered in three dimensions such that the neighbouring octahedron is of different type in all three directions. Each octahedron shares each corner with one other octahedron. Na_2LiAlD_6 crystallizes in the cubic space group $Fm\overline{3}m$ with unit-cell dimension $a = 7.38484(5)$ Å. The structure may also be described as a c.c.p. geometry of (isolated) AlD_6 entities with Li filling the octahedral sites and Na filling all the tetrahedral sites. Sodium is connected to three D atoms from each of the four surrounding AlD_6 octahedra, resulting in a total coordination number of 12.

Keywords: Powder X-ray diffraction; Powder neutron diffraction; Synchrotron radiation; Metal hydrides; Crystal structure; Alanates

1. Introduction

Following the pioneering studies of $NaAlH_4$ with Ti-based additives that were reported by Bogdanovic and Schwickardi in 1997 [1] of $NaAlH_4$, the alanate tetrahydrides $NaAlH_4$ [2–20], $LiAlH_4$ [21–24], $KAlH_4$ [25] and $Mg(AlH_4)_2$ [26–28] have been intensively studied as possible basis for materials for high-capacity reversible hydrogen storage systems. Complex hydrides based on $AlH_6{}^{3-}$ also have a considerable hydrogen content. In addition to Li_3AlH_S 5.6 wt.% for desorption to LiH and Al) and Na_3AlH_6 (3.0 wt.%), the mixed hexahydrides Na_2LiAlH_6 and K_2NaAlH_6 have been reported [1,29–32]. Na_2LiAlH_6 (3.5 wt.%) was synthesized in 1982 by Claudy et al. [29] and was found by Bogdanovic and Schwickardi [1] to be more stable than Na_3AlH_6. Zaluski et al. [32] also found a similar stability for $Na_{1.7}Li_{1.3}AlH_6$. Li_3AlD_6 is less stable than Na_3AlH_6 [33], thus Na_2LiAlH_6 is more stable than either the Li_3 and Na_3 hexahydride end phases.

The crystal structure of Na_2LiAlH_6 has not been determined, but a cubic unit-cell of 7.405 Å has been proposed from powder X-ray diffraction (PXD) data [29]. Furthermore, density functional theory (DFT) has been used to compare the stability of Na_2LiAlH_6 in different crystal structures and symmetries, and an ordered perovskite-type structure (ABX_3) was found to be most stable [34]. The structure was suggested to have space group $P2_1/c$ [34], a lowering in symmetry caused by small rotations of octahedra in the Glazer notation [35] $a^+b^-b^-$ (which gives the frequently encountered space group *Pnma* for perovskites) combined with ordering of Li and Al in the B position of the perovskite.

The aim of this study is to synthesize Na_2LiAlD_6 and determine the crystal structure from powder neutron diffraction (PND) data and compare it to those previously determined for the Li_3 and Na_3 hexahydride end phases.

2. Experimental

The samples were synthesized by ball milling in argon atmosphere. The first sample was synthesized by ball milling

* Corresponding author. Tel.: +47 63 80 64 99; fax: +47 63 81 09 20.
E-mail address: hwbrinks@ife.no (H.W. Brinks).

0925-8388/$ – see front matter © 2004 Published by Elsevier B.V.
doi:10.1016/j.jallcom.2004.09.006

$LiAlD_4$ (>95% chemical purity and >99.8% isotope purity) and NaH at 700 rpm for 3 h. After heat treatment at 150 °C and 50 bar, the sample mainly consisted of $Na_2LiAlD_4H_2$. Another sample for structure determination was synthesized by ball milling at 700 rpm for 3 h of $LiAlD_4$ and $2NaAlD_4$ (single-phase; the synthesis from $LiAlD_4$ and NaF is described elsewhere [19,36]) followed by heat treatment at 180 °C and 30 bar. All operations were performed under argon in a glove box with <1 ppm O_2 and H_2O.

PXD data for were collected at an INEL instrument with Cu $K\alpha_1$ radiation, Bragg Brentano geometry and 120° position sensitive detector. SR-PXD data at 22 °C were collected at the Swiss–Norwegian beam line (station BM1B) at the European synchrotron radiation facility (ESRF) in Grenoble, France. The samples were kept in rotating 0.5 mm boron–silica–glass capillaries. Intensities were measured in steps of $\Delta(2\theta) = 0.005°$. The wavelength 0.79975 Å was obtained from a channel-cut Si(1 1 1) monochromator.

PND data at 22 °C were collected with the PUS instrument at the JEEPII reactor at Kjeller, Norway. Neutrons with wavelength 1.5553 Å were obtained from a Ge(5 1 1) focussing monochromator. The detector unit consists of two banks of seven position-sensitive ^{3}He detectors, each covering 20° in 2θ (binned in steps of 0.05°). Data was collected from 10° to 130° in 2θ. The sample was placed in a rotating cylindrical vanadium sample holder with 5 mm diameter.

Rietveld refinements were carried out using the program Fullprof (Version 2.20) [37]. X-ray form factors and neutron scattering lengths were taken from the Fullprof library. Pseudo-Voigt profile functions were used and the backgrounds were modelled by interpolation between manually chosen points.

3. Results and discussions

The ball milling of $LiAlD_4$ with 2NaH did not directly result in formation of single-phase $Na_2LiAlD_4H_2$, but instead a mixture of $NaAlD_4$ (confirmed by the unit-cell dimensions which are slightly different from $NaAlH_4$), LiH, NaH, Na_3AlH_6 and $Na_2LiAlD_4H_2$. However, DFT calculations had predicted Na_2LiAlH_6 to be more stable than Na_3AlH_6 and Li_3AlH_6 [34]. Thus the sample was heat treated in order to reach equilibrium. Deuterium pressures of >30 bar was used to avoid desorption of the sample. $Na_2LiAlD_4H_2$ with only small amounts of NaH and LiH was obtained at 150 °C and 50 bar.

In order to determine the structure from PND, we attempted to synthesize a sample containing only the deuterium isotope. This was done by ball milling $LiAlD_4$ + $2NaAlD_4$ with subsequent heat treatment under high enough pressure to avoid desorption of Na_3AlD_6 and Na_2LiAlD_6. After heat treatment at 180 °C and 30 bar, the only phases detected in lab PXD data were Na_2LiAlD_6 and Al.

The PXD data from the lab diffractometer do not give any indications of a significant deviation from the proposed cubic unit-cell. The intensities of the reflections are consistent with the atomic arrangement in the unit-cell of an ordered perovskite-type structure—as proposed by the DFT calculations, but without the lowering of symmetry that was proposed from the calculations.

The ideal perovskite structure consists of a network of corner-sharing BX_6 octahedra, where each X atom is shared between two octahedra, and with 12-coordinated A atoms in the interstices. These connected octahedra can be rotated along three axis and give rise to many different symmetries with very related structures. Glazer [35] recognized structural models for 23 different tilt systems for ABX_3 compounds with perovskite-type structure. Furthermore, Woodward [38] has reported the structural models for the $A_2BB'X_6$ with 1:1 ordering on the B position. The simplest of these is the ordered perovskite without any rotation of the octahedra, which gives a $2 \times 2 \times 2$ enlarged unit-cell compared to the ideal perovskite and with the cubic space group $Fm\bar{3}m$. The present Lab PXD data for $Na_2(LiAl)D_6$ agrees with this model.

In order to determine the correct structural model among the possible structures in the perovskite family, PND data (much more sensitive to deuterium) and synchrotron radiation PXD data (superb sensitivity to small deviations from cubic symmetry because of the high resolution) were needed. No extra reflections compared to the cubic model were detected in the PND data. In the SR-PXD data, ~2 wt.% Na_3AlD_6 was detected, and in addition a few unidentified reflections of up to 1% of the intensity of the strongest Na_2LiAlD_6 reflection are present in the data. There is no evident splitting of the reflections from cubic symmetry, even though there are small imperfections in the profile of the cubic (4 0 0) reflection. This could be explained by an impurity reflection, but there is also a possibility that there is a small deformation from cubic symmetry, but even the high-resolution SR-PXD data is not able to reveal what type of a possible deformation.

The fit for two of the PND reflections could be improved by using a model with lower symmetry and thereby a significant increased number of structural parameters. However, it is impossible to find any model that is significantly better than the others from these weak indications of lower symmetry. Hence, it was concluded that a cubic unit-cell with $a = 7.38484(5)$ Å and space group $Fm\bar{3}m$ gives the best description of Na_2LiAlD_6. The structural data are given in Table 1, the fit of the Rietveld refinements in Fig. 1 and the

Table 1
Crystal structure of Na_2LiAlD_6. The space group is $Fm\bar{3}m$ and unit-cell dimension $a = 7.38484(5)$ Å, $Z = 4$

Atom	x	y	z
Na	1/4	1/4	1/4
Li	1/2	1/2	1/2
Al	0	0	0
D	0.238(4)	0	0

Reliability factors are $R_{wp} = 5.78\%$ and $\chi^2 = 1.56$ for PND data and $R_{wp} = 5.17\%$ and $\chi^2 = 3.50$ for PXD data. Standard deviations are given in parentheses.

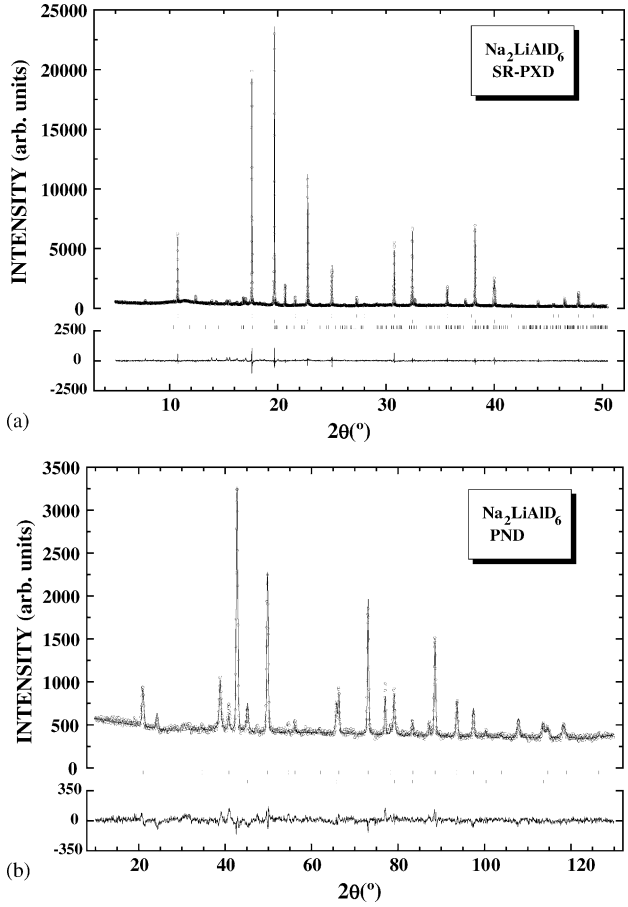

Fig. 1. Observed intensities (circles) and calculated intensities from Rietveld refinements (upper line) of Na_2LiAlD_6 at 295 K for: (a) PXD (BM1B, ESRF) and (b) PND (PUS, Kjeller) data. Positions of Bragg reflections are shown with bars for Na_2LiAlD_6, Al and Na_3AlD_6 (from top). The difference between observed and calculated intensity are shown with the bottom line.

structure of Na_2LiAlD_6 in Fig. 2. Selected inter-atomic distances are shown in Table 2.

The structure consists of a network of corner-sharing AlD_6 and LiD_6 octahedra where each octahedron is surrounded by six octahedral—all of them of the different type. The size difference of the octahedra, Al–D distances being 1.760(3) Å and Li–D 1.933(3) Å, is sufficient to give an ordering of the

Table 2
Selected inter-atomic distances (in Å) and angles (in °) for Na_2LiAlD_6 at 295 K

Atoms	Distances
Al–D	1.760(3)
Li–D	1.933(3)
D–D	2.488(3), 2.734(3)
Al–Al	5.222
Na–Li	3.198
Na–Na	3.692
Li–Li	5.222
Atoms	Angles
D–Al–D	90.00(–), 180.00(–)

Estimated standard deviations in parentheses (for the inter-metallic distances the standard deviations are <0.0005 Å).

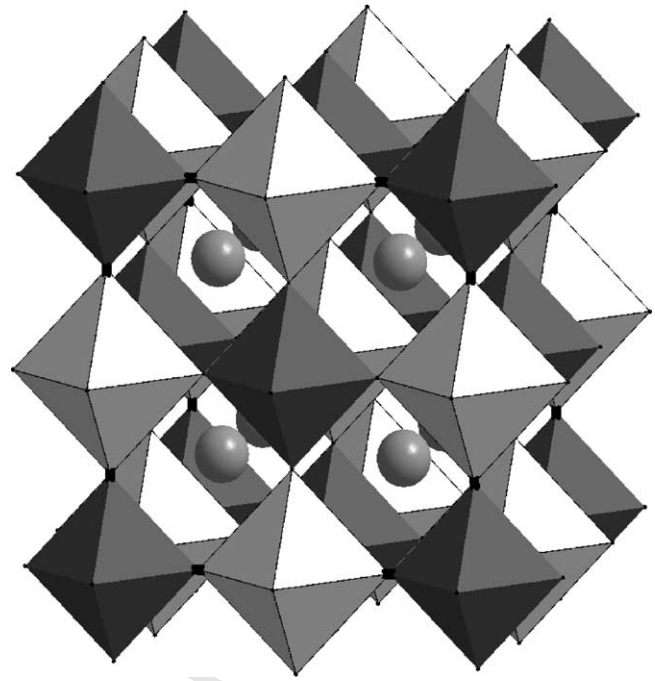

Fig. 2. The crystal structure of Na_2LiAlD_6 at 295 K, showing alternating AlD_6 (dark) and LiD_6 (bright) octahedra in all directions with Na in interstitial 12-coordinated sites.

octahedra in the structure. The AlD_6 octahedra are of similar size as the octahedra in Li_3AlD_6 (1.744 Å on average) [39] and Na_3AlD_6 (1.756 Å) [40]. The AlD_6 octahedra in Na_2LiAlD_6 are ideal with equal Al–D distances and ideal angles.

The Li–D distance of 1.933 Å is also close to the values for Li_3AlD_6:Li–D_{min} = 1.892 Å and Li–$D_{average, CN = 6}$ = 2.001Å. For comparison, the Li–D distance in LiD is 2.031 Å.

The shortest Al–Al distance is 5.222 Å, which is between the corresponding distances for Li_3AlD_6 (4.757 Å) and Na_3AlD_6 (5.390 Å). The AlD_6 octahedra, which are isolated from each other, are oriented such that edges from different octahedra are opposite to each other, thus providing D–D distances between neighbouring AlD_6 octahedra of at least 2.734 Å. Octahedra with corners pointing to each other would have given D–D distances shorter than 2 Å. The shortest D–D distance 2.488(3) Å is found within the AlD_6 octahedron.

Na is 12-coordinated with 12 D atoms from four different octahedra. The Na–D distance, 2.612 Å, is larger than the corresponding distances in Na_3AlD_6 (2.296–2.765 Å with average 2.507 Å). This is probably due to the increased coordination number from 8 to 12. Na in the octahedral sites of Na_3AlD_6 has even shorter bond lengths (2.231–2.266 Å with average 2.253 Å).

The structure of Na_2LiAlD_6 may be described in different ways. It is an ordered perovskite with Li and Al ordered at the B position of the ABX_3 perovskite giving $A_2BB'X_6$, hence with both Al and Li in octahedral position and with Na in a 12-coordinated site. Na_2LiAlD_6 has a very similar structure to Na_3AlD_6; in one of the Na positions Na is substituted by

Li. However, the small distortion of the lattice in Na_3AlD_6 is not present in Na_2LiAlD_6. In a perovskite A and X together (here Na and D) are forming a c.c.p. lattice with B (here Li and Al) filling 1/4 of the octahedral sites.

The structure may also been considered as taking a lattice of c.c.p. geometry of AlD_6 entities (which are not in contact with each other) with Na filling the tetrahedral positions and Li the octahedral position. These coordination numbers are the coordination numbers to the octahedra not the coordination numbers to deuterium, which is 12 for Na and 6 for Li. For comparison, Na_3AlD_6 is a slightly distorted c.c.p. with Na in the same positions and Li_3AlD_6 is a slightly distorted b.c.c. of AlD_6 octahedra with Li in half of the tetrahedral positions.

Acknowledgements

The skilful assistance from the project team at the Swiss–Norwegian Beam Line, ESRF, is also gratefully acknowledged. CMJ gratefully acknowledges financial support received from the Office of Hydrogen, Fuell Cells and Infrastructure Technologies of the US Department of Energy.

References

[1] B. Bogdanovic, M. Schwickardi, J. Alloys Compd. 253 (1997) 1.
[2] C.M. Jensen, R. Zidan, N. Mariels, A. Hee, C. Hagen, Int. J. Hydrogen Energy 24 (1999) 461.
[3] R.A. Zidan, S. Takara, A.G. Hee, C.M. Jensen, J. Alloys Compd. 285 (1999) 119.
[4] A. Zaluska, L. Zaluski, J.O. Strom-Olsen, J. Alloys Compd. 298 (2000) 125.
[5] B. Bogdanovic, R.A. Brand, A. Marjanovic, M. Schwickardi, J. Tolle, J. Alloys Compd. 302 (2000) 36.
[6] C.M. Jensen, K.J. Gross, Appl. Phys. A 72 (2001) 213.
[7] B. Bogdanovic, M. Schwickardi, Appl. Phys. A 72 (2001) 221.
[8] G. Sandrock, K. Gross, G. Thomas, C. Jensen, D. Meeker, S. Takara, J. Alloys Compd. 330 (2002) 696.
[9] D.L. Sun, T. Kiyobayashi, H.T. Takeshita, N. Kuriyama, C.M. Jensen, J. Alloys Compd. 337 (2002) 8.
[10] G. Sandrock, K. Gross, G. Thomas, J. Alloys Compd. 339 (2002) 299.
[11] B. Bogdanovic, G. Sandrock, MRS Bull. 27 (2002) 712.
[12] G.P. Meisner, G.G. Tibbetts, F.E. Pinkerton, C.H. Olk, M.P. Balogh, J. Alloys Compd. 337 (2002) 254.
[13] B. Bogdanovic, M. Felderhoff, S. Kaskel, A. Pommerin, K. Schlichte, F. Schuth, Adv. Mater. 15 (2003) 1012.
[14] M. Fichtner, O. Fuhr, O. Kircher, J. Rothe, Nanotechnology 14 (2003) 778.
[15] B.C. Hauback, H.W. Brinks, C.M. Jensen, K. Murphy, A.J. Maeland, J. Alloys Compd. 358 (2003) 142.
[16] B. Bogdanovic, M. Felderhoff, M. Germann, M. Hartel, A. Pommerin, F. Schuth, C. Weidenthaler, B. Zibrowius, J. Alloys Compd. 350 (2003) 246.
[17] T. Kiyobayashi, S. Srinivasan, D. Sun, C. Jensen, J. Phys. Chem. A 107 (2003) 7671.
[18] E.H. Majzoub, K.J. Gross, J. Alloys Compd. 356 (2003) 363.
[19] H.W. Brinks, C.M. Jensen, S.S. Srinivasan, B.C. Hauback, D. Blanchard, K. Murphy, J. Alloys Compd. 376 (2004) 215.
[20] J. Iniguez, T. Yildirim, T. Udovic, M. Sulic, C. Jensen, Phys. Rev. B 70 (2004) 60101.
[21] V.P. Balema, K.W. Dennis, V.K. Pecharsky, Chem. Commun. 17 (2000) 1665.
[22] J. Chen, N. Kuriyama, Q. Xu, H.T. Takeshita, T. Sakai, J. Phys. Chem. B 105 (2001) 11214.
[23] H.W. Brinks, B.C. Hauback, P. Norby, H. Fjellvåg, J. Alloys Compd. 351 (2003) 222.
[24] B.C. Hauback, H.W. Brinks, H. Fjellvåg, J. Alloys Compd. 346 (2002) 184.
[25] H. Morioka, K. Kakizaki, S. Chung, Y. A., J. Alloys Compd. 2003 (2003) 310.
[26] M. Fichtner, O. Fuhr, O. Kircher, J. Alloys Compd. 356/357 (2003) 418.
[27] A. Fossdal, H.W. Brinks, M. Fichtner, B.C. Hauback, J. Alloys Compd., submitted.
[28] A. Fossdal, H.W. Brinks, B.C. Hauback, M. Fichtner, J. Alloys Compd., in press.
[29] P. Claudy, B. Bonnetot, J.P. Bastide, J.M. Letoffe, Mater. Res. Bull. 17 (1982) 1499.
[30] J. El Hajri, Preparation et caracterisation d'hydroaluminates de potassium $KAlH_4$, K_3AlH_6, K_2NaAlH_6, $K_3AlH_4F_2$, Institut national des sciences appliquees de Lyon, Lyon, 1986.
[31] J. Huot, S. Boily, V. Guther, R. Schulz, J. Alloys Compd. 283 (1999) 304.
[32] L. Zaluski, A. Zaluska, J.O. Strom-Olsen, J. Alloys Compd. 290 (1999) 71.
[33] H.W. Brinks, unpublished results.
[34] O.M. Løvvik, O. Swang, J. Alloys Compd., in press.
[35] A.M. Glazer, Acta Crystallogr. A 31 (1975) 756.
[36] J.P. Bastide, J. Elhajri, P. Claudy, A. Elhajbi, Synth. React. Inorg. Metal-Org. Chem. 25 (1995) 1037.
[37] J. Rodríguez-Carvajal, Physica B 192 (1993) 55.
[38] P.M. Woodward, Acta Crystallogr. B 53 (1997) 32.
[39] H.W. Brinks, B.C. Hauback, J. Alloys Compd. 354 (2003) 143.
[40] E. Rönnebro, D. Noréus, K. Kadir, A. Reiser, B. Bogdanovic, J. Alloys Compd. 299 (2000) 101.

ARTICLE IN PRESS

ELSEVIER

Journal of Alloys and Compounds 1 (2003) 000–000

Journal of ALLOYS AND COMPOUNDS

www.elsevier.com/locate/jallcom

Neutron diffraction structure determination of $NaAlD_4$

B.C. Hauback[a,*], H.W. Brinks[a], C.M. Jensen[b], K. Murphy[b], A.J. Maeland[a]

[a]*Department of Physics, Institute for Energy Technology, P.O. Box 40, NO-2027 Kjeller, Norway*
[b]*Department of Chemistry, University of Hawaii, Honolulu, HI 96822, USA*

Received 2 January 2003; accepted 15 January 2003

Abstract

The structure of $NaAlD_4$ has been determined from Rietveld-type refinements of powder neutron diffraction data at 8 and 295 K. The space group is $I4_1/a$ with $a=501.19(1)$ and $c=1131.47(5)$ pm at 295 K. The Na atoms are surrounded by eight D atoms from eight different $[AlD_4]^-$ tetrahedra in the geometry of a distorted square antiprism. The two different Na–D distances are nearly equal: 240.3(2) and 240.5(2) pm at 8 K and 243.1(2) and 243.9(2) pm at 295 K. The Al–D distance is 162.7(2) and 162.6(2) pm at 8 and 295 K, respectively.

Keywords: Hydrogen absorbing materials; Metal hydrides; Crystal structure; Neutron diffraction

1. Introduction

Following Bogdanovic and Schwickardi's report in 1997 [1] that hydrogenation/dehydrogenation of $NaAlH_4$ becomes reversible when doped with selected Ti-based compounds, there has been a significant focus on the development of dopants for the promotion of the reversible dehydriding of $NaAlH_4$ [2–9]. The total storage capacity of $NaAlH_4$ is 7.5 wt%, but since the last dehydrogenation step of NaH occurs at high temperature (~800 K), the maximum practical available hydrogen storage capacity for $NaAlH_4$ is 5.6 wt%. This is above the aims of the International Energy Agency (task 17) of minimum 5 wt% hydrogen capacity [10]. $NaAlH_4$ is, therefore, now considered to be a very promising material for solid state storage of hydrogen.

In 1979, the structure of $NaAlH_4$ was determined by Lauher et al. through a single-crystal X-ray diffraction study [11]. Refinement in space group $I4_1/a$ gave Al–H bond distances of 153.2(7) pm. Based on IR spectroscopy data, Bel'skii et al. [12] pointed out in 1983 that the Al–H distances should be longer in $NaAlH_4$ than those determined for $LiAlH_4$ (average value of 154.8(17) pm from a single-crystal X-ray diffraction study [13]). Therefore, Bel'skii et al. re-determined the structure from single-crystal X-ray diffraction data. The refinements were again carried out within the space group $I4_1/a$ and the data converged to give an Al–H distance of 161(4) pm [12] that is in agreement with the IR data.

However, Bel'skii et al. [12] recognized the need for neutron diffraction data in order to ascertain the correct description of the location of the hydrogen/deuterium atoms as X-ray diffraction data tends to give erroneously short metal–hydrogen distances and very large uncertainties in the hydrogen coordinates. Detailed knowledge of

Table 1
Refined unit-cell dimensions, atomic coordinates, isotropic displacement factors B (10^4 pm^2)[a] and reliability factors for $NaAlD_4$ at 295 and 8 K. The space group is $I4_1/a$, $Z=4$, and Na is in 4a (0, 1/4, 1/8), Al in 4b (0, 1/4, 5/8), D in 16f (x, y, z). Estimated standard deviations in parentheses

	295 K	8 K
a (pm)	501.19(1)	498.02(1)
c (pm)	1131.47(4)	1114.82(3)
B_{Na}	1.52(8)	0.29(6)
B_{Al}	1.08(8)	0.45(7)
x_D	0.2372(3)	0.2371(3)
y_D	0.3836(3)	0.3867(2)
z_D	0.5469(2)	0.5454(1)
B_D	2.45(4)	1.21(2)
R_{wp} (%)	4.56	4.72
χ^2	1.27	2.41

[a] The isotropic displacement factor is defined by $\exp[-B(\sin^2\theta/\lambda)]$.

*Corresponding author. Tel.: +47-63-80-6078; fax: +47-63-81-0920.
E-mail address: bjorn.hauback@ife.no (B.C. Hauback).

0925-8388/03/$ – see front matter
doi:10.1016/S0925-8388(03)00136-1

the structure, in particular correct coordinates for hydrogen, is required to gain the insight into the hydrogenation/dehydrogenation processes of $NaAlH_4$ that is requisite for the development of related materials with improved hydrogenation properties.

We present here the accurate structure of $NaAlD_4$ that was determined on the basis of powder neutron diffraction data that were collected at 295 and 8 K.

2. Experimental

Sodium aluminium deuteride, $NaAlD_4$ (>99% D) was synthesized by the method of Bastide et al. [14]. The resulting sample was found to contain significant amounts of NaF and Al impurities.

Powder neutron diffraction (PND) data at 8 and 295 K were collected between $2\theta = 10$ and 130° with the PUS diffractometer at the JEEP II reactor at Kjeller, Norway [15]. Monochromatic neutrons with wavelength $\lambda = 155.46$ pm were obtained by reflection from Ge (511) of a focussing composite monochromator with approximately 90° take-off angle. The detector unit consisted of two banks of seven position-sensitive ^{3}He detectors, each covering 20° in 2θ. A cylindrical vanadium sample holder of 5 mm diameter was used. The sample was rotated at 295

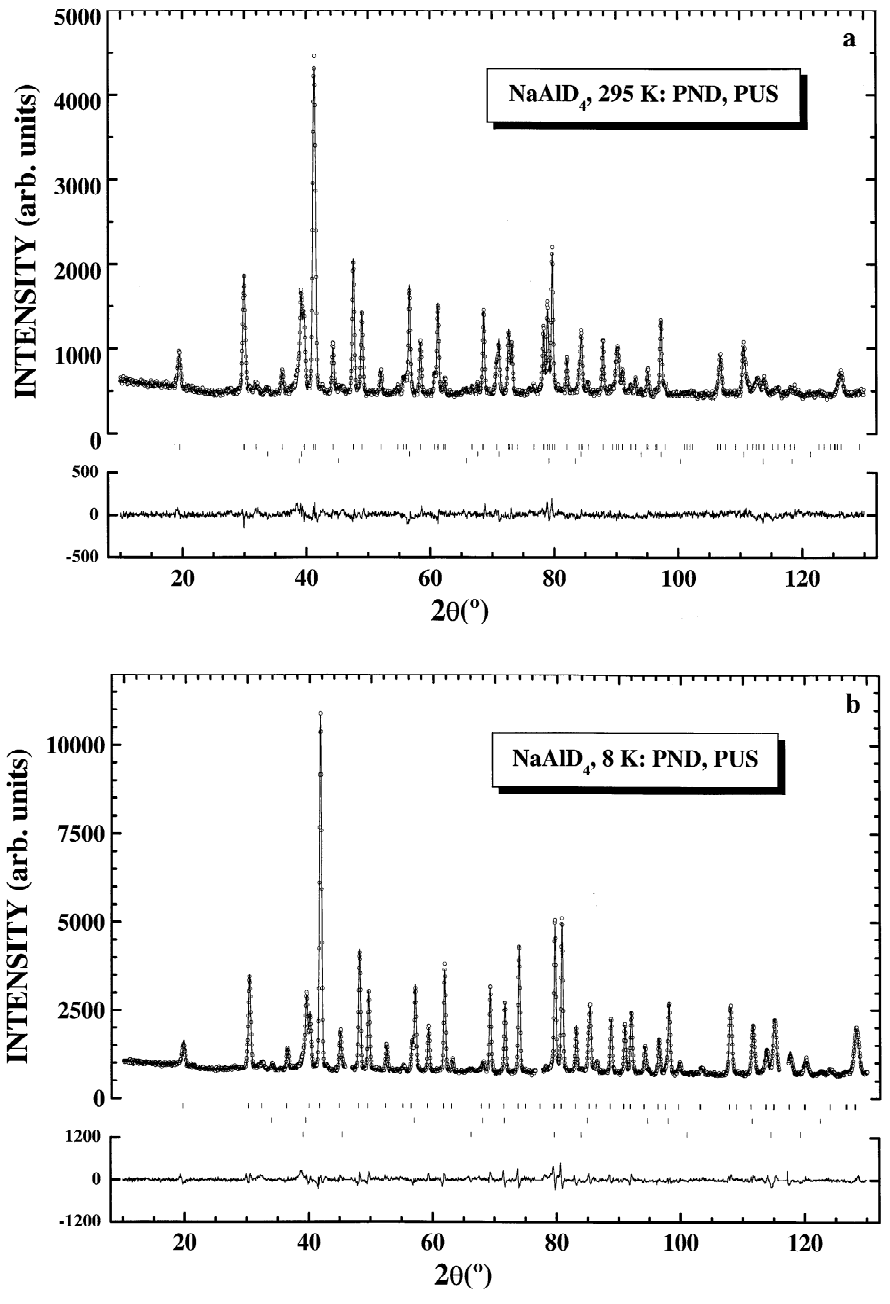

Fig. 1. PND pattern for $NaAlD_4$ at (a) 295 and (b) 8 K showing observed (circles), calculated (upper line) and difference (bottom line) plots. The positions of the Bragg reflections are shown for $NaAlD_4$ (upper), NaF (middle) and Al (lower).

K, but not at 8 K. The temperature of 8 K was obtained by means of a Displex cooling system. An Oxford ITC 503 controller was used and the temperature was measured and controlled by a silicon diode. At both temperatures the data were rebinned in steps of $\Delta(2\theta)=0.05°$ giving 2400 data points. The regions $2\theta=46.00–46.75°$, 76.50–77.60° and 116.00–117.30° were excluded in the analysis of the PND data at 8 K due to additional scattering from the Displex cooling system.

The FullProf program (version 1.9c) [16] was used for the Rietveld profile refinements. The scattering lengths $b_{Na}=3.63$, $b_{Al}=3.45$ and $b_D=6.67$ fm were taken from the FullProf library. The peak profiles were modelled by pseudo-Voigt functions. The backgrounds were described by linear interpolation between manually selected points in the diffraction patterns, 35 and 39 points for the data at 295 K and 8 K, respectively. For both data sets the following 25 parameters were refined: 1 zero point, 3 scale factors (for $NaAlD_4$, NaF and Al), 9 profile (4 each for $NaAlD_4$ and NaF and 1 for Al), 4 unit cell ($NaAlD_4$: 2; NaF: 1; Al: 1) and 8 atom parameters. Isotropic displacement parameters for the individual atoms were applied for $NaAlD_4$ and NaF, but not refined for Al.

3. Results and discussion

The atomic coordinates published by Bel'skii et al. [12] were used as starting parameters in the Rietveld-type refinements. Because of significant amounts of NaF, the unit cell parameters and coordinates were added early in the refinements (space group *F23*, $a=463.42(1)$ pm at 295 K (varied in the refinements), Na in 4*a* (0, 0, 0), F in 4*b* (1/2, 1/2, 1/2)). Peaks corresponding to Al were also found in the data (the *a*-axis was fixed to 404.9 pm in the refinements at 295 K). According to the refinements, the sample contains 57 wt% $NaAlD_4$, 29 wt% NaF and 14 wt% Al.

Structural parameters and reliability factors for the Rietveld-type refinements of $NaAlD_4$ at 295 and 8 K are listed in Table 1. Observed, calculated and difference plots for the PND patterns at 295 and 8 K are shown in Fig. 1.

Table 2
Selected inter-atomic distances (pm) and angles (deg.) in the crystal structure of $NaAlD_4$ at 295 and 8 K. Estimated standard deviations in parentheses

Atoms	295 K	8 K
Al–D (×4)	162.6(2)	162.7(2)
Na–D (×4)	243.1(2)	240.3(2)
(×4)	243.9(1)	240.5(2)
D–D (×2)	261.9(1)	262.0(1)
Na–Na (×4)	377.9(1)	373.7(1)
Al–Na (×4)	354.4(1)	352.1(1)
(×4)	377.9(1)	373.7(1)
D–Al–D (×4)	107.32(1)	107.30(1)
(×2)	113.86(1)	113.90(1)

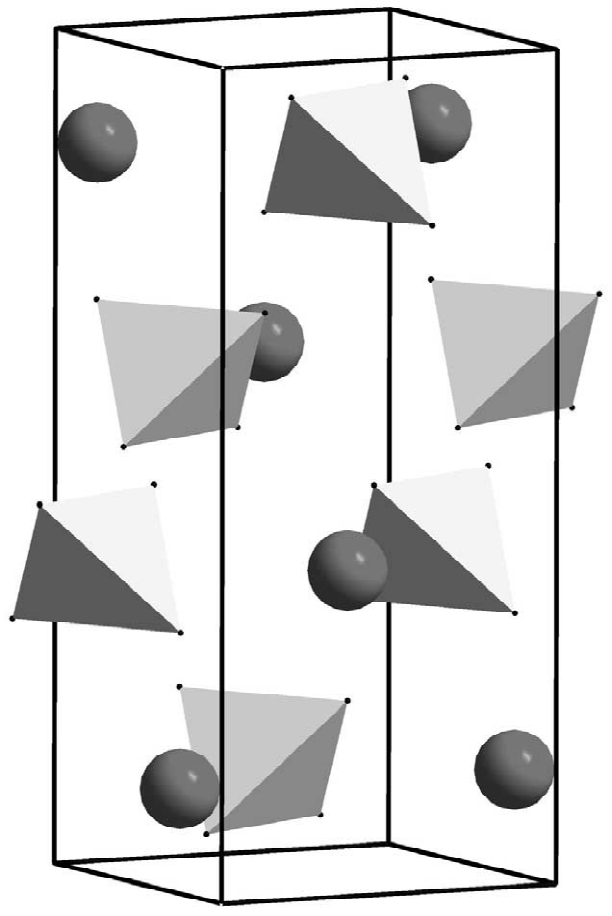

Fig. 2. The crystal structure of $NaAlD_4$. $[AlD_4]^-$ tetrahedra are linked via Na atoms.

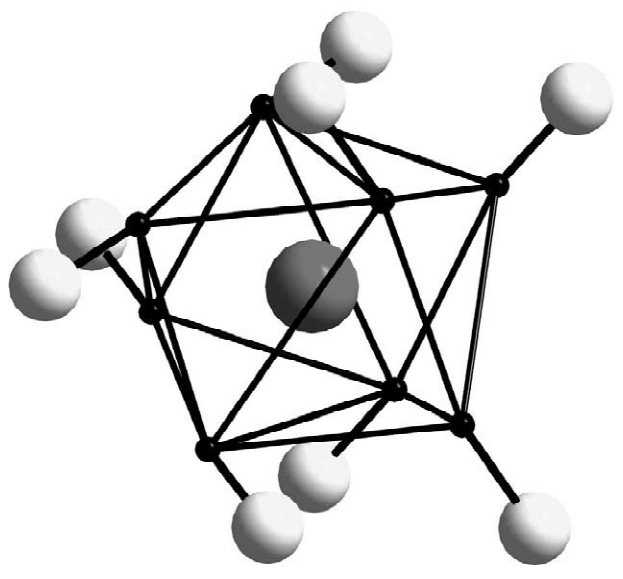

Fig. 3. Each Na atom is connected to eight $[AlD_4]^-$ tetrahedra in a distorted square antiprism.

On cooling, the shrinkage of the tetragonal unit cell is largest along the crystallographic c-axis, $\Delta c/c = -1.5\%$, whereas $\Delta a/a = -0.6\%$. The displacement parameter for the deuterium is relatively large at 295 K. The high thermal motion is possibly related to the low thermal stability of $NaAlD_4$. The same behaviour was found for $LiAlD_4$ [17].

Selected inter-atomic distances and bond angles are given in Table 2. The structure consists of isolated $[AlD_4]^-$ tetrahedra connected via Na atoms. The structure is shown in Fig. 2. The shortest Al–Al separations are 373.7(1) and 377.9(1) pm at 8 and 295 K, respectively. Each Na atom has eight D atoms as nearest neighbours, each from different $[AlD_4]^-$ tetrahedra, in the geometry of a distorted square antiprism (Fig. 3).

The shortest D–D distances at 295 K of 261.9(1) pm are found within the tetrahedron, whereas the shortest D–D distance between different tetrahedra are slightly larger: 271.9(1) pm. If the Al–D bonds in neighbouring tetrahedra were pointed directly towards each other, the D–D distance would have been as low as 52.7 pm, but the tetrahedra are in fact oriented with all four faces pointed towards neighbouring tetrahedra. The D–D distances are thereby maximized.

The two unique Na–D bond distances are nearly equal, 240.3(2) and 240.5(2) pm at 8 K and 243.1(2) and 243.9(2) pm at 295 K (Fig. 3). The Al–D distance is 162.7(2) and 162.6(2) pm at 295 and 8 K, respectively. For comparison, the X-ray data by Bel'skii et al. [12] gave a shorter and much more uncertain Al–D distance: 161(4) pm. The two unique D–Al–D bond angles in the $[AlD_4]^-$ tetrahedron are 107.32 and 113.86° at 295 K.

The Al–D distance is slightly longer in $NaAlD_4$ (162.6 pm) at 295 K than the average 161.9(7) pm determined in the recent study of $LiAlD_4$ [17]. At 8 K, the Al–D distances are 162.7(2) and 162.4(9) for $NaAlD_4$ and $LiAlD_4$, respectively. The similarity of the Al–D distances is also present for the $[AlD_6]^{3-}$ octahedra in Na_3AlD_6 [18] and Li_3AlD_6 [19]. It is also interesting to note that, for $NaAlD_4$ and $LiAlD_4$, the Al–D distances do not change on cooling from 295 to 8 K.

References

[1] B. Bogdanović, M. Schwickardi, J. Alloys Comp. 253/254 (1997) 1.
[2] R.A. Zidan, S. Takara, A.G. Hee, C.M. Jensen, J. Alloys Comp. 295 (1999) 119.
[3] K.J. Gross, S. Guthrie, S. Takara, G. Thomas, J. Alloys Comp. 297 (2000) 270.
[4] A. Zaluska, L. Zaluski, J.O. Ström-Olsen, J. Alloys Comp. 298 (2000) 125.
[5] B. Bogdanović, R.A. Brand, A. Marjanović, M. Schwickardi, J. Tölle, J. Alloys Comp. 302 (2000) 36.
[6] B. Bogdanović, M. Schwickardi, Appl. Phys. A 72 (2001) 221.
[7] K.J. Gross, G.J. Thomas, C.M. Jensen, J. Alloys Comp. 330–332 (2002) 683.
[8] G. Sandrock, K.J. Gross, G.J. Thomas, J. Alloys Comp. 339 (2002) 299.
[9] B. Bogdanović, G. Sandrock, MRS Bulletin September (2002) 712.
[10] G. Sandrock, IEA, task 17 http://hydpark.ca.sandia.gov/iea.html
[11] J.W. Lauher, D. Dougherty, P.J. Herley, Acta Crystallogr. B35 (1979) 1454.
[12] V.K. Bel'skii, B.M. Bulychev, A.V. Golubeva, Russ. J. Inorg. Chem. 28 (1983) 1528.
[13] N. Sklar, B. Post, Inorg. Chem. 6 (1967) 669.
[14] J.P. Bastide, J. El Hajri, P. Claudy, Synth. React. Inorg. Met.-Org. Chem. 25 (1995) 1037.
[15] B.C. Hauback, H. Fjellvåg, O. Steinsvoll, K. Johansson, O.T. Buset, J. Jørgensen, J. Neutron Res. 8 (2000) 215.
[16] J. Rodríguez-Carvajal, Physica B 192 (1993) 55.
[17] B.C. Hauback, H.W. Brinks, H. Fjellvåg, J. Alloys Comp. 346 (2002) 184.
[18] E. Rönnebro, D. Noréus, K. Kadir, A. Reiser, B. Bogdanović, J. Alloys Comp. 299 (2000) 101.
[19] H.W. Brinks, B.C. Hauback, J. Alloys Comp., in press.

Point Defect Dynamics and Evolution of Chemical Reactions in Alanates by Anelastic Spectroscopy

Oriele Palumbo,[†] Rosario Cantelli,[*,†] Annalisa Paolone,[†,‡] Craig M. Jensen,[§] and Sesha S. Srinivasan[§]

Dipartimento di Fisica, Università di Roma "La Sapienza", Piazzale A. Moro 2, I-00185 Roma, Italy, Istituto Nazionale per la Fisica della Materia, Corso Perrone 24, I-16152 Genova, Italy, and Department of Chemistry, University of Hawaii, Honolulu, Hawaii 96822

Received: August 30, 2004; In Final Form: October 26, 2004

We report the first measurements of elastic modulus and energy dissipation in Ti-doped and undoped sodium aluminum hydride. It is shown that the chemical reactions that occur by varying the sample temperatures or by aging most sensitively affect the elastic constants, such that the modulus variations allow the time and temperature evolution of decomposition to be monitored. After a well-defined thermal treatment at 436 K, a thermally activated relaxation process appears at 70 K in the kilohertz range, denoting the existence of a new species, likely involving hydrogen, having a very high mobility, that is, 10^3 jumps/s at the peak temperature corresponding to a relaxation rate of about 10^{11} s^{-1} at room temperature. The activation energy of the process is 0.126 eV and the preexponential factor 7×10^{-14} s, which is typical of point defect relaxation. The peak is very broad with respect to a single Debye process, indicating strong interaction or/and multiple jumping type of the mobile entity. The present data suggest that the models aiming at interpreting the decomposition reactions and kinetics should take into account the indicated point-defect dynamics and stoichiometry defects.

Introduction

Sodium/lithium aluminum hydride compounds ($NaAlH_4$ and $LiAlH_4$), called "alanates", have attracted renewed attention in the last years for their high hydrogen storage capacity. Early studies on alanates evidenced their poor absorption/desorption kinetics and lack of reversibility of that process. In 1997 Bogdanovic and Schwickardi[1] reported that, upon doping with Ti, the dehydrogenation of $NaAlH_4$ becomes reversible and the dehydrogenation kinetics are greatly accelerated,[2−9] thus opening new perspectives to the use of these compounds as hydrogen reservoirs for fuel cells and on-board applications. Further kinetic enhancement was subsequently attained by varying the doping methods.[2−5]

The discharge process of hydrogen from $NaAlH_4$ proceeds following three chemical reactions:

$$NaAlH_4 \rightarrow {}^1/_3Na_3AlH_6 + {}^2/_3Al + H_2(\uparrow) \quad (1)$$

$$Na_3AlH_6 \rightarrow 3NaH + Al + {}^3/_2H_2(\uparrow) \quad (2)$$

$$NaH \rightarrow Na + {}^1/_2H_2(\uparrow) \quad (3)$$

The series of chemical reactions has been extensively studied, and it is believed that the reacted compounds have the perfect stoichiometry reported in the previous formulas. The dehydrogenation of NaH occurs only at extremely high temperature and thus the theoretical reversible storage capacity of the sodium compound is generally considered to be 5.6 wt %. The actual hydrogen cycling capacity of Ti-doped $NaAlH_4$ under conditions relevant to practical operation of a PEM fuel cell has been found to be 3.4−4.0 wt %.[6]

The nature of the active Ti species in Ti-doped $NaAlH_4$ remains an enigma. It was initially speculated that the remarkable enhancement of the hydrogen cycling kinetics in Ti-doped $NaAlH_4$ was due to surface-localized catalytic species consisting of titanium metal or a Ti−Al alloy.[1,9,10] It was also hypothesized that during the dehydriding and rehydriding reactions titanium is present in alanates as Ti^0, Ti^{2+}, and Ti^{3+} and that it can form complexes with Al on the surface of the powder grains.[11] A later work pointed out that Ti ions should substitute Na cations in the lattice, so that the enhancement of dehydriding kinetics arising upon doping $NaAlH_4$ should be associated with lattice distortions induced by the dopant rather than a catalytic effect.[12] Recent ab initio calculations[13] and kinetic studies[14] have provided support for this model of the doped hydride. However, recent papers have also reported the detection of zerovalent titanium species in doped $NaAlH_4$.[15−18] From the present scenario it is evident that many aspects of the chemical reactions and of the hydriding/dehydriding mechanisms of alanates, in particular the role of the catalyst, need to be elucidated.

In the present paper we report an elastic modulus and energy dissipation study in $NaAlH_4$ during its decomposition reactions, where we show that the formation and evolution of different phases are detected also at extremely low concentrations and that a species having a very high mobility, likely a point defect complex containing hydrogen, enters the existence field during one of the decomposition reactions. As a consequence, new models involving the H mobility, the trapping effect of Ti on H, the presence of nonstoichiometric compounds, and their role in the dehydriding process should be considered.

* Corresponding author: phone +39-06-49914388; fax +39-06-4957697; e-mail Rosario.Cantelli@roma1.infn.it.
[†] Università di Roma "La Sapienza".
[‡] Istituto Nazionale per la Fisica della Materia.
[§] University of Hawaii.

10.1021/jp0460893 CCC: $30.25
Published on Web 12/31/2004

Experimental Section

Sodium aluminum hydride was obtained from Albemarle Corp. The aluminum metal was removed from the raw hydride via Soxlet extraction with dry, oxygen-free tetrahydrofuran (THF) under a nitrogen atmosphere by the standard Schlenk technique. The final purification was accomplished through recrystallization from THF/pentane. The doping was performed by the mechanical milling method[2,3,19] in which the hydride was combined with 2 mol % TiF_3 (Aldrich, purity 99%) and ball-milled under an argon atmosphere in a stainless steel bowl by use of a Fritsch 6 planetary mill at 400 rpm and a grinding ball-to-powder ratio of 35:1.

To obtain samples from the alanate powder for the anelastic spectroscopy measurements, the alanate was mixed with pure KBr, finely ground, and pressed in dies having rectangular form and dimensions of 40×6 mm^2. After this procedure, in which KBr has the role of compactant, solid prismatic bars were obtained with thickness varying, according to the amount of material used, from 0.7 to 1.3 mm. This method, introduced by us, was fruitfully used in a study on organic molecules[20] and opened new perspectives to the anelastic spectroscopy, as it allows measurements to be conducted on systems that are not available as solid samples. Two bars doped with 2% Ti, Ti2-1 and Ti2-2, and two undoped bars, U-2 and U-3, were prepared for the present study. Some bars made of pure KBr were also prepared for comparison. As the alanate powder reacts with oxygen, all the operations were accomplished in a flowing nitrogen atmosphere.

The complex dynamic elastic modulus, $E(\omega, T) = E'(\omega, T) + iE''(\omega, T)$, was measured as a function of temperature by suspending the prepared samples on their nodal lines and electrostatically exciting their first and third flexural modes, whose frequencies, $\omega_i/2\pi$, are in the ratio 1:5.4. The real part of the elastic modulus, or dynamic Young's modulus, can be obtained from the vibration frequency by means of the relationship $E_i'(\omega,T) = \alpha_i\rho\omega_i^2$, where ρ is the density and α_i are geometrical factors. As ρ usually varies much less than ω as a function of T, the temperature dependence of E' is practically due to the variation of ω^2. The elastic energy loss coefficient, or the reciprocal of the mechanical quality factor,[11] is $Q^{-1}(\omega, T) = E''/E'$, where $E = E' + iE''$ is the stiffness elastic constant. The loss coefficient Q^{-1} was measured from the decay of the free oscillations or from the width of the resonance peak.

Results

Figure 1 displays the coefficient of elastic energy dissipation of samples Ti2-1 and U-2 from room temperature to 4 K, which shows a monotonic decrease with decreasing temperature without visible processes. The dissipation of a pure KBr sample, to be considered as the background, is also drawn in Figure 1.

The energy loss Q^{-1} and vibration frequency f of sample Ti2-2 during thermal cyclings at progressively increasing temperatures are reported in Figure 2. On heating the sample from room temperature (RT) to 322 K, f decreases as usually expected and Q^{-1} increases, while on cooling back to room temperature both the f and Q^{-1} curves form a hysteresis loop which, however, practically closes at RT. Also, a previous cycle at 316 K (result not shown in Figure 2 for clarity reasons) displayed similar features. After the maximum temperature of the cycle was increased to 343 K, the frequency curve did not close and the modulus softened irreversibly by 2%, indicating the occurrence of a permanent modification in the material. Indeed, the modulus measurements are very sensitive to detect phase transformations or to monitor the evolution of chemical reactions, as the presence or the formation of different phase particles strongly affects the mechanical properties. Also the dissipation curve remained open after heating to 343 K, but an interpretation of the Q^{-1} behavior is certainly less direct in this case and therefore will not be discussed further. Figure 2 reports for reference also the f and Q^{-1} curves of a KBr sample along a cycle up to 346 K; this compound does not show any modification upon cycling up to this temperature. When thermal cycles were performed on alanates up to a maximum temperature not exceeding that of the previous cycle, the f and Q^{-1} cooling curves retraced the heating ones, indicating complete reversibility (see fourth cycle in Figure 2).

The fifth cycle was conducted up to the maximum temperature of 368 K. At 348 and 355 K on heating the temperature was intentionally arrested, but the modulus continued decreasing and so did the dissipation, as shown in Figure 3. Simultaneously, moderate gas evolution out of the sample was monitored by

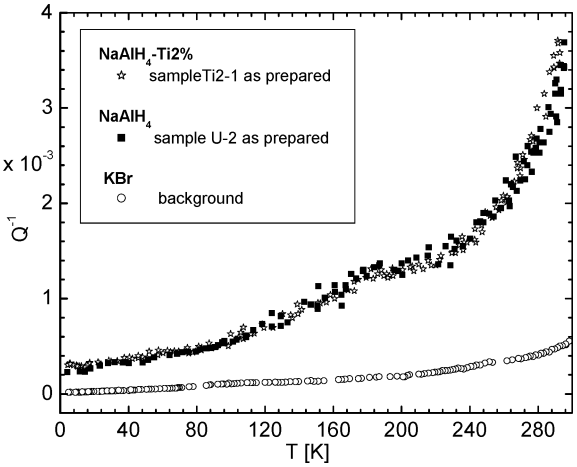

Figure 1. Elastic energy loss below room temperature of as-prepared samples of $NaAlH_4$ doped with TiF_3, undoped $NaAlH_4$, and pure KBr.

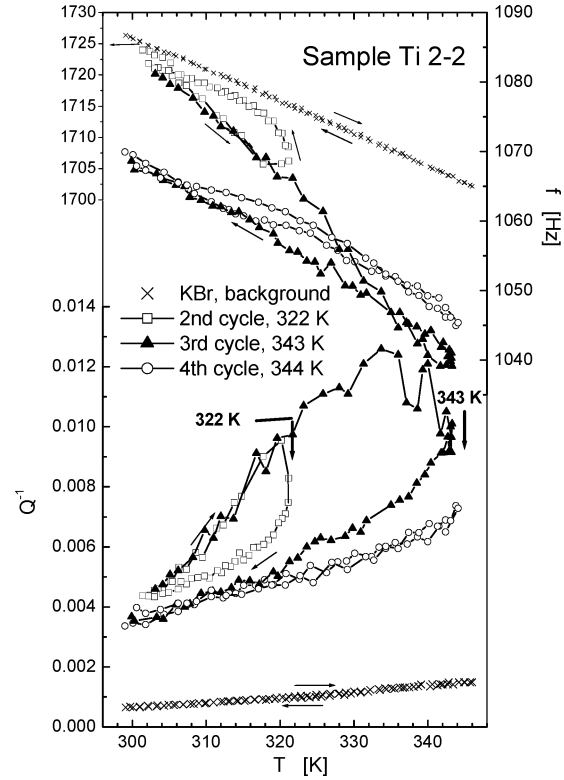

Figure 2. Temperature dependence of the elastic energy loss and frequency of Ti-doped $NaAlH_4$ during thermal cycles up to 343 K.

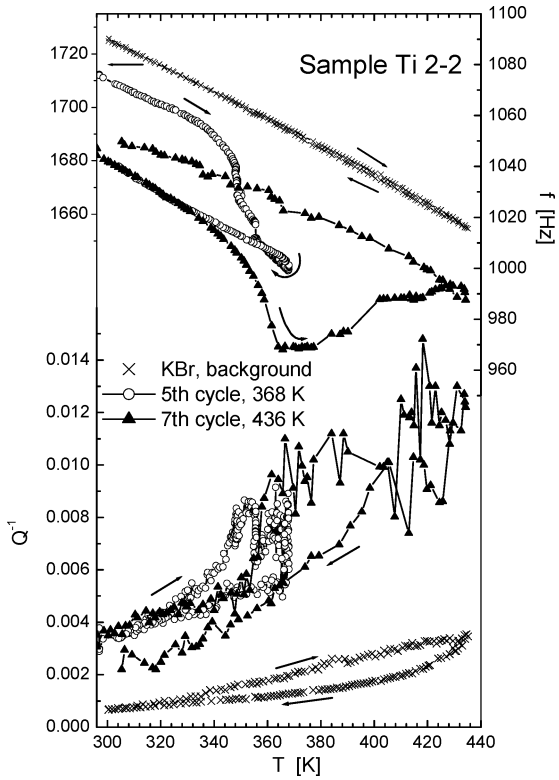

Figure 3. Temperature dependence of the elastic energy dissipation and frequency of Ti-doped $NaAlH_4$ during thermal cycles up to 435 K.

the Pirani gauge. After cooling back to the starting temperature, the modulus remarkably and irreversibly softened by about 6.6%.

In the sixth cycle the maximum temperature was lower than the previous ones (332 K; result not reported in Figure 3) and complete reversibility between heating and cooling was again observed. The cycle up to 436 K behaved qualitatively differently with respect to the previous ones. The monotonic modulus decrease on heating was followed by a steep lowering starting at 340 K, and at about 365 K the modulus inverted its trend and slow hardening was measured up to the maximum temperature reached; simultaneously, the dissipation displayed a marked scattering indicating instability; on cooling back to room temperature the *f* curve was constantly above the heating one and the sample remained hardened.

Due to the qualitatively different modulus behavior of sample Ti 2-2 during the cycle to 436 K, the low-temperature measurement was promptly repeated at two different frequencies, and the result is shown in Figure 4 (▲ and ◆) together with the dissipation before cycling (☆) already shown in Figure 1. Surprisingly, a well-developed peak appeared at about 70 K that shifts to higher temperature at the higher frequency, indicating that the peak is caused by a thermally activated relaxation process. After a 1 h aging of Ti 2-2 at 415 K, the measurements were repeated on the two vibration modes; the peak was still present but its height was lower (Figure 4).

To verify whether the modulus variations observed in Ti 2-2 during the thermal cycles may be connected to the chemical reaction that transforms the sodium aluminum hydride from tetrahydride to hexahydride, the cycling sequence was carried out also in the undoped sample U-3, where it is well-known from literature that all chemical reactions take place at higher temperature. The *f* and Q^{-1} measurements were carried out during thermal cycles up to 316, 327, 344, 365, 390, and 430

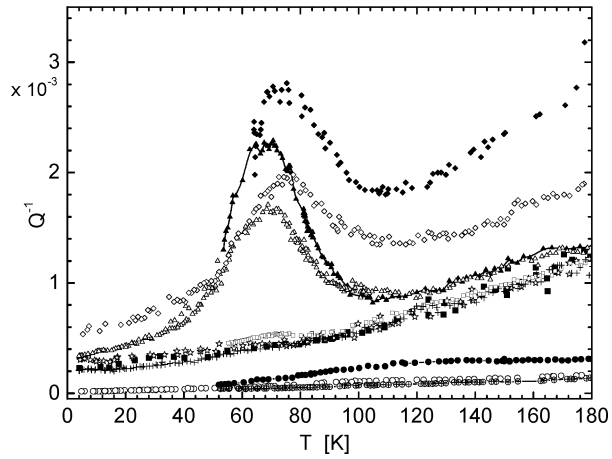

Figure 4. Low-temperature dependence of the elastic energy loss function of $NaAlH_4$−Ti2% sample Ti2-1 as prepared (☆); of $NaAlH_4$−Ti2% sample Ti2-2 after cycling up to 436 K (▲, 1.1 kHz; ◆, 4.8 kHz); of $NaAlH_4$−Ti2% sample Ti2-2 after subsequent aging of 1 h at 415 K (△, 1.1 kHz; ◇, 4.8 kHz); of undoped $NaAlH_4$ sample U-2 as prepared (■) and sample U-3 after cycling up to 430 K (□) and after subsequent aging of 8 days (+); and of KBr as prepared (○), KBr after H_2 treatment (⊕), and KBr after H plasma (●).

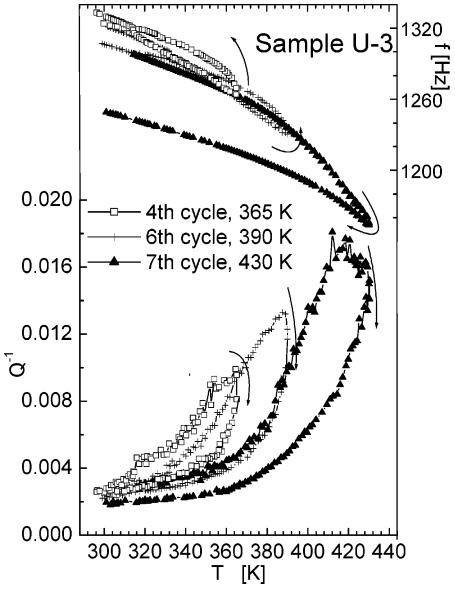

Figure 5. Temperature dependence of the elastic energy loss and frequency of undoped $NaAlH_4$ during thermal cycles up to 430 K.

K (Figure 5). The first four cycles gave closed loops. We note in particular that also after the cycle to 365 K the modulus and dissipation were recovered on cooling back to room temperature, while the corresponding cycle in the Ti-doped sample (○ in Figure 3) resulted in a marked modification of the material. The 390 K cycle of sample U-3 displayed a slight modification of the modulus, while the one at 430 K (to be compared with the 436 K cycle of the Ti 2-2 sample) showed a more visible but still moderate variation (3%).

The low-temperature dissipation curve of sample U-3 after the seventh thermal cycle is drawn in Figure 4 (□), where it is seen that only a small trace of the 70 K peak is visible, which, however, completely disappeared after aging of the sample for 8 days at room temperature (+).

We point out that the phenomena observed in samples Ti2-2 and U-3 are strictly due to intrinsic properties of the alanates and cannot be attributed to KBr, as its modulus displays a perfect

reproducibility of the heating and cooling curves and the dissipation shows only small modifications (see Figures 2 and 3).

Discussion

Monitoring of the Chemical Reaction. The elastic modulus is extremely sensitive to the formation of new phases or of atomic complexes in materials. The present data show that the modulus changes when temperature varies and its permanent modifications when the samples reassume their initial temperature after thermal cycling, are closely connected with the evolution of the decomposition reactions occurring in the alanates. Strong support for this assertion is also provided by comparison of the thermal cycles in the Ti-doped and undoped samples (Figures 2 and 5). It is clearly seen that the irreversibility behavior of the elastic modulus displayed by the latter samples is shifted to higher temperatures, because the chemical reactions are correspondingly shifted, as is known from literature.

After sample Ti2-2 was cycled to 343 K (70 °C) and 368 K, the value of the modulus is not recovered (Figure 2), and it is known that the first reaction occurring at the lowest temperatures is that described in eq 1. Therefore, we ascribe the permanent modifications of the modulus and its softening after cycling up to 343 and 368 K to the evolution of reaction 1.

Actually, the onset of the hydrogen discharging process (reaction 1) indicated by thermal desorption spectroscopy measurements is revealed at quite higher temperatures.[2] However, it is likely that this is due to the rather severe temperature rate that was used in these experiments ($dT/dt > 2$ °C/min) in order to attain the sensitivity necessary to detect the H_2 outgassing of the sample, and this fact may lead to an overestimation of the transformation temperature. The present measurements do not require high temperature rates and in principle they can be done with a quasi-static temperature variation. We emphasize, therefore, that the tetrahydride to hexahydride reaction in Ti-doped samples was observed to readily occur at 70 °C, and heating of the material above 100 °C is not required for discharging, as previously reported. As visibly indicated by the third cycle in Figure 2, desorption occurs at temperatures even lower than those indicated by X-ray diffraction observations in catalyzed samples (100 °C).[13] Modulus measurements are in progress to verify previous reports that doped alanates can undergo the reaction from $NaAlH_4$ to Na_3AlH_6 also at room temperature, at extremely slow rates.[22]

The sensitivity of the present modulus measurements is also confirmed by the results obtained from the undoped samples; in fact, the modulus irreversibility is observed in these samples after heating to only 390 K (Figure 5), while X-ray results[23] report stability even up to 423 K.

After heating to a temperature not exceeding that of the previous cycle, the modulus and dissipation heating curves are retraced on cooling (fourth cycle in Figure 2); this constitutes strong indication that the chemical reaction does not proceed appreciably in this case.

In the seventh cycle (Figure 1) the sample was heated to 436 K, and it is known[14] that at those temperatures reaction 2 occurs. Therefore, the marked instability and the modulus hardening measured during this cycle is clearly linked to the evolution of decomposition (reaction 2).

Hydrogen Dynamics. The peak appearing at about 70 K in the Ti-doped sample after the thermal treatment (TT) at 436 K is of a thermally activated nature and is caused by a species that was absent before the TT. This entity is very mobile, as it performs about 5×10^3 jumps/s at 70 K, corresponding to a relaxation rate of about 10^{11} s^{-1} at room temperature.

To check that the peak is due to a mechanism originating from the sodium aluminum hydride rather than the compactant with which it is mixed, we prepared pure KBr prismatic bars as described in the Experimental Section and conducted the following tests:

(i) In order to see whether molecular hydrogen is absorbed in KBr, one sample was heated to 550 °C in a vacuum in a sensitive apparatus for volumetric absorption tests and subsequently exposed to H_2 atmospheres of 0.4 and 4 mbar; absorption was not detected in either case.

(ii) One KBr sample was exposed to a H_2 atmosphere of 870 mbar for 90 min at 435 K, followed by slow cooling for 2 h in the same H_2 atmosphere. This was the maximum temperature of the seventh cycle, after which the low-temperature peak appeared. This test eliminates the possibility of process entailing the absorption of hydrogen by KBr upon its evolution out of the alanate.

(iii) A KBr prismatic bar was exposed to a hydrogen plasma of 5 mbar dynamic flow at 250 °C for 5 h, with the aim of producing atomic hydrogen. In fact, the nonmetallic KBr surface does not split the H_2 molecule, thus not providing the conditions for hydrogen entry in the solid.

The Q^{-1} curves measured below room temperature in the samples of the second and third tests are reported in Figure 4, where it is seen that the peak is totally absent.

Once it was ascertained that the observed peak originates in the sodium aluminum hydride, we carried out a quantitative analysis of it. In the Debye model the elastic energy loss function can be expressed as[21]

$$Q^{-1} = \frac{M v_0 (\lambda_1 - \lambda_2)^2 n_1 n_2}{T} \frac{1}{(\omega\tau)^{\alpha} + (\omega\tau)^{-\alpha}} \qquad (4)$$

where M is the Young modulus; v_0 is the unit cell volume; λ_1 and λ_2 are the elastic dipoles of the defects in the two configurations in which the defects can relax; n_1 and n_2 the fractions of defects in each state; $\omega = 2\pi f$, with f the vibration frequency of the sample; τ is the relaxation time, which in the case of classical processes follows the Arrhenius law, $\tau = \tau_0 e^{E/kT}$; and $\alpha = 1$.

The activation energy and the preexponential factor derived from the peak shift with frequency gave the approximate values of 0.126 eV and 7×10^{-14} s. Those values of E and τ_0 were then inserted in the single-time Debye formula and the obtained curve is drawn in Figure 6. By a comparison with the data, the experimental curve is remarkably broader than a single Debye process, indicating either that the relaxing complexes are strongly interacting, or that they perform different types of jumps having close relaxation rates; this fact implies a distribution of the relaxation parameters (E and τ_0). To obtain an evaluation of the broadening, the approximate Fuoss−Kirkwood fitting procedure was adopted, and a value of $\alpha = 0.27$ was obtained, which is typical of extremely broad processes.

To perform a more accurate analysis, we introduced a Gaussian distribution[10] of τ_0 and E in the Q^{-1} expression:[4]

$$Q^{-1} = C \int\int \frac{1}{\omega\tau + (\omega\tau)^{-1}} P(E) P(\tau)\, dE\, d\tau \qquad (5)$$

where C is a constant, τ follows the usual Arrhenius law, and $P(E)$ and $P(\tau)$ are two normalized Gaussian distribution functions for E and τ, respectively.

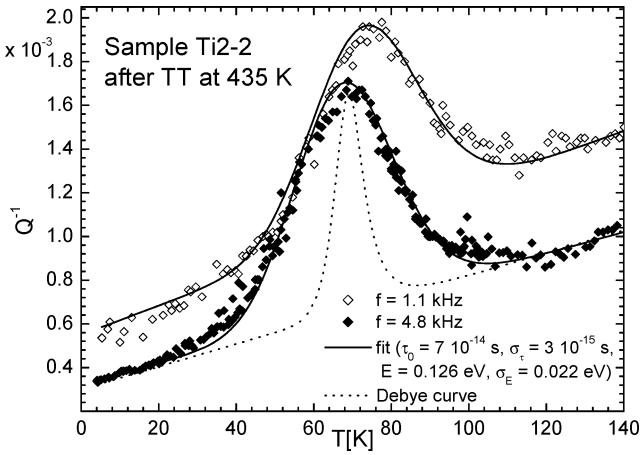

Figure 6. Elastic energy loss function of the Ti-doped alanate (symbols) and best curves (solid lines) obtained by means of the model with Gaussian distribution functions of the activation energy and relaxation time. For comparison, the corresponding Debye curve is reported (dotted line).

The best fit is satisfactory as seen in Figure 6 and gave the following mean values for E, τ_0, and the respective widths:

$$E = 0.126 \text{ eV}, \sigma(E) = 0.022 \text{ eV}$$

$$\tau_0 = 7 \times 10^{-14} \text{ s, and } \sigma(\tau_0) = 3 \times 10^{-15} \text{ s}$$

Important information is obtained from the prefactor; in fact, its value is typical of point defect relaxation and thus may provide the key to the interpretation of the nature of the relaxing entity. Preliminarily, we suggest that, in view of the fast dynamics of the mobile species causing the peak, as well as of the observation of H_2 outgassing during the reactions, hydrogen is very likely involved in the point-defect complex causing the detected relaxation. To ascribe the peak to a possible physical mechanism, we will consider the decomposition reactions 1 and 2 separately.

The first decomposition, reaction 1, was well monitored by the modulus softening of Ti 2-2 during the third and fifth cycles (Figures 2 and 3), and it was accompanied by hydrogen outgassing. Additionally, the absence of the peak in the measurement carried out after the fifth cycle, at 368 K (result not shown), suggests that the peak cannot be ascribed to spurious phases introduced during the powder preparation; the products of reaction 1, that is, Na_3AlH_6; aggregated Al; an altered form of $NaAlH_4$ resulting immediately upon treatment with the dopant precursor; or interstitial hydrogen (if any is left in the crystal lattice after its evolution out of the sample). It should be pointed out that the monitoring of the hydrogen molecule during hydrogen evolution out of the sample is only the final step of the outgassing process and does not give information about the state of hydrogen inside the compound. Possible states for interstitial hydrogen, however, not yet identified in the present compounds, are in atomic (or protonic) form, in H−H pairs, in complexes with other impurities, and so forth.

The low-temperature peak appeared after the sample was heated to 436 K, during which reaction 2 evolved, and correspondingly the modulus anomaly manifested itself. Therefore, the mechanism causing the peak apparently involves one of the possible point defects or point defect complexes produced by reaction 2. Provided that the peak is absent in the Na_3AlH_6 produced by reaction 1, it may be caused by (i) a stoichiometry defect of Na_3AlH_6 (indeed, if one or more of the six H atoms are missing, jumping is possible for the remaining H atoms, and in other words H vacancy dynamics may take place); (ii) the relaxation of H in the NaH compound produced by the decomposition reaction 2; (iii) the reorientation of H around Ti, or a Ti−Al complex, or a vacancy which acts as an attracting cluster for H after the transformation at 150 °C. In the latter case, we must suppose that a small part of the hydrogen made available by reaction 2 does not evolve out of the sample but is retained in the lattice by the trap. The potent trapping effect of substitutional Ti on H in a crystal lattice was first reported in 1977 for Nb−Ti alloys by G. Cannelli and one of the present authors (R.C.), as reviewed in the work of ref 24. It was found that the Ti atom locally distorts the lattice and introduces sites for easy H reorientation, resulting in relaxation processes around 100 K (at 20 kHz), and that the H migration proceeds via long range from trapping site to trapping site.

Although much systematic work is still needed in order to have a better understanding of the complex processes occurring in alanates, the present results clearly indicate that new models involving the H mobility should be considered to understand the catalytically enhanced kinetics.

Conclusions

In conclusion, we report the first measurements of complex elastic modulus in alanates. The dynamic Young modulus allowed us to monitor the evolution of the decomposition reactions as a function of temperature and time, whereas the elastic energy dissipation, after a thermal treatment up to 436 K, revealed the presence of a thermally activated relaxation process due to the fast dynamics of a point-defect cluster, very likely involving hydrogen. The present data suggest that models aiming at interpreting the decomposition reactions and kinetics should consider the hydrogen mobility and trapping and stoichiometry defects.

The nonconventional way introduced by us to obtain solid vibrating samples from the alanate powders made the present study possible and opened new perspectives to the anelastic spectroscopy, as it allows elastic modulus and dissipation measurements to be extended to all compounds that cannot be obtained in bulky form.

Acknowledgment. We acknowledge F. Cordero for carrying out the volumetric tests on hydrogen absorption in KBr. C.M.J. and S.S.S. gratefully acknowledge financial support received from the Office of Hydrogen, Fuel Cells, and Infrastructure Technologies of the U.S. Department of Energy.

References and Notes

(1) Bogdanovic, B.; Schwickardi, M. *J. Alloys Compd.* **1997**, *253−254*, 1.

(2) Zidan, R. A.; Takara, S.; Hee, A. G.; Jensen, C. M. *J. Alloys Compd.* **1999**, *285*, 119.

(3) Jensen, C. M.; Zidan, R. A. U.S. Patent 6,471,935, 2002.

(4) Bogdanovic, B.; Felderhoff, M.; Kaskel, S.; Pommerin, A.; Schlichte, K.; Schüth, F. *Adv. Mater.* **2003**, *15*, 1012.

(5) Fichtner, M.; Fuhr, O.; Kircher, O.; Rothe, J. *Nanotechnology* **2003**, *14*, 778.

(6) Srinivasan, S. S.; Brinks, H. W.; Hauback, B. C.; Sun, D.; Jensen, C. M. *J. Alloys Compd.* **2004**, *377*, 283.

(7) Bogdanovic, B.; Schwickardi, M. U.S. Pat. Appl. 08/983.320, 1998; corresponding to World Pat. Appl. PCT WO 97/03919, 1997, and German Pat. Appl. 19526434.7, 1995.

(8) Jensen, C. M.; Gross, K. *J. Appl. Phys.* **2001**, *A72*, 213.

(9) Bogdanovic, B.; Brand, R. A.; Marjanovic, A.; Schwickardi, M.; Tolle, J. *J. Alloys Compd.* **2000**, *302*, 36.

(10) Thomas, G. J.; Gross, K. J.; Yang, N. Y. C.; Jensen, C. M. *J. Alloys Compd.* **2002**, *330−332*, 702.

(11) Chen, J.; Kuriyama, N.; Qiang, X.; Takeshita, H. T.; Tetsuo, S. *J. Phys. Chem.* **2001**, *B105*, 11214.

(12) Sun, D.; Kiyobayashi, T.; Takeshita, H. T.; Kuriyama, N.; Jensen, C. M. *J. Alloys Compd.* **2002**, *337*, L8.

(13) Iniguez, J.; Yildirim, T.; Udovic, T. J.; Sulic, M.; Jensen, C. M. *Phys. Rev. B* **2004**, *70*, 60101.

(14) Kiyobayashi, T.; Srinivasan, S. S.; Sun, D.; Jensen, C. M. *J. Phys. Chem. A* **2003**, *107*, 7671.

(15) Bogdanovic, B.; Felderhoff, M.; Germann, M.; Hartl, M.; Pommerin, M. A.; Schuth, F.; Weidenthaler, G.; Zibrowius, A. *J. Alloys Compd.* **2003**, *350*, 136.

(16) Brinks, H. W.; Jensen, C. M.; Srinivasan, S. S.; Hauback, B. C.; Blanchard, D.; Murphy, K. *J. Alloys Compd.* **2004**, *376*, 215.

(17) Graetz, J.; Reilly, J. J.; Johnson, J.; Ignatov, A. Y.; Tyson, T. A. *Appl. Phys. Lett.* **2004**, *85*, 500.

(18) Leon, A.; Kircher, O.; Rothe, J.; Fichtner, M. *J. Phys. Chem. B* **2004**, *108*, in press.

(19) Jensen, C. M.; Zidan, R. A.; Mariels, N.; Hee, A.; Hagen, C. *Int. J. Hydrogen Energy* **1999**, *24*, 461.

(20) Paolone, A.; Cantelli, R.; Caciuffo, R.; Arduini, A. *Phys. Rev.* **2002**, *B65*, 214304.

(21) Nowick, A. S.; Berry, B. S. *Anelastic Relaxation in Crystalline Solids*; Academic Press: New York, 1972.

(22) Sandrock, G.; Gross, K.; Thomas, G.; Jensen, C.; Meeker, D.; Takara, S. *J. Alloys Compd.* **2002**, *330*−*332*, 696.

(23) Gross, K. J.; Guthrie, S.; Takara, S.; Thomas, G. *J. Alloys Compds* **2000**, *297*, 270.

(24) Cannelli, G.; Cantelli, R.; Cordero, F.; Trequattrini, F. Tunnelling of H and D in Metals and Semiconductors; monography (80 pp), in *Tunnelling Systems in Amorphous and Crystalline Solids*; Esquinazi, P., Ed.; Springer, 1998.

Preparation of Ti-Doped Sodium Aluminum Hydride from Mechanical Milling of NaH/Al with Off-the-Shelf Ti Powder

Ping Wang* and Craig M. Jensen*

Department of Chemistry, University of Hawaii, Honolulu, Hawaii 96822

Received: July 7, 2004; In Final Form: August 3, 2004

Ti-doped $NaAlH_4$ can be directly prepared by mechanical milling a 1:1 mixture of NaH and Al together with a few mole percent of off-the-shelf metallic Ti powder under an argon or hydrogen atmosphere. The hydrogen storage materials that are produced through this process exhibit stable hydrogen capacities through 10 cycles of hydrogenation/dehydrogenation. We have conducted a systematic investigation of this new method for the preparation of Ti-doped $NaAlH_4$. Consideration of these results, together with those previously obtained for $NaAlH_4$ that was doped with Ti powder through milling under a hydrogen atmosphere, has provided insight into the nature of active Ti species.

Introduction

Sodium aluminum hydride has been found to undergo reversible elimination of hydrogen at moderate temperatures upon doping with a few mole percent of selected transition metal compounds.[1,2] This finding has stimulated extensive study of doped $NaAlH_4$ and other light-metal complex hydrides as viable candidates for onboard hydrogen storage applications.[3−29] Studies of Ti-doped $NaAlH_4$ have led to considerable improvement in the kinetic and cycling performance at conditions that are relevant to the practical operation of a PEM fuel cell.[3−13] However, despite this progress, practical hydrogen storage capacities of only 3∼4 wt % have been achieved for Ti-doped $NaAlH_4$. This is far from the theoretical value of 5.6 wt % for $NaAlH_4$ undergoing dehydrogenation to NaH and Al as seen in eq 1.

$$NaAlH_4 \leftrightarrows 1/3\ Na_3AlH_6 + 2/3Al + H_2 \leftrightarrows NaH + Al + 3/2H_2 \quad (1)$$

The current state-of-the-art doping technology involves the use of high-valance Ti compounds as dopant precursors. Utilization of these precursors is known to result in the production of nonvolatile byproducts that occupy a significant weight percentage and constitute "dead weight" in the doped materials. For example, it has been well established that the use of $TiCl_3$ or $TiCl_4$ as the dopant precursor gives rise to the production of NaCl.[11,14,27] The incorporation of Na and/or Al in these byproducts also results in a significant reduction in the amount of the parent hydride that is available for hydrogen storage.[11] Clearly, the identification of a method for effectively doping $NaAlH_4$ without generating "dead weight" byproducts would be an important advance in the development of doped $NaAlH_4$ as practical hydrogen storage media. Limited success toward this goal has been achieved through ball milling $NaAlH_4$ with Ti13·6THF.[12,13]

We recently reported a method whereby off-the-shelf Ti powder could be used directly to prepare Ti-doped $NaAlH_4$ through mechanical milling.[28] Unfortunately, the hydride that was obtained through this direct Ti doping process suffers from serious cycling degradation and dehydriding kinetics that are inferior to doped hydride produced by mechanical milling with Ti(III) or Ti(IV) precursors.[3−11] These results did, however, suggest that more than one Ti species might be produced by the doping process. Thus, current thinking concerning the nature of active Ti species in the doped hydrides might be oversimplified; it is possible that more than one Ti species contributes to the kinetic enhancement of the dehydrogenation of $NaAlH_4$.

The practical and economical advantages of introducing dopants into sodium aluminum hydride during its "direct synthesis" from NaH and Al have long been appreciated.[8,23] As an alternative approach to our direct utilization of Ti powder as dopant precursor, we have explored mechanical milling the mixture of NaH and Al with off-the-shelf Ti powder. The materials obtained through this doping procedure, unlike the material that is prepared through mechanical milling of $NaAlH_4$ with Ti powder under a hydrogen atmosphere, have been found to undergo a stable hydrogenation/dehydrogenation cycle. We have also observed that variation of the conditions that are employed for milling of the NaH/Al mixtures together with Ti powder leads to significant differences in the hydrogen storage performance.

Experimental Section

The starting materials, NaH (95%, ∼200 mesh), Al powder (99.95+%, ∼200 mesh), and Ti powder (99.98%, ∼325 mesh), were all purchased from Aldrich Co. The mixture of NaH + Al + Ti in a mole ratio of 1:1:0.04 was mechanically milled using a Fritsch 6 Planetary mill at 400 rpm in a stainless steel bowl together with eight 7-mm diameter steel balls. The milling was performed under a hydrogen or argon atmosphere, with initial pressures of about 0.8 and 0.1 MPa, respectively. The ball-to-powder ratio varied between 30:1 and 40:1.

Hydrogen absorption/desorption behavior was monitored with a carefully calibrated Sievert's-type apparatus (LESCA Co., Japan). Precise pressure measurement and temperature controlling were accomplished by using a high-precision pressure transducer and a silicon oil bath, respectively. A typical cyclic experiment entailed absorption at 120 °C and desorption at 150

* To whom correspondence may be addressed. E-mail: jensen@gold.chem.hawaii.edu; pwang@hawaii.edu; Fax: +1 808 956 5908.

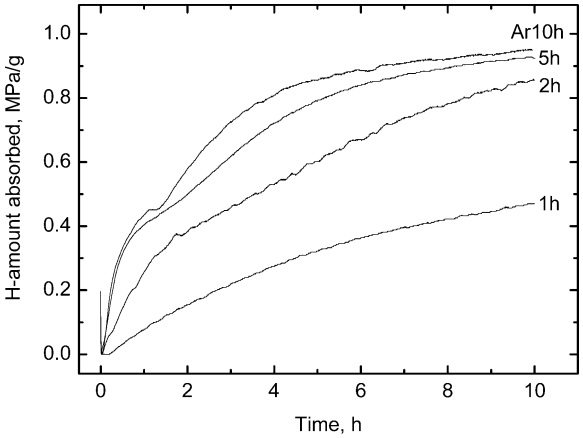

Figure 1. First hydrogenation profiles at 120 °C of NaH + Al + 4 mol % Ti mechanically milled under an Ar atmosphere for different periods.

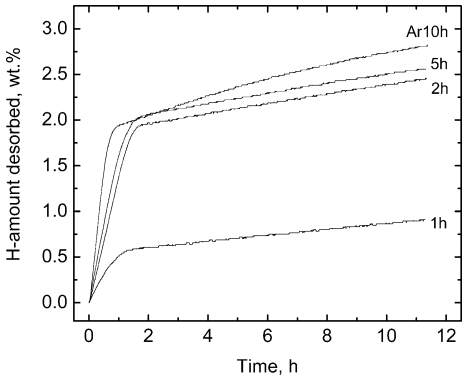

Figure 2. First dehydrogenation profiles at 150 °C of NaH + Al + 4 mol % Ti mechanically milled under an Ar atmosphere for different periods.

°C. The initial pressure conditions were ~12 MPa and <1 Torr, respectively. To allow a practical evaluation of the hydrogen storage performance, the weight of metallic Ti was taken into account in the determination of H capacity.

Results and Discussion

We had previously found that a reactive H_2 atmosphere was required to achieve effective Ti doping of $NaAlH_4$ using Ti powder.[28] Thus, it was surprising to find that effective Ti doping could be achieved upon mechanical milling of 1:1 mixtures of NaH and Al with prescribed amounts of Ti powder under an argon atmosphere. The reversible hydriding/dehydriding behaviors of thus-prepared materials were found to be highly dependent on the milling time. This is inconsistent with the findings of our earlier study of the doping of $NaAlH_4$ with off-the-shelf Ti powder.[28] Kinetic studies were carried out on samples that were mechanically milled under an argon atmosphere for different lengths of time. All of the samples were hydrogenated under identical conditions (including time and initial hydrogen pressure) before being subjected to dehydrogenation. We experienced difficulties in precisely determining the amount of absorbed hydrogen during the high-pressure hydrogenation process; thus, the change in hydrogen pressure was directly used to characterize the hydrogenation kinetics. Representative initial hydrogenation and dehydrogenation profiles are presented in Figures 1 and 2, respectively. The rate of both hydrogenation and dehydrogenation increased with increased milling time. Remarkably, the marked difference in

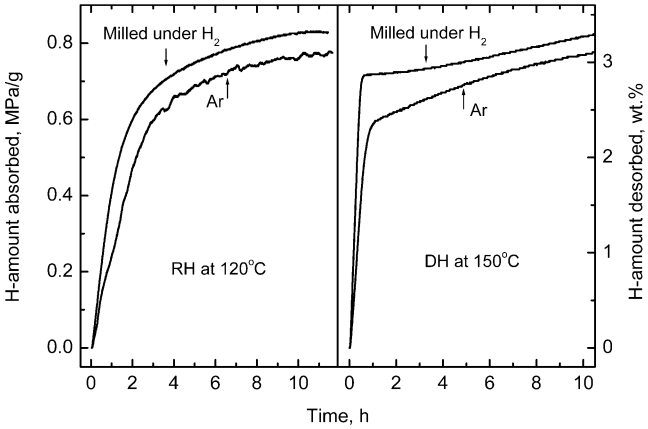

Figure 3. Comparison of the hydrogenation/dehydrogenation profiles in the third cycle between the materials that were prepared by mechanically milling the mixture of NaH + Al + 4 mol % Ti for 10 h under H_2 and Ar atmospheres, respectively. RH, rehydrogenation; DH, dehydrogenation.

kinetic performance arising upon variation of the milling time persisted in the following cycles of hydrogenation/dehydrogenation.

Mechanical milling of NaH/Al mixture with Ti powder under H_2 rather than argon was found to significantly influence the hydrogen storage performance of the doped hydride. Figure 3 compares typical hydrogenation and dehydrogenation profiles of 1:1 mixtures of NaH and Al that were mechanically milled with Ti powder under the differing atmospheres for 10 h. It was observed that the material prepared under a H_2 atmosphere exhibited significant improvements in both the hydrogenation rate and attainable hydrogen capacity vs the material that arises upon milling under an argon atmosphere. Additional, the kinetic behaviors during dehydrogenation were also affected. Similar small, but significant, improvements in hydrogen storage behaviors were also observed in analogous comparison studies of the doped hydrides that were prepared through mechanical milling for 2 and 5 h.

We initially considered the possibility that the mechanical milling of the mixture of NaH and Al with Ti powder under a H_2 atmosphere might result in the direct synthesis of Na_3AlH_6. To explore this possibility, several samples were intensively milled for long periods. Following only the mechanical milling, none of the samples were found to undergo substantial dehydrogenation at 150 °C, clearly indicating that Na_3AlH_6 was not formed. Apparently, the applied hydrogen pressure was lower than the plateau pressure of Na_3AlH_6 at the local temperatures that were reached during the mechanical milling process.[6,9]

The hydrogen capacity of the material obtained from the milling of 1:1 NaH and Al with off-the-shelf Ti under a H_2 atmosphere was found to be highly stable. This markedly contrasts with the behavior of the doped hydride obtained through milling $NaAlH_4$ with Ti powder under a H_2 atmosphere, in which a serious cycling degradation on hydrogen capacity was detected.[28] Figure 4 compares the cycling dehydrogenation performance between these two materials that were both prepared through mechanical milling under a H_2 atmosphere for 10 h. No signs of degradation of either hydrogen capacity or dehydrogenation kinetics are detectable for the present material after 10 cycles. Unfortunately, the potential for an improved hydrogen capacity upon the elimination of doping byproducts was not realized as only 3.3 wt % hydrogen is available from the material after desorption at 150 °C for 10 h. The low hydrogen cycling capacity is, at least partly, due to the slow kinetics in the second dehydriding step, which is

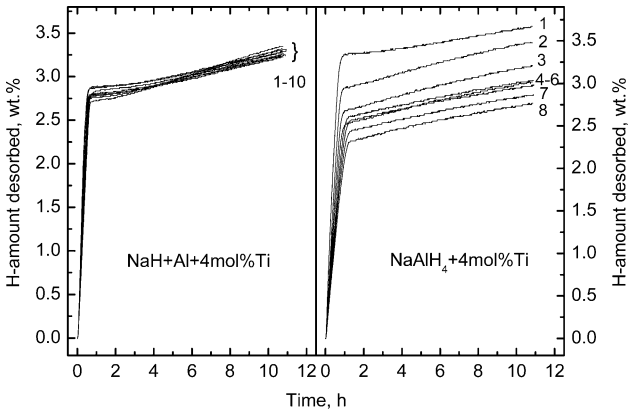

Figure 4. Comparison of the cycling dehydrogenation profiles between NaH + Al + 4 mol % Ti and $NaAlH_4$ + 4 mol % Ti. Both samples were prepared by mechanical milling under a H_2 atmosphere for 10 h.

significantly inferior to those arising upon doping the hydride with Ti(III) or Ti(IV) dopant precursors.[3−9,11,14,15] Additionally, the persistent problem of incomplete conversion of Na_3AlH_6 to $NaAlH_4$ in the rehydrogenation process contributes to the wide gap between the practically attained values and the theoretical values for the available weight percent of hydrogen.[21] The results of our attempts to resolve the problem of low available hydrogen capacity through a functionally designed, structural modification of doped material (inspired by this study) will be presented in forthcoming publications.

The finding of hydrogen storage performances that are characteristic of the variations in this method of preparation of the Ti-doped hydride has several important implications about the nature of the active Ti species in these materials. Clearly, mechanical milling accomplishes more than merely the high dispersion of the atomic Ti on the surface of the hydride[1,6,9] as changes in the milling atmosphere and/or the bulk environment (hydrogenated vs dehydrogenated form) exert influences that are as pronounced as those resulting from variation in milling time.[28] Furthermore, our findings suggest that these materials do not all contain the same active Ti species; rather, they contain a variety of related active Ti species. Kinetic studies have indicated that the abilities of active Ti species to migrate within the bulk of the hydride and interact with complex Alanate anions are the factors that dictate the kinetics of dehydrogenation and rehydrogenation of the doped hydride.[22] Thus, the observed differences in the hydrogen storage performance of these materials can be ascribed to variations in the active Ti species that effect its stability, bulk mobility in the hydride, and/or interaction with the complex Alanate anions.

Conclusions

We have developed a method for the preparation of Ti-doped $NaAlH_4$ by mechanically milling a 1:1 mixture of NaH and Al with a few mole percent of off-the-shelf Ti powder. This method has practical advantages over the doping of $NaAlH_4$ with (1) Ti(III) and Ti(IV) precursors that result in the incorporation of dead weight byproducts or (2) Ti13•6THF, which is much more expensive and less generally available. Moreover, our results clearly demonstrate that kinetic enhancement of the reversible dehydrogenation of Ti-doped $NaAlH_4$ can be induced upon milling the hydride with simple Ti powder. Thus, there is no requirement for exotic nanostructured precursors. The doped Alanate that is prepared through our novel method shares several common characteristics with $NaAlH_4$ that is doped through mechanical milling with off-the-shelf Ti powder under a H_2 atmosphere. However, it has the important practical advantage that its hydrogen storage capacity does not diminish upon cycling. The kinetic enhancement of the dehydrogenation process observed in the thus-prepared Alanate has been found to be inferior to that arising from doping $NaAlH_4$ with Ti(III) and Ti(IV) precursors. As a result, the material does not exhibit an improved hydrogen cycling capacity despite not containing any doping byproducts. We have found that this problem is partially alleviated when the mechanical milling is carried out under an atmosphere of H_2 rather than of argon. Thus, it is evident that the presence of hydrogen in the milling process affects the nature of the active Ti species. Further investigation into the nature of this modification may lead to the elucidation of the mechanism of action of the active Ti species in the dehydrogenation of the complex Alanate anions. Thus, further investigation could provide insight into means of improving the hydrogen storage properties of Ti-doped $NaAlH_4$.

Acknowledgment. This work was financially supported by The Office of Hydrogen, Fuel Cells, and Infrastructure Technologies of the U.S. Department of Energy.

References and Notes

(1) Bogdanović, B.; Schwickardi, M. *J. Alloys Compd.* **1997**, *253−254*, 1−9.

(2) Bogdanović, B.; Schwickardi, M. U.S. Patent Appl. S. N. 08/983.320 (1998), corresponding to PCT/EP 96/03333076; German Patent Appl. 195 26 434.7, July 19, 1995.

(3) Jensen, C. M.; Zidan, R.; Mariels, N.; Hee, A.; Hagen, C. *Int. J. Hydrogen Energy* **1999**, *24*, 461−465.

(4) Zidan, R. A.; Takara, S.; Hee, A. G.; Jensen, C. M. *J. Alloys Compd.* **1999**, *285*, 119−122.

(5) Jensen, C. M.; Zidan, R. A. U.S. Patent 6,471,935, 2002.

(6) Bogdanović, B.; Brand, R. A.; Marjanovic, A.; Schwickardi, M.; Tölle, J. *J. Alloys Compd.* **2000**, *302*, 36−58.

(7) Jensen, C. M.; Gross, K. J. *Appl. Phys. A* **2001**, *72*, 213−219.

(8) Bogdanović, B.; Schwickardi, M. *Appl. Phys. A* **2001**, *72*, 221−223.

(9) Gross, K. J.; Thomas, G. J.; Jensen, C. M. *J. Alloys Compd.* **2002**, *330−332*, 683−690.

(10) Sandrock, G.; Gross, K.; Thomas, G.; Jensen, C.; Meeker, D.; Takara, S. *J. Alloys Compd.* **2002**, *330−332*, 696−701.

(11) Sandrock, G.; Gross, K.; Thomas, G. *J. Alloys Compd.* **2002**, *339*, 299−308.

(12) Bogdanović, B.; Felderhoff, M.; Kaskel, S.; Pommerin, A.; Schlichte, K.; Schüth, F. *Adv. Mater.* **2003**, *15*, 1012−1015.

(13) Fichtner, M.; Fuhr, O.; Kircher, O.; Rothe, J. *Nanotechnology* **2003**, *14*, 778−785.

(14) Gross, K. J.; Sandrock, G.; Thomas, G. J. *J. Alloys Compd.* **2002**, *330−332*, 691−695.

(15) Bogdanović, B.; Sandrock, G. *MRS Bull.* **2002**, *27*, 712−716.

(16) Zaluska, A.; Zaluski, L.; Ström-Olsen, J. O. *J. Alloys Compd.* **2000**, *298*, 125−134.

(17) Gross, K. J.; Guthrie, S.; Takara, S.; Thomas, G. J. *J. Alloys Compd.* **2000**, *297*, 270−281.

(18) Thomas, G. J.; Gross, K. J.; Yang, N. Y. C.; Jensen, C. *J. Alloys Compd.* **2002**, *330−332*, 702−707.

(19) Sun, D.; Kiyobayashi, T.; Takeshita, H. T.; Kuriyama, N.; Jensen, C. M. *J. Alloys Compd.* **2002**, *337*, L8−L11.

(20) Meisner, G. P.; Tibbetts, G. G.; Pinkerton, F. E.; Olk, C. H.; Balogh, M. P. *J. Alloys Compd.* **2002**, *337*, 254−263.

(21) Bogdanovi'c, B.; Felderhoff, M.; Germann, M.; Härtel, M.; Pommerin, A.; Schüth, F.; Weidenthaler, C.; Zibrowius, B. J. *Alloys Compd.* **2003**, *350*, 246−255.

(22) Kiyobayashi, T.; Srinivasan, S. S.; Sun, D.; Jensen, C. M. *J. Phys. Chem. A* **2003**, *107*, 7671−7674.

(23) Majzoub, E. H.; Gross, K. J. *J. Alloys Compd.* **2003**, *356−357*, 363−367.

(24) Balema, V. P.; Dennis, K. W.; Pecharsky, V. K. *Chem. Commun.* **2000**, 1665−1666.

(25) Fichtner, M.; Fuhr, O.; Kircher, O. *J. Alloys Compd.* **2003**, *356−357*, 418−422.

(26) Züttel, A.; Rentsch, S.; Fischer, P.; Wenger, P.; Sudan, P.; Mauron, Ph.; Emmenegger, Ch. *J. Alloys Compd.* **2003**, *356−357*, 515−520.

(27) Brinks, H. W.; Jensen, C. M.; Srinivasan, S. S.; Hauback, B. C.; Blanchard, D.; Murphy, K. *J. Alloys Compd.* **2004**, *376*, 215.

(28) Wang, P.; Jensen, C. M. *J. Alloys Compd.*, in press.

PHYSICAL REVIEW B **70**, 060101(R) (2004)

Structure and hydrogen dynamics of pure and Ti-doped sodium alanate

Jorge Íñiguez,[1,2] T. Yildirim,[1] T. J. Udovic,[1] M. Sulic,[3] and C. M. Jensen[3]
[1]*NIST Center for Neutron Research, National Institute of Standards and Technology, Gaithersburg, Maryland 20899, USA*
[2]*Department of Materials Science and Engineering, University of Maryland, College Park, Maryland 20742, USA*
[3]*Department of Chemistry, University of Hawaii, Honolulu, Hawaii 96822, USA*
(Received 2 June 2004; published 3 August 2004)

We have studied the structure, energetics, and dynamics of pure and Ti-doped sodium alanate ($NaAlH_4$), focusing on the possibility of substitutional Ti doping in the bulk. Our *ab initio* calculations reproduce well the measured neutron inelastic scattering spectrum, which exhibits surprisingly strong and sharp two-phonon features. The calculations also reveal that substitutional Ti doping is energetically possible, and imply that Ti prefers to substitute for Na and is a powerful hydrogen attractor that facilitates multiple Al-H bond breaking. Our results hint at ways of improving the hydrogen dynamics and storage capacity of the alanates.

DOI: 10.1103/PhysRevB.70.060101 PACS number(s): 61.12.−q, 63.20.Dj, 68.43.Bc, 81.05.Zx

Developing safe, cost-effective, and practical means of storing hydrogen is crucial for the advancement of hydrogen and fuel cell technologies. Presently, there are three generic routes for the solid-state storage of hydrogen: (i) physisorption as in many porous carbon and zeolite materials; (ii) chemisorption as in metal hydrides; and (iii) chemical reaction such as in complex metal hydrides. Among the type (iii) materials, sodium alanate ($NaAlH_4$) has received considerable attention because of its high hydrogen weight capacity and low cost. The release of hydrogen from $NaAlH_4$ occurs via a two-step reaction

$$NaAlH_4 \leftrightarrow \frac{1}{3}Na_3AlH_6 + \frac{2}{3}Al + H_2 \ (3.7 \text{ wt } \%),$$

$$Na_3AlH_6 \leftrightarrow 3NaH + Al + \frac{3}{2}H_2 \ (1.8 \text{ wt } \%), \qquad (1)$$

yielding a total of 5.5 wt % hydrogen. It was recently reported that a few percent of Ti doping in $NaAlH_4$ renders accelerated and reversible hydrogen release under moderate conditions.[1] In spite of the extensive investigations of Ti-doped $NaAlH_4$ that have resulted, little is known about the mechanism by which Ti enhances the cycling kinetics of hydrogen.[2,3] In fact, even the location of the Ti atoms remains unclear. While it is widely believed that they reside on the surface of the material,[4] the possibility that Ti is substituted for Na has also been suggested,[5] but convincing experimental or theoretical evidence is still lacking.

Here we present first-principles total energy and dynamics calculations of pure and Ti-doped sodium alanates, focusing on the possibility of substitutional Ti doping in the bulk. Along with the calculations, we report neutron inelastic scattering (NIS) measurements of the phonon density of states, which allow us to validate our computational approach. We succeed in characterizing the main features in the observed spectrum, which displays surprisingly strong two-phonon contributions. Furthermore, the calculations show that it is most energetically favorable for Ti to substitute for Na, breaking several Al-H bonds in its vicinity. We also find that Ti-doped $NaAlH_4$ can accommodate extra hydrogen near the dopant. In addition, we examine the effect of the Ti dopants on the vibrational spectrum of neighboring AlH_4 groups, which could allow probing the Ti location in doped samples using high resolution spectroscopic techniques.

Three powder samples were investigated: pure $NaAlH_4$, 2% Ti-doped $NaAlH_4$, and Na_3AlH_6. $NaAlH_4$ was prepared as described in Ref. 6. $NaAlH_4$ was doped with 2 mol percent TiF_3 through mechanical milling according to standard procedure.[7] Na_3AlH_6 was synthesized and purified by the method of Huot *et al.*[8] The NIS measurements were performed using the filter analyzer neutron spectrometer at the NIST Center for Neutron Research (Gaithersburg, Maryland)[9] under conditions that provided energy resolutions of 2-4.5 % in the range probed.

The calculations were performed within the plane-wave implementation of the generalized gradient approximation[10] to density functional theory in the ABINIT package.[11] We used Troullier-Martins pseudopotentials[12,13] treating the following electronic states as valence: 3*d* and 4*s* of Ti, 3*s* and 3*p* of Al, 3*s* of Na, and 1*s* of H. We carefully tested the convergence of our calculations with respect to the plane-wave cutoff and *k*-point mesh. For example, for the Ti-doped alanate supercells (containing 96 atoms) we used a cutoff of 1250 eV and a $3\times3\times2$ *k*-point mesh. The phonon spectrum of the pure compound was computed using density functional perturbation theory[14] as implemented in ABINIT. We calculated the phonons corresponding to two $2\times2\times2$ *q*-point grids. An interpolation scheme was then used so that the powder-averaged NIS phonon spectra were computed for a $4\times4\times4$ *q*-point grid within the incoherent approximation.[15]

We first optimized the tetragonal $NaAlH_4$ and monoclinic Na_3AlH_6 structures. The results, summarized in Table I, agree reasonably well with previous x-ray[16] and neutron[17,18] studies. For example, the reported $NaAlH_4$ lattice parameters (at 8 K)[17] are 4.98 and 11.15 Å, respectively, while we obtain 4.98 and 11.05 Å. The reported H position (0.237, 0.384, 0.547) is in good agreement with our result.

We also calculated the energy change associated with the two reactions in Eq. (1) and obtained, respectively, 24 and 42 kJ/mol of H_2 released, compared to the experimental enthalpies of reaction of 37 and 47 kJ/mol.[19] The agreement is reasonably good taking into account (i) we cannot directly

TABLE I. Calculated structural parameters of $NaAlH_4$ and Na_3AlH_6.

$NaAlH_4$	$I4_1/a$	$a=4.98$ Å,	$c=11.05$ Å	
Atom	Wyc.	x	y	z
Al	4b	0	1/4	5/8
Na	4a	0	1/4	1/8
H	16f	0.2335	0.3918	0.5439
Na_3AlH_6	$P2_1/n$			
$a=5.33$ Å,	$b=5.53$ Å,	$c=7.68$,	$\beta=90.103°$	
Atom	Wyc.	x	y	z
Al	2a	0	0	0
Na	2b	0	0	1/2
Na	4e	0.9897	0.4532	0.2535
H	4e	0.1000	0.0481	0.2164
H	4e	0.2281	0.3307	0.5437
H	4e	0.1608	0.2673	0.9366

compare our energy differences with the experimental enthalpies (because we do not consider contributions from vibrational entropies, etc.) and (ii) the error associated with our first-principles approach is of the order of 5–10 kJ/mol. This error is estimated from the error in the calculated cohesive energies of individual compounds; e.g., we get $E_{coh}=4.53$ eV for the H_2 molecule, while the experimental value is 4.49 eV.

The vibrational spectrum of $NaAlH_4$ is shown in Fig. 1. The calculated one-phonon spectrum does not reproduce several experimentally observed features. Yet, including two-phonon processes yields results that are in excellent agreement with the observed spectrum. [We also obtained very good agreement between theory and experiment for the phonon spectrum of Na_3AlH_6 (not shown here).] The two-phonon peak in Fig. 1 comes from the combination of one-phonon processes associated with the peaks around 55 and

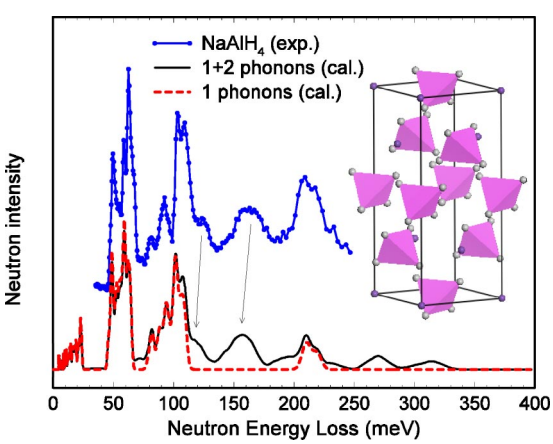

FIG. 1. (Color online) Measured (top) and calculated (bottom) NIS spectra of $NaAlH_4$. The calculated 1 and 1+2 phonon contributions are shown. The structure of $NaAlH_4$ is shown in the inset; grey tetrahedra represent AlH_4 units. The measurements were performed at 8 K.

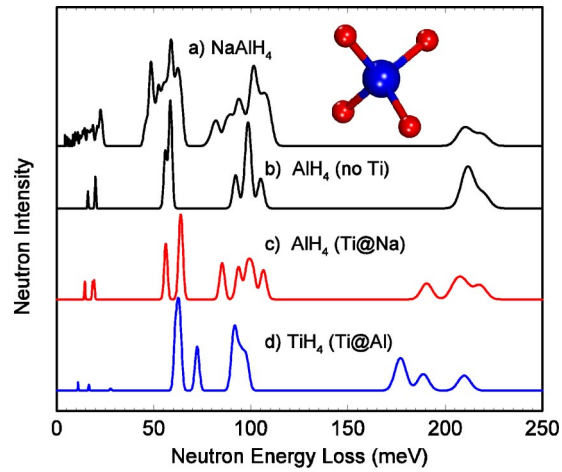

FIG. 2. (Color online) Calculated one-phonon NIS spectra for (a) $NaAlH_4$ and for a single MH_4 tetrahedron for various cases: (b) pure alanate, (c) Ti→Na, and (d) Ti→Al.

100 meV. The AlH_4 units seem to be weakly interacting, which results in sharp one-phonon peaks and relatively sharp two-phonon features as well. These latter features are similar to overtones observed in Raman or IR molecular spectra. Such strong multiphonon contributions are unusual, but they seem to be typical of materials with MH_x groups, where M is a metal atom.[20]

The nature of the different phonon bands in Fig. 1 can be determined by computing the modes of the individual AlH_4 groups in the crystalline matrix. (Note that the NIS spectrum is dominated by hydrogen modes.[15]) The dynamical matrix of the AlH_4 group is constructed using the the finite displacement technique[21] and then diagonalized. As shown in Fig. 2(b), we obtain four distinct groups of modes that correspond to the largest features in the one-phonon spectrum of Fig. 2(a). Inspection of the eigenvectors allows the characterization of the modes. The lowest-frequency modes are AlH_4 translations, while the peak above 200 meV consists of stretching modes of the AlH_4 tetrahedron. The modes in the two intermediate sets are a mixture of rotations and stretches.

Now we extend our calculations to investigate the possibility of substitutional Ti doping of alanates. First we study whether Ti-doped alanate is energetically stable and, if so, where the Ti dopant goes. From the many substitutional and interstitial doping models that could be tried, we choose two that are experimentally motivated. Doping sodium alanate with solid $TiCl_3$ by dry ball-milling results in the formation of NaCl and partial desorption of $NaAlH_4$, which leads to the formation of aluminum crystallites.[22] Hence, it seems pertinent to study the substitution of Al and Na by Ti. In the following we denote these doping models by "Ti→Al" and "Ti→Na."

We consider supercells containing 16 $NaAlH_4$ formula units, and substitute only one of the Al or Na atoms by Ti. The cohesive energies are obtained as the sum of the individual atom energies minus the energy of the system. The results are given in Table II; E_{coh} of the pure alanate has been chosen as zero energy, so that positive entries indicate greater stability than the pure system.

Note that the results in Table II give minus the energy

TABLE II. Calculated cohesive energies, given in eV and per 96-atom supercell. The result for pure $NaAlH_4$ (231.922 eV) is taken as the zero of energy. E_{coh}^{atom} is the cohesive energy obtained by allowing the atoms to relax but imposing the $NaAlH_4$ relaxed supercell (V=1095.48 Å^3); E_{coh}^{atom}(SP) is the same but obtained from spin-polarized calculations; E_{coh}^{full} is the result obtained when allowing both atoms and cell to relax, and V the resulting volume of the 96-atom supercell in $Å^3$.

System	E_{coh}^{atom}	E_{coh}^{atom}(SP)	E_{coh}^{full}	V
Ti→Al	0.075	0.408	0.113	1051.10
Ti→Na	0.911	1.192	1.024	1079.96
Ti→Na+Na^v	−0.665	0.073	−0.562	1059.52
Ti→Na+2Na^v	−2.866		−2.778	1059.27
Ti→Na(H)	1.316			
Ti→Na+H	1.317			

change in reactions of the form $Ti+Na_{16}Al_{16}H_{64} \rightarrow Al+Na_{16}Al_{15}TiH_{64}$, which involve isolated atoms (Ti and Al in this case). These results thus measure the relative stability of pure and doped systems. A positive (and large) entry in the table indicates that, in principle, it is feasible to obtain the doped structure.

We find both Ti→Na and Ti→Al are energetically more stable than pure alanate; i.e., the system gains energy by accepting a Ti dopant into the bulk and releasing a Na or Al atom. In addition, Ti→Na is found to be the most favorable substitution.

The relaxed Ti→Na structure presents H atoms that come close to the Ti dopant. The shortest Ti-H distance is 2.05 Å, to be compared with the 2.39 Å Na-H distance in the pure system. Consequently, the distance between the hydrogens close to the dopant and their neighboring Al atoms is longer than the Al-H distance in the pure system; we obtain 1.70 and 1.64 Å, respectively. This type of relaxation is to be expected, since Ti has more electrons than Na to share with neighboring hydrogens.

It may seem surprising that Ti→Na has a higher cohesive energy than Ti→Al. The typical valences of these atoms certainly suggest otherwise. However, Ti seems to be relatively large for the Al site. In the relaxed Ti→Al structure we get a Ti-H bond of 1.82 Å, which is much longer than the 1.64 Å Al-H bonds in pure sodium alanate. This size mismatch is the most likely cause for Ti→Al to be energetically less favorable.

The above results do not change significantly when the electrons are allowed to spin polarize or when we allow both atoms and cell to relax (see E_{coh}^{atom}(SP) and E_{coh}^{full} columns in Table II). The spin-polarized calculations predict the Ti ion retains one unpaired electron in both Ti→Na and Ti→Al.

A meaningful modification of the Ti→Na doping model is to introduce Na vacancies close to the Ti. Na vacancies should yield a more balanced sum of valence charges and have been invoked in the literature to argue that the Ti dopants reside in the bulk of the system.[5] Our results for one and two Na vacancies are in Table II denoted by "Ti→Na+Na^v" and "Ti→Na+2Na^v," respectively. When spin polarization is allowed, the Ti→Na+Na^v structure is found to be more stable than the pure system, but significantly less stable than the doping models considered above. On the other hand, the Ti→Na+2Na^v structure is predicted to be quite unlikely. All these calculations preserve the basic $NaAlH_4$ lattice. Hence, our results imply that, if Na vacancies really occur, they will involve strong local distortions of the sodium alanate structure.

The dynamics of the neighboring H atoms could be used as a local probe for the Ti location. However, dynamical calculations for the whole 96-atom supercell are very computationally demanding. Instead, we calculated the vibrational spectrum of a single AlH_4 group near the Ti dopant. The results are shown in Fig. 2. In the Ti→Na case (panel c), the Ti dopant mainly affects the high-frequency modes, i.e., those involving stretching of the AlH_4 tetrahedron. All the modes in that group soften. The mode that softens most, approximately from 210 to 190 meV, is dominated by the displacement of H that is closest to the Ti, and essentially corresponds to its oscillation along the Al-Ti direction. This clearly indicates that the presence of Ti could facilitate breaking of the Al-H bond.

In the Ti→Al case [Fig. 2(d)], the dynamics are modified quite differently since we deal with a TiH_4 group. This suggests that, by investigating the phonon spectrum of Ti-doped $NaAlH_4$, one might determine whether Ti dopants go into the bulk of the system and, if so, where they are located. Motivated by this possibility, we measured the phonon spectrum of a 2% Ti-doped sample, but obtained a result essentially identical to that of pure alanate shown in Fig. 1. However, it should be noted that this does not rule out the possibility of substitutional doping in our sample since the amount of Ti is very small, and thus any dopant-induced feature in the spectrum should also be very small and hard to distinguish from the noise. In addition, the NIS spectrum of pure sodium alanate presents significant two-phonon intensity in the 175–200 meV energy range (see Fig. 1), which makes it difficult to identify fine details. Higher resolution spectroscopic measurements, such as Raman scattering, might help elucidate this issue.

The above results suggest that Ti dopants may facilitate the breaking of the Al-H bond. We explored this possibility by moving one H atom to the immediate vicinity of the dopant and then relaxing the system. The resulting structure, which we denote by "Ti→Na (H)," is considerably more stable than the original Ti→Na doping model (see E_{coh} in Table II). In fact, we found that it has not one but two H atoms very close to the Ti. The shortest Ti-H distance is

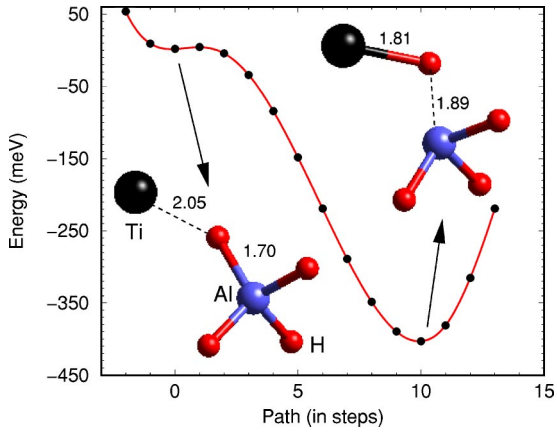

FIG. 3. (Color online) Energy along the path from Ti→Na to Ti→Na (H) structures (see text). Insets show the local structure and bond distances at the two minima. The zero of energy is arbitrary.

1.81 Å, and the corresponding Al-H distance is 1.89 Å, i.e., 0.25 Å longer than in pure $NaAlH_4$. Thus the Ti dopant can indeed induce Al-H bond breaking, a necessary step for H_2 release.

These results indicate that the Ti→Na structure is a local minimum. In Fig. 3 we show the energy change along the transition path leading from Ti→Na to Ti→Na (H). The Ti→Na minimum is very shallow. The calculated energy barrier is around 2.5 meV≈30 K, indicating that Al-H bonds would immediately break in the presence of Ti. Associated with the shallow well is a collective mode of the Ti→Na structure whose frequency can be roughly estimated to be ~80 meV. Yet, the frequency of the AlH_4 mode that we related to the Al-H bond breaking is about 190 meV [see the discussion of Fig. 2(c)]. The reduction from 190 to 80 meV is related to other atomic rearrangements, e.g., the second H coming close to the Ti atom, displacements of the AlH_4 groups, etc.

Along these lines, we also considered a less obvious possibility, namely, that Ti drags extra hydrogens into the system. Table II shows the result for "Ti→Na+H," which corresponds to placing one extra H in the vicinity of the Ti atom. (In the calculation of this cohesive energy, the extra hydrogen was assigned one half of the energy of the H_2 molecule, so that the resulting E_{coh} measures stability against H_2 release.) This structure turns out to be very stable. We find a Ti-H bonding distance of 1.82 Å and several AlH_4 groups approaching the Ti dopant.

In conclusion, we have used first-principles methods and neutron inelastic scattering to study pure and Ti-doped sodium alanate ($NaAlH_4$), a material that holds great promise for reversible hydrogen storage. The total energy calculations indicate that substitutional Ti doping in $NaAlH_4$ is energetically stable. We find that the dopant prefers to substitute for Na and attracts several hydrogen atoms, softening and breaking the corresponding Al-H bonds. We also find it energetically favorable for the Ti to drag extra H atoms into the system. These results point to an interesting direction for future research, namely, the possibility of producing a material, sodium-titanium alanate, that might benefit from the ability of Ti to accommodate extra hydrogens in its vicinity and thus exhibit improved H-storage capabilities.

The authors thank Eric H. Majzoub for providing us with some of the samples used in this work. The authors acknowledge fruitful discussions with D. A. Neumann and Mei-Yin Chou.

[1] B. Bogdanovic and M. Schwickardi, J. Alloys Compd. **253**, 1 (1997).
[2] K. J. Gross, G. J. Thomas, and C. M. Jensen, J. Alloys Compd. **330–332**, 683 (2002).
[3] T. Kiyobayashi, S. S. Srinivasan, D. Sun, and C. M. Jensen, J. Phys. Chem. A **107**, 7671 (2003).
[4] G. J. Thomas, K. J. Gross, N. Y. C. Yang, and C. M. Jensen, J. Alloys Compd. **330–332**, 702 (2002).
[5] D. Sun, T. Kiyobayashi, H. T. Takeshita, N. Kuriyama, and C. M. Jensen, J. Alloys Compd. **337**, L8 (2002).
[6] G. Sandrock, K. Gross, and G. Thomas, J. Alloys Compd. **339**, 299 (2002).
[7] R. A. Zidan, S. Takara, A. Hee, and J. M. Jensen, J. Alloys Compd. **285**, 119 (1999).
[8] J. Huot, S. Boily, V. Guther, and R. Schultz, J. Alloys Compd. **283**, 304 (1999).
[9] J. R. D. Copley, D. A. Neumann, and W. A. Kamitakahara, Can. J. Phys. **73**, 763 (1995).
[10] J. P. Perdew, K. Burke, and M. Ernzerhof, Phys. Rev. Lett. **77**, 3865 (1996).
[11] X. Gonze *et al.*, Comput. Mater. Sci. **25**, 478 (2002). See also http://www.abinit.org
[12] N. Troullier and J. L. Martins, Phys. Rev. B **43**, 1993 (1991).
[13] M. Fuchs and M. Scheffler, Comput. Phys. Commun. **119**, 67 (1999).
[14] S. Baroni, S. de Gironcoli, A. Dal Corso, and P. Giannozzi, Rev. Mod. Phys. **73**, 515 (2001).
[15] G. L. Squires, *Introduction to the Theory of Thermal Neutron Scattering* (Dover, New York, 1996).
[16] V. K. Bel'skii, B. M. Bulychev, and A. V. Golubeva, Acta Crystallogr., Sect. B: Struct. Crystallogr. Cryst. Chem. **24**, 1968 (1982).
[17] B. C. Hauback, H. W. Brinks, C. M. Jensen, K. Murphy, and A. J. Maeland, J. Alloys Compd. **358**, 142 (2003).
[18] V. Ozolins, E. H. Majzoub, and T. J. Udovic, J. Alloys Compd. **375**, 1 (2004).
[19] B. Bogdanovic, R. A. Brand, A. Marjanovic, M. Schwickardi, and J. Tolle, J. Alloys Compd. **302**, 36 (2000).
[20] J. Íñiguez, T. Yildirim, and T. J. Udovic (unpublished).
[21] T. Yildirim, Chem. Phys. **261**, 205 (2000).
[22] K. J. Gross, G. Sandrock, and G. J. Thomas, J. Alloys Compd. **330–332**, 691 (2002).